UNIVERSITÁ DEGLI STUDI DI MILANO

Dottorato in Scienze Farmacologiche Biomolecolari, Sperimentali e Cliniche

PhD in Pharmacological Biomolecular Sciences, Experimental and Clinical

XXXIV cycle

DEPARTMENT OF PHARMACOLOGICAL AND BIOMOLECULAR SCIENCES

DEPARTMENT OF HEALTH SCIENCES

DEPARTMENT OF ONCOLOGY AND HEMATO-ONCOLOGY

TARGETED DELIVERY OF DIAGNOSTIC AGENTS TO NEOPLASTIC TISSUES: PRECLINICAL DEVELOPMENT OF NANOPARTICLES-BASED SYSTEMS FOR THE INTRAOPERATIVE LABELLING OF TUMOUR SITES

BIO/14

Daniela CRESCENTI

Matr. n. R12241

Tutor: Prof. Paolo CIANA

Coordinator: Prof. Giuseppe Danilo NORATA

A.A. 2020/2021

SUMMARY

1 ABSTRACT

English

Despite the advances made in surgical and medical therapies, cancer is still a major cause of death in the world: patients often develop resistance to therapy and relapses due to the incomplete removal of cancer cells. In cancer therapy, the surgical tumour resection aims to remove the neoplastic tissue, along with a surrounding margin of normal non-tumoral tissue, in order to reduce the risk of relapses and improve patients' survival. However, the procedure lacks an objective tool to intraoperative map the exact portion of tissue interested by the neoplastic growth.

The aim of the present project was the preclinical development of an objective tool to label and circumscribe the tumour area, to guide surgeons in the intraoperative safe removal of cancer tissues.

Here, we investigated novel drug delivery systems of natural origin named Extracellular Vesicles (EV) for the specific delivery of diagnostics at tumour sites, in order to allow the detection of tumours during the surgical procedure with increased sensitivity and accuracy. We encapsulated fluorescent dyes into EV from different biological sources and characterized the biodistribution of fluorescence in mouse models of cancer by *in vivo* and *ex vivo* imaging methodologies. In this experimental setting, we have identified EV isolated from cancer patients showing a selective tropism for neoplastic tissues; this tumour tropism is conserved among EV of tumoral origin and is independent from the tumour type and the species originating the vesicles. In PDX models we demonstrated that patient-derived EV recognize corresponding human tumours and deliver fluorescent agents inside cancer cells, providing a proof-of-principle demonstration of the possible translational use of patients' EV in clinic.
Taking advantage of *omics* technologies, we have identified a protein "signature" characterizing the PDEVs and candidate molecules for the mechanism of tumour targeting. From this signature we also discovered a novel promising biomarker for the prediction of CRC disease in liquid biopsy.

In conclusion, this thesis presents the discovery and characterization of pathotropic nanoparticles derived from the blood of oncological patients as useful drug delivery tool to selectively target cancer cells. The biological properties of these autologous EV and their innate abilities to recognize tumours pave the way to the design of novel strategies of personalized diagnosis and therapies in cancer patients, where EV are loaded with diagnostics for the

detection of neoplastic tissues, therapeutics (e.g. chemotherapeutic drugs) for targeted cancer therapies or theranostics for combined diagnostic and therapy.

Italiano

Nonostante i progressi fatti nel campo delle terapie mediche e chirurgiche, il cancro rappresenta ancora una maggiore causa di morte nel mondo: i pazienti sviluppano spesso resistenza alle terapie antitumorali e recidive a causa della non completa deplezione di tutte le cellule tumorali. Tra le terapie antitumorali, la chirurgia mira alla rimozione completa del tessuto neoplastico, tipicamente asportato insieme ad un margine di tessuto sano non tumorale circostante allo scopo di ridurre il rischio di recidive ed aumentare la sopravvivenza dei pazienti. Tuttavia, ad oggi la procedura chirurgica di resezione tumorale manca ancora di uno strumento oggettivo in grado di mappare esattamente, nel contesto intraoperatorio, le porzioni di tessuto interessate dalla crescita neoplastica.

Scopo di questo progetto era quindi lo sviluppo preclinico di uno strumento in grado di definire e circoscrivere in maniera oggettiva l'area tumorale, per guidare i chirurghi in una rimozione intraoperatoria più sicura del tessuto tumorale.

Nello sviluppare questo progetto, ci siamo occupati dello studio di sistemi innovativi di origine naturale per la veicolazione di farmaci, chiamati Vescicole Extracellulari (EV), con i quali veicolare agenti diagnostici in maniera specifica ai siti tumorali, allo scopo di consentire la rilevazione di tumori durante l'operazione chirurgica con maggior sensibilità e precisione. Abbiamo incapsulato dei coloranti fluorescenti all'interno di vescicole extracellulari ottenute da diverse fonti biologiche e caratterizzato la biodistribuzione della fluorescenza veicolata in modelli tumorali murini tramite sistemi di *imaging* in vivo ed ex vivo. In questo contesto sperimentale abbiamo individuato vescicole extracellulari isolate da pazienti oncologici che mostrano un tropismo selettivo per i tessuti neoplastici; questo tropismo tumorale risulta conservato tra vescicole extracellulari di origine tumorale ed è indipendente sia dal tipo di tumore che dalla specie di origine delle vescicole. In modelli di xenotrapianto (PDX) abbiamo dimostrato che le vescicole derivate da pazienti sono in grado di riconoscere i corrispondenti tumori umani e veicolare i traccianti fluorescenti all'interno delle cellule tumorali stesse, fornendo così una prova di principio del possibile utilizzo delle vescicole di pazienti in clinica. Grazie all'utilizzo di tecniche *omiche*, abbiamo identificato una "firma" proteica caratterizzante le vescicole dei pazienti e delle molecole candidate per spiegare il meccanismo di targeting dei tumori.
Da questa firma abbiamo inoltre scoperto un nuovo promettente biomarcatore per la predizione del tumore del colon-retto attraverso la biopsia liquida.

In conclusione, questo lavoro di tesi presenta la scoperta e la caratterizzazione di nanoparticelle patotropiche derivate dal sangue di pazienti oncologici come utili strumenti per la veicolazione selettiva di sostanze attive alle cellule tumorali. Le proprietà biologiche di queste vescicole autologhe e le loro innate abilità di riconoscere i tumori aprono la strada allo sviluppo di nuove strategie per diagnosi e terapie personalizzate in pazienti oncologici, dove le vescicole extracellulari vengono caricate con agenti diagnostici per la rilevazione dei tessuti neoplastici, agenti terapeutici (es. farmaci chemioterapici) per terapie antitumorali mirate o agenti teranostici per diagnosi e terapia combinate.

2 INTRODUCTION

2.1 Cancer impact

Cancer is a generic term for diseases in which abnormal cells divide without control and can invade nearby tissues (definition from NCI [1]). Cancer ranks as a leading cause of death in many countries of the world and its rising prominence partly reflects the decline in mortality rates of stroke and coronary heart disease, reduced by successful prevention therapies.

Worldwide, 19.3 million new cancer cases and almost 10.0 million cancer deaths occurred in 2020 (data collected before SARS-CoV-2 pandemic). Female breast cancer was the most diagnosed cancer (11.7% of the new cases), followed by lung (11.4%), colorectal (10.0 %), prostate (7.3%), and stomach (5.6%) cancers, while lung cancer remained the leading cause of cancer death (18% of deaths), followed by colorectal (9.4%), liver (8.3%), stomach (7.7%), and female breast (6.9%) cancers [2]. In Italy prostate, lung and colorectal cancer are the most frequent and with the highest mortality in men, while breast, colorectal and lung cancer are the most common and deadly among women [3].

Global cancer burden is expected to grow as consequence of both aging and growth of the population as well as of changes in the prevalence and distribution of the main cancer risk factors [2].

2.1.1 Colorectal Cancer

Colorectal cancer (CRC) is the third most common cancer and the second leading cause of death among cancers worldwide [4]. In Italy 52,228 new CRC cases were documented in 2017 and 20,982 deaths due to CRC were recorded [3]. Italian incidence rates are among the highest in the world and similar to those reported in high-income countries [4]. The disease is quite rare before the age of 40 and more widespread in patients between 60-75 years. CRC incidence is generally higher among males than females at all anatomic sites, however the male-female ratio tends to increase progressively from the colon to the cecum and the rectum [5].

Colorectal cancer usually develops from the glandular epithelial cells of the large intestine. Cancer arises when certain cells of the epithelium acquire a series of genetic or epigenetic mutations conferring them selective advantages in proliferation and survival leading to the develop of carcinomas [6]. CRC occurs in half of the cases in the sigmoid and rectum, in a quarter of patients it affects the ascending colon, while the transverse and descending colon are affected one in five cases [7].

Most colorectal cancers generally develop over time from adenomatous precancerous polyps, which grow from proliferations of intestinal mucosal cells. **Risk factors** for CRC include family history of colon or rectal cancer (first grade relatives), genetic predisposition, lifestyle and diet, alcohol intake, smoking and inflammatory bowel disease [8].

Primary colorectal cancers can be classified in **epithelial** (adenocarcinomas), **neuroendocrine** (NETs), **non-epithelial** (leiomyosarcomas, GIST) and **haematopoietic system tumours** (non-Hodgkin lymphomas), according to the World Health Organization classification (WHO). Colorectal adenocarcinomas are the most frequent malignant tumours of colon rectum and account for 95% of all tumours in these sites [9].

DIAGNOSIS

A diagnosis of colorectal cancer either results from the assessment of a patient with symptoms or as a result of screening. Symptoms associated with CRC disease include blood in stools, change in bowel habits, abdominal pain, fatigue, anaemia-related symptoms and weight loss [8]. As the onset and evolution of the disease take years to show, regular screening represents a fundamental tool for early diagnosis and treatment. Currently, faecal occult blood test is the examination employed for screening in the general population. In symptomatic patients, colonoscopy is the preferred method of investigation; alternatively, flexible sigmoidoscopy associated with double contrast barium enema or CT colonography (virtual colonoscopy) can be used [10].

After diagnosis, disease staging and assessment of metastasis is addressed. Staging identifies the severity of cancer and correlate with prognosis and survival. According to the TNM classification system, staging of CRC describes the primary tumour and the depth of invasion through the wall of the intestine (T), the involvement of lymph nodes (N), and the spread to other organs (metastases, M) [11]. Colorectal cancer frequently metastasizes in the liver: about 10-20% of patients display liver metastases at the first diagnosis (synchronous metastasis), while almost 50% develop them after surgery on the primary tumour (metachronous metastasis) [12]. Imaging test like thoracic and abdominal CT scan, MRI, PET, and X-rays are performed in order to detect metastases [10].

Blood test offers a non-invasive test for molecular detection of colorectal cancer through serum quantitation of tumour markers: CEA and CA 19.9. CEA (carcinoembryonic antigen) is a

marker of disease and the most frequent indicator of recurrence in asymptomatic patients (standard plasma levels are less than 5 ng/ml), often used in combination with carbohydrate antigen (CA) 19-9 [13].

TREATMENT

The goal of CRC treatment is to achieve complete removal of the tumour and metastases, which requires surgical intervention. Surgery is the first curative option for patients with non-metastasized colorectal cancer; the outcome is strongly related to the quality of surgery, the quality of pre-operative staging and treatment selection [8]. In more-advanced cases, neoadjuvant treatment (for example preoperative chemotherapy or (chemo)radiotherapy) might be necessary to reduce tumour burden and increase the chances for a successful resection [8,14].

Surgery is essentially represented by total o segmental resection, preferentially laparoscopic over laparotomy open surgery [15,16], unless contraindications such as obesity, previous abdominal surgeries and advanced-stage disease [15]. Video-laparoscopic resections offer to patients several advantages, such as less postoperative pain, faster recovery times and return to normal daily activities, and better aesthetic result, with comparable outcomes to the laparotomy technique [16] (Figure 1). The basic surgical principles are the removal of the major vascular pedicle feeding the tumour along with its lymphatics, and en bloc resection of any organs or structures attached to the tumour [14]. To ensure radical intervention and decrease the risk of local or distant recurrence, proximal and distal **disease-free resection margins** of at least 8-10 cm in colon cancer and 2 cm in rectal cancer are recommended [14,17].

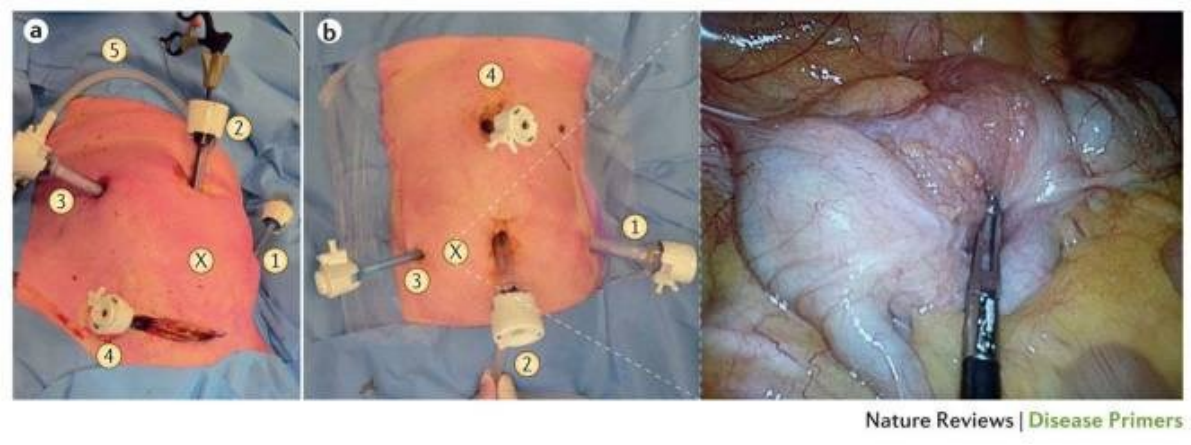

Figure 1. Laparoscopic surgery for colorectal cancer. Image from [8].

In addition to surgery, radiotherapy and chemotherapy are the leading strategies to reduce tumour growth and spread in patients with unresectable lesions or intolerant to surgery. In some cases, chemotherapy and radiotherapy are also applied as neoadjuvant or adjuvant treatment before or after surgery to reduce or stabilize the tumour mass. Current chemotherapy for CRC includes single-agent therapies with 5-fluorouracil and multiple-agent treatments with different drugs, including oxaliplatin, irinotecan, and capecitabine [18]. Another treatment option for CRC patients is represented by targeted therapies, with cetuximab and bevacizumab the first monoclonal antibodies approved for metastatic CRC targeting the *Epidermal Growth Factor Receptor* (EGFR) and the angiogenetic factor VEGF-A (*Vascular endothelial growth factor-A*), respectively [19,20].

In metastatic CRCs, only 10–20% of patients with metastasis are eligible for curative treatment strategies [21]. For patients with unresectable stage IV CRC survival has substantially improved to a median overall survival of ~ 30 months [22]; this improvement can be attributed to the use of chemotherapeutics (oxaliplatin and irinotecan), introduction of targeted therapies (cetuximab, panitumumab, bevacizumab) and surgical resection of liver metastases [8]. With surgery, eligible patients with R0 resectable metastasis [23] have a 5-year overall survival rate of about 20% [24]. However, in most patients with isolated metastases, a R0 resection cannot be primarily achieved; nevertheless, if metastases can be downsized and combined with adjuvant chemotherapy, the 5-year overall survival rate come close to that of R0 resections [25].

RECURRENCE

The 5-year survival rate for CRCs is about 64% but drops to 12% for metastatic CRC [26]. The liver is the most common site of metastatic disease from colorectal cancer; nearly a quarter of CRC are diagnosed at an advanced stage with metastases, and 20% of the remaining cases may develop metachronous metastases, resulting in more difficult curative surgery and subsequent tumour-related deaths [18]. The liver is affected in 65% of patients with metachronous metastases; lungs are the second most-common site of metachronous metastasis, affecting 43% of patients, while in 12% of patients liver and lung metastases are present together [21].

After curative treatment 30% of patients with stage I-III and up to 65% of patients with stage IV CRC develop recurrent disease. 60 to 80% of recurrences after curative surgery occur within the first 2-years of therapy [22]; therefore, follow-up monitoring is more intensive during this time. The goal of surveillance after treatment of primary CRC is the detection of local recurrent

disease, metachronous lesions, and distant metastases at an early, asymptomatic and treatable stage [22]. Imaging scans (CT, MRI, CT-colonography, colonoscopy, ultrasonography, PET) and serum biomarkers are used for detection of non-luminal local recurrences and distant metastases during follow-up assessments, whereas endoscopic investigations (colonoscopy, CT-colonography) enable diagnosis of intraluminal recurrent disease and metachronous lesions [22].

Several factors are known to influence the risk of CRC recurrence. These include tumour clinical stage and molecular subgroup, KRAS mutations, mismatch repair genes and microsatellite instability, adjuvant/neoadjuvant chemotherapy, emergency surgery in case of perforating and obstructive tumours, anastomotic leakages, postoperative bacterial infections, perioperative blood transfusions, tumour location, and presence of micro metastases in lymph nodes and around vessels and nerves [27]. In colorectal liver metastasis, dedifferentiation and tumour infiltrating inflammation of metastatic lesions are considered predictive factors of tumour recurrence [28]. The mechanism of recurrence may include inadequate resection margins or missed lesions from the primary tumour [29]; margin status and RFA (radiofrequency ablation) [30] were factors associated with intrahepatic recurrence, while risk of extrahepatic recurrence was associated with a more aggressive tumour phenotype (e.g. multiple, large metastasis) [31].

2.2 The surgical practice of tumour resection

In clinical oncology, tumour resection is a surgical practice aimed at completely eradicate the neoplastic tissue from the body. Complete removal of the tumour tissue improves patients' prognosis and decreases the chance of recurrence of disease for many types of cancer, thus influencing the long-term efficacy of the anti-cancer therapy [32]. Since the beginning of medicine, intraoperative tumour resection is primarily based on human vision and tactile information: surgeons rely on experience, training, visual, and tactile information to delineate and resect most solid tumours [33]. During surgery, the eyes and hands of the surgeon are the instrument used to decide the tissues, healthy or not, that need to be resected or preserved [34].

To plan surgical interventions, tests and imaging scans (predominantly x-ray computed tomography (CT), magnetic resonance imaging (MRI), and ultrasound (US)) are usually performed before surgery to help the surgeon have a view of the tumour appearance and location within the body [35]; in some cases, CT, MRI, and US are even used during cancer surgery to detect tumours and define tumour vasculature [36]. Depending on the area affected by

the tumour growth and on tumour size, surgery is then performed using open field or less invasive techniques.

Surgeons perform tumour resection by removing the neoplastic tissue along with a surrounding amount of normal healthy tissue, defined as **resection margin**, in order to completely remove cancer cells and reduce the risk of relapses. The residual disease is in fact the prevalent cause of local recurrence and affects prognosis. Studies have reported up to 40% of intended curative resections containing microscopic evidence of residual tumour [37,38], even in endoscopic procedures, such as laparoscopic colorectal surgery [38,39]. The need to obtain a complete resection of the malignant tissue with sufficient tumour-free margins is balanced with preservation of the surrounding structures to minimise tissue damage of vital structures, such as nerves, functional impairment and postoperative complications [33]. Often, lymph nodes and other tissues near the tumour are excised to search for evidence of cancer infiltration and occult disease into the nearby tissues or lymphatic drainage. Assessment of margins (i.e. identification of complete resection or presence of positive margins indicative of an incomplete excision) and infiltrations of cancer cells is currently evaluated by the histopathological examination of the resected specimen, which is conducted postoperative [40]; several hours to days after surgery may be required before specimens are analysed and the presence of positive margins eventually confirmed [32]. With evidence of cancer cells in the margins (meaning *positive margins*), the best follow-up treatments, including radiotherapy and chemotherapy, are planned.

2.3 Intraoperative imaging

Imaging techniques have a crucial role in the diagnosis and management of disease. For diagnostic purposes they are normally undertaken within 24 h before surgical interventions to guide delineation and localization of regions of surgical interest or in the postoperative period to ensure correct performance of surgery or exclude operative adverse events [41]. During surgery, oncologic surgeons need to assess tumour margins, the borders between healthy and cancerous tissue, and take note of nerves and blood vessels in order to optimize resection of malignant tissues while minimizing harm [35]. Palpation and visual inspection are not always sufficient for discriminating between malignant and normal tissues and can lead to incomplete resections, resulting in residual disease, or to the unnecessary removal of healthy tissue. Moreover, human vision does not have the sensitivity to detect cells, disease infiltration or cancer-related

processes affecting deep structures because human eyes cannot visualize under the tissue surface [32].

Currently, several imaging techniques are used during surgery with the aim of supporting the surgeon, including ultrasound, x-ray, computed tomography (CT) and magnetic resonance imaging (MRI). However, these techniques have limited contrast imaging capabilities or limitations due to their size and geometry, toxicity, require direct contact with the body, cannot get images in real-time for fast intraoperative decision-making and continuous workflow, they are challenging in maintaining a sterile surgical field and ultimately costs [35].

More recently, new imaging techniques have been successfully introduced as intraoperative tools for surgical image guidance, including optical (fluorescence imaging [36] and Raman spectroscopy [42]), acoustic (photoacoustics [43] and radiofrequency-acoustics [44]), and nuclear imaging-based modalities (SPECT and PET [45]). These approaches, used alone or combined with imaging agents to increase contrast and specificity, can improve the signal coming from the disease tissue, enhancing its identification beyond the direct visual inspection and palpation [35].

Fluorescence imaging is a simple, low-cost, and contact-free method based on excitation of fluorophores by an appropriate light source and detection of emitted photons by appropriate detection systems [36]. The technique is highly compatible with the intraoperative setting, allowing for real-time imaging during surgery and offering superior sensitivity compared to preoperative imaging or visual inspection and palpation [46].

2.3.1 Real-time fluorescence imaging in surgery

To improve surgical vision and distinction of disease and healthy tissues during surgery, the intraoperative imaging using near-infrared (NIR) fluorescent light has been introduced as a new method to fill the gap between the preoperative imaging and the intraoperative reality based on human vision [32].

NIR light works in the optical window at wavelengths between 700-1000 nm and is usually preferred for *in vivo* imaging applications due to the lower autofluorescence, deeper tissue penetration (from several millimetres up to centimetres) and reduced interference and light scattering of biological chromophores in the NIR spectrum, that improve the sensibility of the technique [47,48]. Since NIR fluorescence is invisible to the human eye, sensitive photodetectors

are required: several imaging fluorescence systems with an integrated light source and camera are commercially available and have already been employed in the intraoperative setting [49].

Intraoperative NIR fluorescence imaging relies on NIR fluorescent agents labelling tissues and structures of interest (i.e. tumour) and on intraoperative imaging systems able to both excite and detect the fluorophore, allowing to visualize the fluorescence signal after milliseconds [50] (Figure 2).

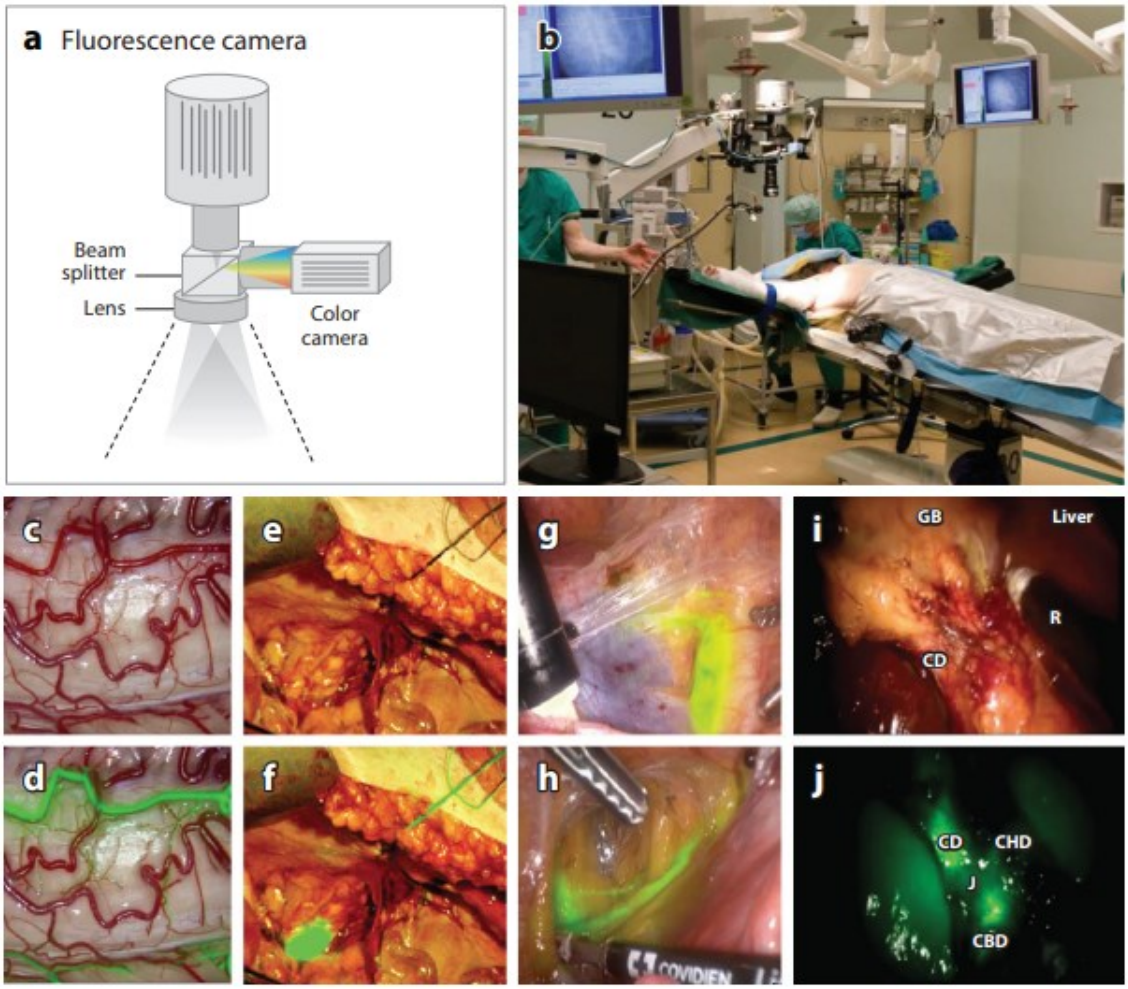

Figure 2. Intraoperative fluorescence imaging. (a) Typical intraoperative fluorescence imaging system simultaneously collecting fluorescence and white light (colour) images from the same camera and field of view. (b) Photograph of an imaging fluorescence system inside the operating room. (c) Colour reflection image of the spinal cord and (d) overlay of colour and fluorescence images of spinal cord during indocyanine green (ICG)-video angiography visualizing microvascular flow and anatomical orientation for precise resection of spinal intramedullary tumours. (e) White light reflection and (f) fluorescence overlaid image showing a lymph node in early-stage cervical cancer surgery. (g) Endoscopic sentinel lymph node (SLN) mapping in the right external iliac region in endometrial cancer and (h) endoscopic lymph node mapping in the left obturator region. (i) Colour reflection image and (j) fluorescence pseudo-colour image of intraoperative fluorescent cholangiography during cholecystectomy. Picture from [32].

In order to visualize tumours using NIR fluorescence imaging, a contrast agent should accumulate in or around a tumour. For accurate tumour delineation or identification of occult lesions, the targeting efficacy of the fluorescent agent should be able to provide high contrast between tumour and surrounding tissue (high tumour-to background ratio) to distinguish the labelled fluorescent tumour area from non-fluorescent areas free of tumour [33,51].

2.3.2 Near-InfraRed fluorescent agents

Currently, only two NIR dye are approved for clinical use: indocyanine green (ICG) and methylene blue (MB). ICG is the most commonly used NIR fluorescent agent, approved by the regulatory agencies Food and Drug Administration (FDA) and European Medicines Agency (EMA) for clinical fluorescence imaging applications, including angiography, perfusion imaging, and sentinel lymph node (SLN) mapping, and also used for intraoperative detection of tumours [52]. Methylene blue (MB) has traditionally been used at high doses as a visible dye in thyroid and parathyroid surgery [53]; at low doses, MB acts as NIR fluorophore at 700nm in different NIR guided surgical techniques, including visualization of ureters, thyroid and parathyroid surgery, pancreatic neuroendocrine tumours, localization of breast cancers [36,54].
5-aminolevulinic acid (5-ALA) is another fluorophore approved and used in clinic but not considered a NIR agent since its fluorescence is outside the NIR spectrum. 5-ALA and its derivate 5-ALA hexyl ester are prodrugs used for fluorescence imaging detection of high-grade gliomas and bladder cancer and for tumour treatment in photodynamic therapy by inducing the synthesis of protoporphyrin IX, a red-fluorescent protein which preferentially accumulates in epithelia and neoplastic tissues [55].

However, ICG, MB and 5-ALA are nonspecific contrast agents, labelling tumour or tumour vessels not specifically. To highlight tumours, new strategies have been investigated over the years to improve the specificity of cancer detection during surgery, including fluorescent agents targeting specific ligands overexpressed by tumour cells (e.g. EGFR, folate receptor-α, CEA, EpCAM, c-MET, CAIX), tumour vessels or stroma (e.g. VEGF, integrin αvβ3, uPAR) [56]. In many cases, NIR fluorophores were combined to specific tumour-targeting ligand, such as peptides, affibodies, activatable tracers, small molecules, and antibodies already clinically available as therapeutics (like cetuximab or bevacizumab), to provide a real-time system for the identification and delimitation of tumours or adjacent vital structures [32,57,58].

Strategies based on nanoparticles have been also explored to overcome the problems of NIR dyes, including their low photostability, hydrophobicity, and non-specific targeting, and therefore to improve the delivery of NIRs to tumours by actively targeting cell-specific moieties or through passive targeting by the enhanced permeability and retention (EPR) effect [59]. Most of these nanoparticle carriers included liposomes and micelles, polymeric nanoparticles, dendrimers, quantum dots, carbon nanotubes, gold and silica-based nanoparticles [60].

2.3.3 Indocyanine Green

Indocyanine green (ICG) is a water soluble amphiphilic tricarbocyanine iodide dye (Figure 3), used as fluorescent contrast medium in various clinical settings, from cardiology, ophthalmology, and neurosurgery to evaluation of tissue perfusion and cancer treatment [61]. It was 1959 when ICG was first approved by the Food and Drug Administration (FDA) for clinical and research use in humans.

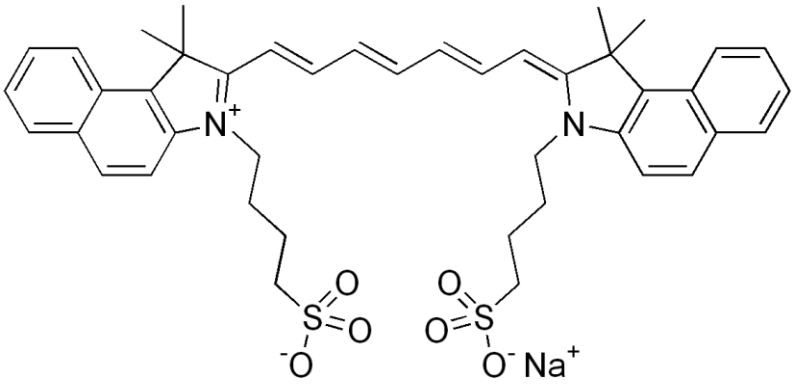

Figure 3. Chemical structure of indocyanine green (ICG).

ICG has an absorption and fluorescence spectrum in the near infrared region (the region of the electromagnetic spectrum within the wavelengths range from 700 to 2.500 nm), both depending on solvent and concentration used. The molecule is generally excited between 750 and 800 nm (800-805nm in blood) and fluorescence is viewed around the maximum peak of 832 nm [62]. These properties allow high contrast, sensitivity and detection of ICG fluorescence with proper detection systems through up to 10 mm of tissue [63]. The wavelength of the light source used and the absorbance of molecules constituting human tissues, especially water and haemoglobin, influence how deep through tissues it is possible to observe; however, little interference in

fluorescence measurements is given by tissue autofluorescence and light absorption of biological chromophores at ICG working wavelengths [63,64].

ICG is a relatively nontoxic, fluorescent iodide dye with rapid hepatic clearance. The dye has a LD_{50} lethal dose of 60 mg/kg in mice and 87 mg/kg in rats [65], resulting essentially non-toxic with a standard dose of less than 2 mg/kg in humans [61]. Some side effects of minor to moderate entity are sporadically reported (1 case over 42,000) and include: nausea, angyalgia, hot flushes and low-grade fever. Severe side effects like anaphylactic shock, hypotension, tachycardia, dyspnea and urticaria are also reported [64,66] .

Once injected, the molecule highly binds to plasma proteins, especially serum albumin and α- and β-lipoproteins, which restrict ICG into the intravascular space until hepatic uptake and excretion into bile [62,67]. ICG is cleared from the systemic circulation exponentially in the first 10 to 20 minutes after administration, with a half-life of about 3-4 minutes in healthy subjects depending on single organs vascularization. After this initial phase, the clearance rate slows allowing trace amounts of ICG to remain in the plasma for more than an hour [61,68]. Sinusoidal uptake and canalicular excretion are the two main processes involved in ICG hepatic clearance: selective uptake of ICG occurs across the sinusoidal plasma membrane by 1B3 and Na+ - taurocholate co-transporting polypeptides, after which ICG is excreted unchanged and almost completely (97%) into the bile in the non-conjugated form [69].

FDA granted approval of ICG in 1959 for the use in:

i) determining cardiac output, exploiting the pharmacokinetic characteristics of ICG [70];
ii) determining hepatic function and liver blood flow, thanks to the absence of metabolism and the entero-hepatic recirculation allowing to correlate ICG clearance with hepatic function [69];
iii) ophthalmic angiography, where ICG can be used as contrast medium to better visualize retinal vascularization [71].

In surgery, ICG is used as a contrast agent for the evaluation of organ and tissue perfusion [62] in video-assisted laparoscopic and thoracoscopic surgery and in traditional open surgery, taking advantage of near-infrared technologies where the light source needed to excite ICG is incorporated in the near-infrared video camera system; fluorescence emitted by excited ICG is made visible by detection systems, allowing a real-time augmented-reality view of the surgical

field [72]. In gastrointestinal and colorectal surgery ICG is often used to guide the identification of the optimal resection site and help estimate the blood flow after anastomosis [73]. Since the 97% of ICG is excreted in the bile, ICG can also be used as a contrast agent in the visualization of the biliary tree to guide cholecystectomies and resection of malignancies [74]. ICG also find application in lymphatic mapping and sentinel lymph node (SLN) identification, allowing visualization of the lymphatic drainage of the tumour and SLN after peritumoral injection [52,75].

Indocyanine green has been reported as a biologically safe photothermal and photosensitizer agent too, able to kill tumour cells by producing singlet oxygen species and photothermal heat upon NIR irradiation [76]. These photosensitizing properties of ICG are exploited in oncologic therapy for photothermal (PTT) and photodynamic therapy (PDT), where necrosis of malignant tumours can be induced with minimal side effects [77]. PDT is a non-invasive treatment that combines a photosensitizer and an activating light source: after administration and accumulation of the photosensitizer in tumour cells, exposure of the molecule to light of an appropriate wavelength leads to activation of the compound which subsequently releases reactive oxygen species (ROS) and singlet oxygen, exhibiting anti-tumour effects [78]. In PTT and PDT ICG's use is restricted by limited accumulation in tumours, photobleaching, easy aggregation, rapid aqueous degradation, and short half-life of ICG. To address these limitations and improve ICG stability and pharmacokinetics, resulting in efficient PTT, nanoparticles delivery systems such as polymers, micelles, liposomes, dendrimers, and magnetic, gold and mesoporous nanomaterials conjugated with ICG have been developed [77].

ONM-100 is a nanoparticle-based fluorescent imaging agent consisting of an ultra-pH sensitive amphiphilic polymer, conjugated with indocyanine green, which rapidly and irreversibly dissociates to fluoresce in the acidic extracellular microenvironment that characterizes many solid tumours [79]. In a phase I study on human patients, ONM-100 fluorescence-guided surgery enabled detection of tumour-positive surgical margins and occult disease [79].

2.4 Extracellular Vesicles (EV)

Extracellular vesicles (EV) are defined as particles naturally released into the extracellular environment by both eukaryotic and prokaryotic cells, delimited by a lipid bilayer and unable to replicate [80]. EV represent an elegant, efficient, robust and economical strategy for intercellular communications, evolutionally conserved from bacteria, plants, lower eukaryotes up to higher organisms. In intercellular communication, cells continuously crosstalk by using different paracrine and endocrine networks of signals. These signalling systems have been historically linked with the activity of single messenger molecules including hormones, growth factors, cytokines. More recently, a novel layer of communication has been described involving extracellular vesicles.

The significance of EV lies in their physiological role of carriers of bioactive molecules (protein, lipids, nucleic acids and sugars), by transferring many and different kinds of information from donors to recipient cells in order to influence biological functions [81]. Their content has been described as a full package of regulatory molecules that may efficiently change the phenotype of target cells.

The first observations leading to the identification of EV date back to 1946 when Chargaff and West discovered that platelet-free plasma possessed clotting properties that were lost after high speed centrifugation [82]. More than twenty years later, in 1967, Wolf published evidence of coagulant particulate material released from activated platelets, which could be separated by ultracentrifugation and referred to as "platelet dust" [83]; it was only in 1971 in a manuscript of Bonucci that the term "extracellular vesicle" was first used [84]. Initially, the secretion of extracellular vesicles was considered as means used by cells to eliminate unneeded compounds and waste material [85]. Years later, particularly in 2006–2007, EV acquired renewed interest as mediators for cell-cell communication with the discovery that EV contain RNAs, including microRNAs. Since then, the interest of the scientific community for extracellular vesicles has grown exponentially and the field has rapidly developed. Not surprisingly, in 2013 James E. Rothman, Randy W. Schekman and Thomas C. Südhof were awarded with the Nobel Prize in Physiology or Medicine *for their discoveries of machinery regulating vesicle traffic, a major transport system in our cells*.

2.4.1 Essentials of EV

"Extracellular vesicles" is an umbrella term endorsed by the International Society for Extracellular Vesicles (ISEV; www.isev.org) to indicate all types of membrane vesicles secreted by cells, including exosomes and microvesicles, because at present no biochemical or biophysical distinction of EV generated by a particular biogenesis pathway can be made [80,86].

Extracellular vesicles are a heterogeneous group of cell-derived membranous structures differing in size, cargo content, function and biogenetic mechanism. Cargo, size and membrane composition of EV are highly heterogeneous and dynamic and dependent on the cell of origin, state and environmental conditions. Currently. three main EV subtypes have been identified and classified according to size, subcellular origin, their biophysical and/or biochemical properties, their receptor composition, and possibly their content: i) exosomes, originating from the endosomal system, ii) microvesicles, which are shed from the plasma membrane, and iii) apoptotic bodies, released during cellular apoptosis after blebbing of the plasma membrane [87] (Figure 4).

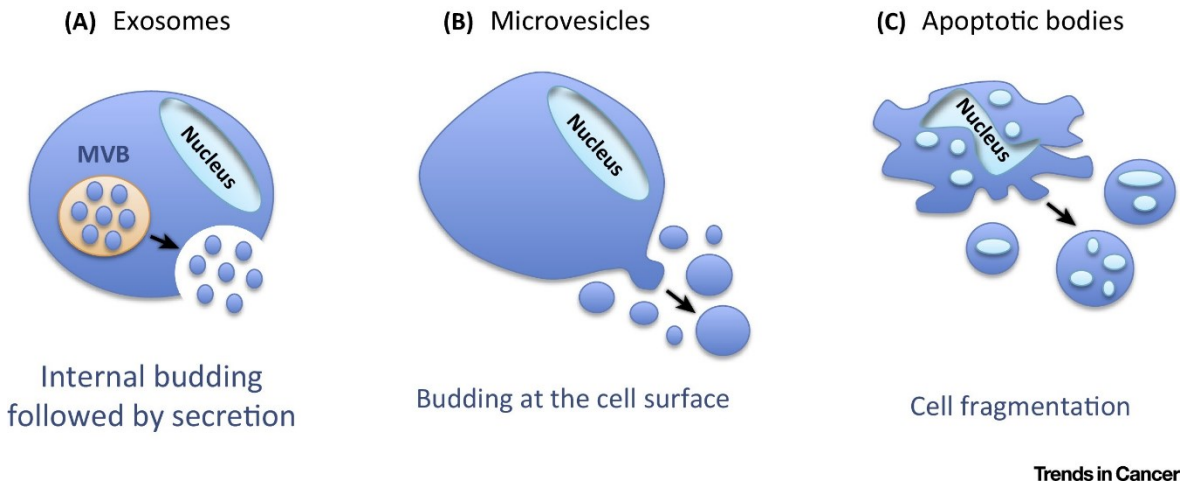

Figure 4. Main classes of Extracellular Vesicles. (A) Exosomes generated by inward budding of endosomal membranes. (B) Microvesicles formed by outward budding of the plasma membrane. (C) Apoptotic bodies release by apoptotic cells. Picture from [88].

EXOSOMES

Exosomes are nano-sized extracellular vesicles, span 40-150 nm in diameter and have spherical or cup-shaped structure given by a lipid bilayer membrane with similar orientation of the cell of origin [89]. Exosomes originate from endocytic invaginations of the plasma membrane called "early endosomes", where intraluminal vesicles (ILVs) are formed by inward budding of the endosomal membrane, leading to formation of multivescicular bodies (MVB). ILVs and MVB biogenesis can occur in an ESCRT- or sphingomyelinase-dependent manner; the process is mediated by at least two distinct pathways and involves the sorting of various molecules, including proteins, lipids, and cytosol, specifically into ILVs. The first pathway leading to MVB formation requires the multimolecular machinery *endosomal sorting complex required for transport* (ESCRT). The machinery consists of four multi-protein complexes (ESCRT0, ESCRTI, ESCRTII and ESCRTIII): ESCRT0, ESCRTI and ESCRTII recognize ubiquitinated cargo proteins outside the endosomal membrane, ESCRTI and ESCRTII mediate the invagination of the late endosomal membrane, ESCRTIII promotes deubiquitination of cargo proteins, vesicle excision and the final generation of ILVs [90,91]. The second pathway of MVB formation is based on the lipid composition of the endosomal membrane and involve sphingomyelinase: this enzyme is responsible for the hydrolysis of sphingomyelin to ceramide which in turn creates microdomains and negative curvatures on the endosomal membrane leading to ILVs formation [90]. Another way for ILVs formations involves some proteins of the tetraspanin family, including CD63, CD81, CD82 and CD9, which create clusters on the endosomal membrane leading to internal invagination and formation of ILVs [87]. Following formation, MVB are fated for the degradative lysosomal pathway or the secretory pathway. Although the mechanism by which MVB are degraded or secreted is still unknown, it may be dependent on cholesterol: MVB rich in cholesterol are generally secreted, while MVB poor in cholesterol are more easily degraded by fusion with lysosomes [92]. The final release of ILVs into the extracellular milieu occurs upon fusion of MVB with the cellular plasma membrane, mediated by proteins of the SNAREs family (*soluble N-ethylmaleimide-sensitive fusion attachment protein SNAP REceptors*) [93]. Once secreted, ILVs are finally termed exosomes [90] (Figure 5).

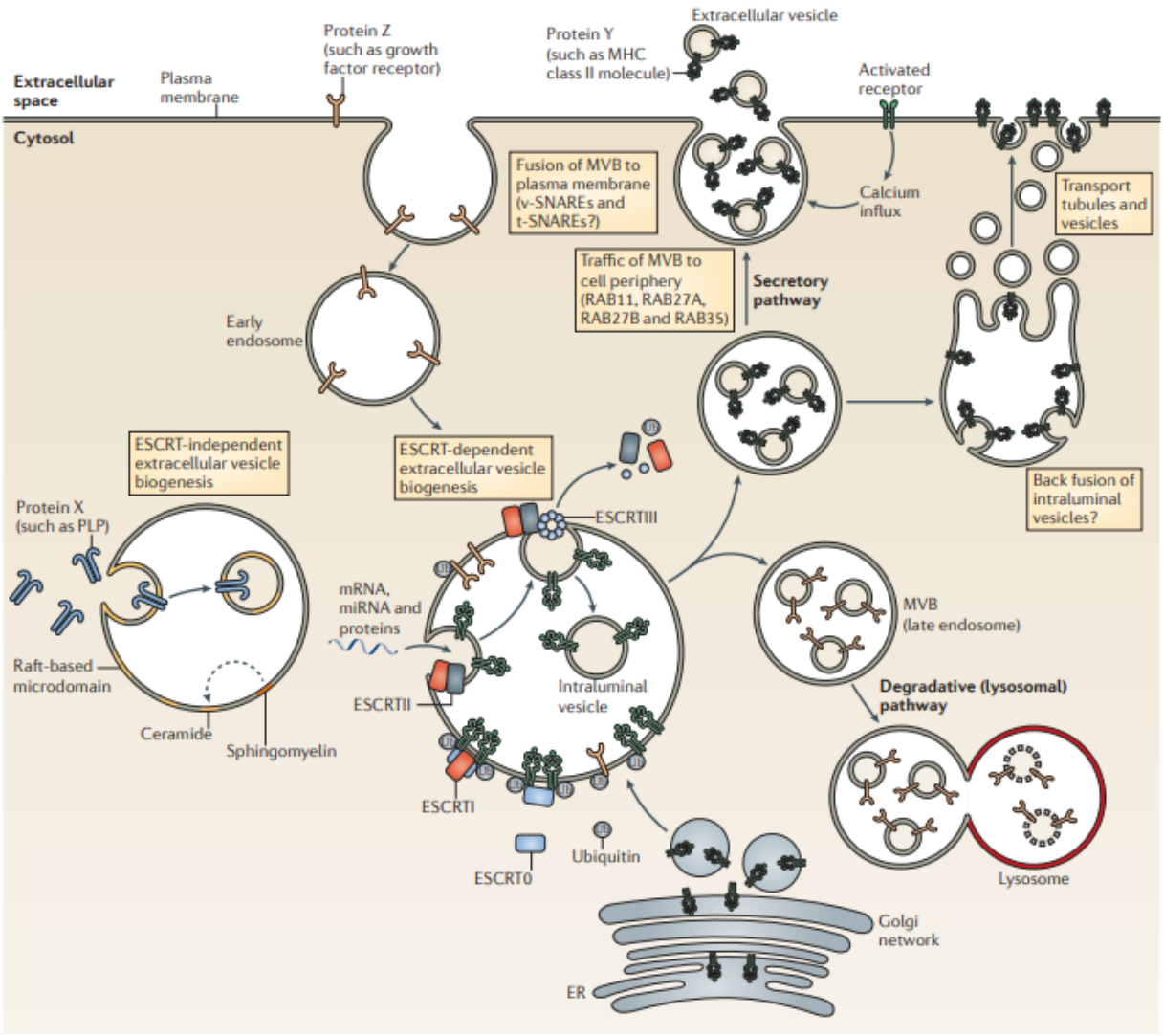

Figure 5. Biogenesis and secretion of exosomes. Picture detailing the biogenetic pathways leading to exosomes formation and secretion described in the text. Picture from [90,94].

MICROVESICLES

Microvesicles, also referred to as shedding vesicles, ectosomes, oncosomes, shedding bodies, and microparticles, are heterogenous extracellular vesicles with a diameter spanning from 100 and 1000nm, shed from the surface of many cell types [95]. Unlike exosomes, the cellular processes leading to their generation are less understood. Membrane-remodelling and membrane-sorting events seem implicated in the constitutive or stimulated release of microvesicles from the cell surface [90]: trafficking of molecular cargo to the plasma membrane, redistribution of membrane protein and lipids (including phosphatidylserine placement on the outer side of the membrane) which induce changes in membrane curvature and rigidity, and use

of the actin and myosin contractile machinery and fusion machinery (SNAREs and tethering factors) at the surface to allow vesicle budding are involved in their biogenesis [96] (Figure 6).

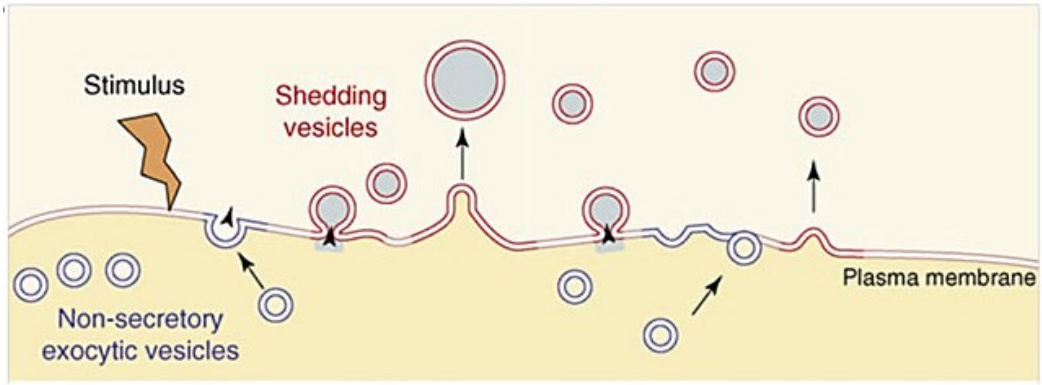

Figure 6. Biogenesis of microvesicles. Membrane-remodelling and membrane-sorting events proposed to be implicated in the constitutive or stimulated generation of microvesicles (MV). Non-secretory exocytic vesicles contribute to MV biogenesis by releasing their cargo at the sites of microvesicle generation. Areas of plasma membrane of distinct composition from surrounding area, but similar to those of shed vesicles, are formed and then budded off from the plasma membrane, thereby secreting microvesicles into the extracellular space. [90]

APOPTOTIC BODIES

Apoptotic bodies (ApoEV) are the largest category of vesicles in terms of size, with a dimension usually from 1 up to 5 µm in diameter, that carry nuclear fragments and cellular organelles, such as mitochondria and endoplasmic reticulum, as a result of apoptosis [97]. Apoptotic bodies are produced from dying cells undergoing programmed cell death; in this process, apoptotic bodies are formed during plasma membrane blebbing and later phagocytosed by macrophages and fused with lysosomes in phagolysosomes to prevent damage to the surrounding cells or tissues [98]. ApoEV have been suggested to have similar functional properties to EV released from healthy cells (which undergo normal turnover in physiological conditions), in relation to their molecular cargo [97]. Since apoptosis occurs in normal but also in many immunological and disease conditions, ApoEV have two main proposed functions, one in supporting apoptotic cell clearance and the second as intercellular mediators in immune-regulated processes such as inflammation, infection, autoimmunity and cancer [97,99].

EV COMPOSITION

Extracellular vesicles contain a wide range of bioactive molecules, including proteins, lipids, DNA, RNAs (mRNAs and miRNAs), and the nature and abundance of EV cargos vary in relation to cell-type, physiological or pathological state of the donor cell, external stimuli, molecular mechanisms of biogenesis and subpopulation considered [87]. During their biogenesis, several molecules are loaded into EV lumen: from proteins like major histocompatibility complex (MHC) class I and II molecules, costimulatory molecules, tetraspanins, proteases, cytokines, growth factors, and enzymes, to lipids (especially phosphatidylserine and ceramide) and RNAs. In general, EV include proteins typical of the biogenesis and secretion pathways, which are common in EV even across different cell types (e.g. TSG101, Alix, or Rab proteins), and proteins specifically loaded into EV by certain cell types thus characterizing EV functions (e.g. cytokines; surface receptors, signalling molecules and enzymes) [100].

Exosomes cargo reflects the composition of their parental cells and includes membrane transport and fusion proteins, tetraspanins, heat shock proteins (HSPs), proteins involved in the biogenesis of MVB, phospholipases and integrins [101]. In addition to these components, which are common to exosomes and used as positive markers to detect their presence, many others have been identified, varying according to the cell of origin and possibly representing the "message" for the target cells [102]. Exosomes are rich in lipids such as sphingomyelin, phosphatidylcholine, phosphatidylethanolamine, phosphatidylserine, cholesterol, ceramide, phosphoglycerates and saturated fatty acids [103], contributing at the maintenance of vesicles spherical shape and participating in the biogenesis process and at homeostasis in recipient cells [101]. In addition, exosomes contain mRNAs and miRNAs encoding for proteins or silencing specific target genes upon release into recipient cells; exosomal miRNAs were shown to be involved in immunological synapse formation, viral infections, induction of endothelial cell migration and pro-metastatic inflammatory responses, as well as in the suppression of T lymphocytes [104].

Several classes of proteins are also expressed on microvesicles such as CD40, integrins and cytoskeletal proteins. Moreover, microvesicles are characterized by Ras-associated (Rab) binding proteins, including Rab27a and Rab27b, that being specific of their budding mechanism could be useful for microvesicles and exosomes distinction [105]. Microvesicles are highly enriched in cholesterol, phosphatidylcholine and diacylglycerol [106] and like exosomes contain various types of miRNA and mRNA [104].

Apoptotic bodies cargo also reflects the composition of their progenitor cells, but unlike exosomes or microvesicles they can also contain cellular components and organelles, including mitochondria, endoplasmic reticulum, components of the nucleus, deriving from the cell in apoptosis [97].

While much has been learned about the content of exosomes, microvesicles, and apoptotic bodies, the identification of cargo specific of each vesicle subtype to be used as unique marker is still lacking [87] (Figure 7).

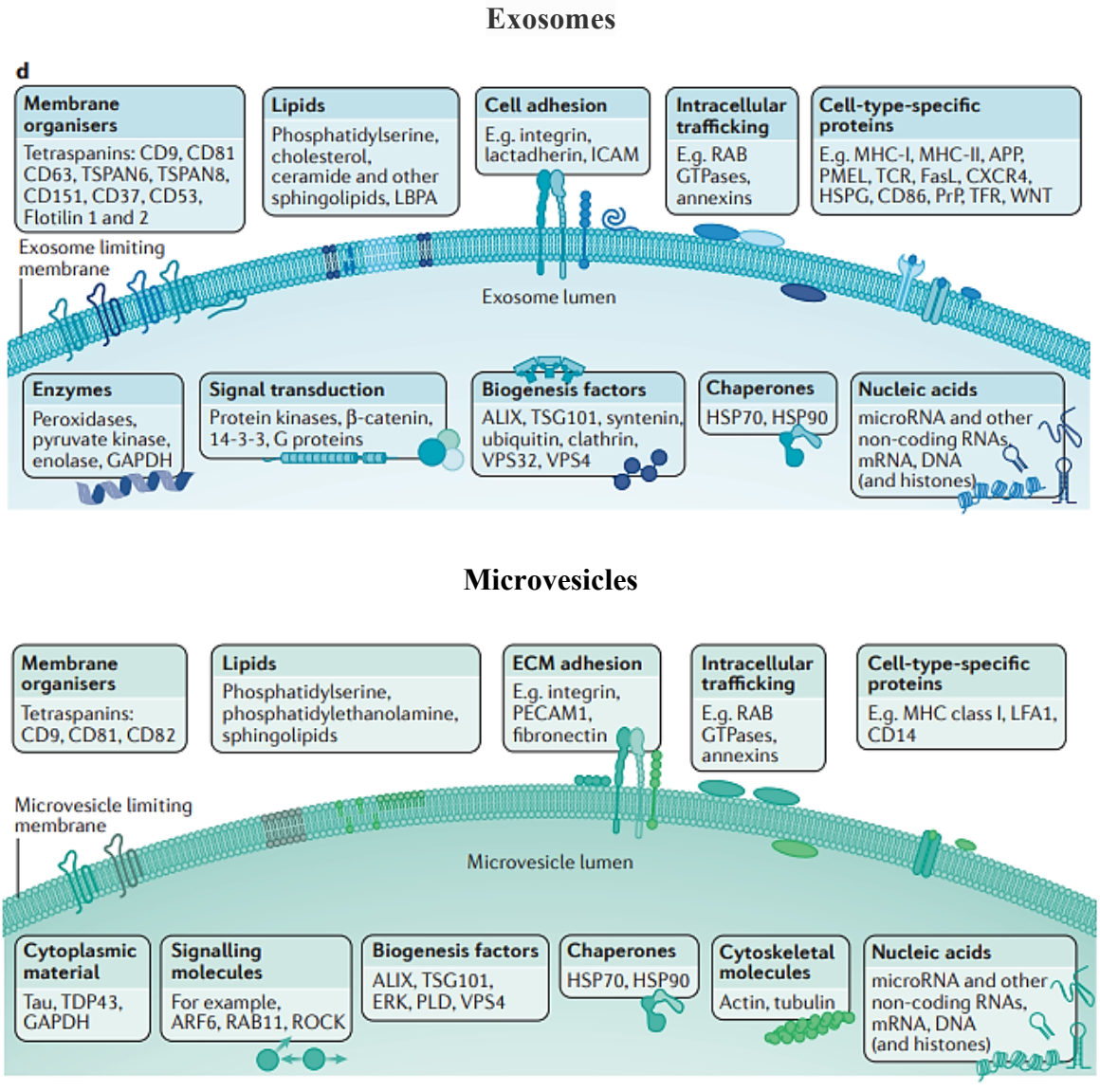

Figure 7. Exosomes and microvesicles cargo composition. Comparison of proteins, lipids and nucleic acids cargo of exosomes and microvesicles. Despite the different biogenesis, exosomes and microvesicles display a common composition of surface and lumen molecules that make difficult to establish their origin. [87]

TARGETING OF EV TO RECIPIENT CELLS

Upon release into the extracellular space, extracellular vesicles reach and interact with recipient cells to deliver their cargo, elicit functional responses and induce changes in their physiological or pathological status. This interaction requires docking of EV at the cell plasma membrane followed by activation of surface receptors and signalling, and vesicle internalization by endocytosis or fusion with target cells [87]. Binding of EV to the cell surface involves specific interactions between EV and the plasma membrane of target cells: although the mechanisms are not fully elucidated, the specificity of this interaction is probably determined by specific proteins and receptors enriched at the surface of EV and target cells, both dependent on the origin of EV and the recipient cell type [87,89]. Some molecules such as tetraspanins, integrins, immunoglobulins, lipids, lectins, heparan sulphate proteoglycans and extracellular matrix (ECM) components are known to mediate EV-cell interactions [87,89,107].

UPTAKE AND FATE OF EV WITHIN RECIPIENT CELLS

Sometimes, binding of EV to recipient cells is sufficient to induce changes in the physiological state of recipient cells, like during antigen presentation by antigen-presenting cell-derived EV to specific T cells [46]. In other cases, the content of EV must be transferred inside the recipient cell to elicit cellular responses [28]. Cells take up EV by several endocytic pathways, including clathrin-dependent endocytosis, caveolin-mediated uptake, phagocytosis, macropinocytosis, and lipid raft–mediated internalization [107] (Figure 8).

- In **clathrin-mediated endocytosis** membrane bound-EV are internalized into cells through the assembly of clathrin-coated vesicles, which deform the plasma membrane leading to invagination and internalization; then, intracellular vesicles undergo clathrin un-coating and fusion with the endosome where the content is released [109].
- In **caveolin-dependent endocytosis**, small invaginations in the plasma membrane called caveolae can lead to internalization of EV into cells, like with clathrin-coated pits; caveolae are formed at glycolipid rafts domains of the plasma membrane formed by cholesterol, sphingolipids and caveolins [110].
- **Phagocytosis** is a receptor-mediated route of uptake that involves the progressive formation of membrane invaginations around the material to be incorporated [111]. The mechanism of phagocytosis is similar to that of **macropinocytosis**, which requires the participation of enveloping membrane extensions but not direct contact with the internalized material [107,111].

- EV could be also internalized by cells through **lipid raft** domains: lipid rafts are microdomains within the plasma membrane with altered phospholipid compositions, rich in protein receptors, cholesterol, and sphingolipids such as sphingomyelin; they are known to contribute to the uptake of viral particles by mediated the binding of glycoproteins [107,112].
- The direct **fusion** of EV and cell **plasma membranes** is another possible mechanism of EV uptake: when lipid bilayers come into close proximity and contact in an aqueous environment, the outer-leaflets can fuse resulting in a single structure with the two hydrophobic cores mixed [107,113].

Once endocytosed or phagocytosed, EV can be degraded and their components and cargo used by cells for many different processes and purposes.

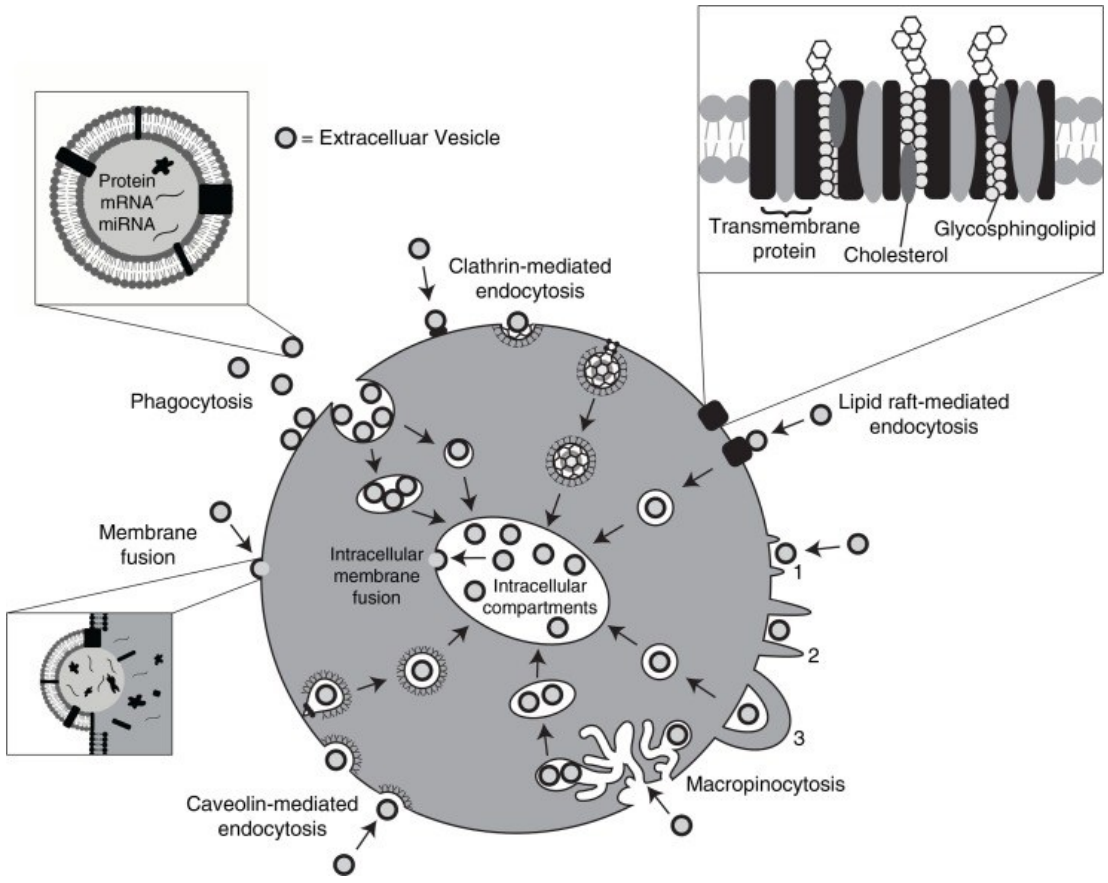

Figure 8. Pathways participating in EV uptake by target cells. Phagocytosis, membrane fusion, clathrin or caveolin-mediated endocytosis, macropinocytosis and lipid raft-mediated endocytosis are the main mechanisms proposed for EV entry inside target cells .Picture from [107].

2.4.2 EV roles in tumorigenesis

EV exchange cargos between cells as a means of intercellular communication at both paracrine and systemic levels. EV participate in various normal physiological processes, including blood coagulation [114], immunity and immunomodulation [94], stem cell differentiation [115], tissue regeneration and angiogenesis [116], autophagy [117], embryo implantation [118], pregnancy [119], development and physiology of the nervous system [120,121]. In addition to their physiological role, EV also participate in many pathological processes such as neurodegenerative diseases, cardiovascular diseases, infectious diseases and cancer [122]: in malignant cells, EV package of molecules fosters the acquisition of different hallmarks of cancer, including inflammation, cell proliferation, cell migration and invasion, angiogenesis, immune suppression, and metastasis [121,123] (Figure 9).

During carcinogenesis, accumulated mutations constitutively activate the expression of proto-oncogenes while inactivate tumour suppressor genes [123]. Neoplastic transformation correlates with an increased number of secreted tumour-derived EV that may contribute to the spread of tumour DNAs or oncogenic proteins in normal recipient cells, inducing cellular transformation towards a tumorigenic phenotype [88,124].

To survive and grow, cancer cells need to elaborate strategies that limit or elude apoptosis. EV have been shown to transfer antiapoptotic signals, such as anchorage-independent growth and survival capability in nutrient-limiting conditions, to neighbouring cells like normal fibroblasts and epithelial cells [88,125]. The transfer of oncogenic materials via tumour-derived EV can affect non-cancer cells, like endothelial cells, fibroblasts, and immune cells, to generate a favourable tumour microenvironment for tumour growth and metastasis. For example, tumour-derived exosomes contain pro-angiogenic miRNAs, mRNAs and proteins (i.e. EGFR or tissue factor [88]) that influence endothelial cells to stimulate neo angiogenesis, and consequently tumour growth, the formation of pre-metastatic niches [126] and facilitate metastasis by inducing vascular permeability [127]. Exosomes also trigger differentiation of stromal fibroblasts into cancer-associated fibroblasts (CAFs): EV containing TGF-β and other biomolecules can promote differentiation of fibroblasts into myofibroblasts [128], a fibroblast cell type involved in wound healing and inflammation and in supporting cancer cell proliferation and angiogenesis [129,130]. CAFs also contribute to create an inflammatory microenvironment by secreting high amounts of IL-6 and TGF-β and other cytokines [131]. Since CAFs are important in invasion and metastasis of cancer cells, CAF-secreted EV may promote these activities too [27,132]. Indeed, stromal cells

also participate in cancer progression by releasing exosomes and microparticles that continuously traffic to cancer cells to transfer functional proteins and RNAs that support tumour growth, invasion, and metastatic dissemination, and confer drug resistance [121].

Cancer-derived EV modulate the phenotype of multiple recipient cells by transferring functional oncoproteins able to activate tyrosine kinase receptors and their signalling pathways (e.g. MAPK/ERK, WNT and PI3K–AKT–mTOR pathways) [121,133], miRNAs to attenuate expression of target genes and evade growth suppressor signalling [134], mutated proteins, fusion gene mRNAs and oncogenic lncRNAs from cancer cells to neighbouring cells in the tumour microenvironment [133]. For instance, exosomes derived from glioma cells transfer a mutated form of EGFR to other cancer cells to spread their growth capacity [124]. Fragments of mutated DNA and oncoproteins included as cargo in cancer-derived EV may increase genome instability and generate genetic tumour heterogenicity when transferred to other cancer cells [133].

Tumour-derived exosomes can initially suppress immune cells to evade immune detection of tumours, while later modify immune cells towards pro-tumorigenic and pro-metastatic phenotypes [121]. Tumour-derived EV can inhibit T-cell activation and proliferation and promote their apoptosis [135]. EV produced by tumour cells also suppress immune-cell responses by inhibiting the cytotoxic actions of CD8+ T cells and NK cells or by modifying regulatory T cells and myeloid precursors toward a more tolerogenic phenotype (MDSCs) [100]. TGF-β, PD-L1 and miRNAs molecules associated to EV can induce an immunosuppressive M2-like phenotype on macrophages, educate Mesenchymal Stromal Cells (MSCs) to secrete large amounts of IL-8 and other immunosuppressive cytokines, and stimulate B and T cells to secrete tumour supporting cytokines [133].

Tumour-derived EV carry Matrix Metalloproteases (MMPs) able to activate Epithelial to Mesenchymal Transition (EMT), tumour invasion and metastasis upon internalization by nearby cancer cells [136]. At the same time, cancer-EV can act on distant tissues to establish pre-metastatic niches; it has been shown that expression of distinctive integrin pattern on EV derived from different tumours determine organ-specific metastasis: EV containing $\alpha_6\beta_4$ and $\alpha_6\beta_1$ were associated with lung metastasis, whereas expression of integrin $\alpha_v\beta_5$5 was linked to liver metastasis [137].

EV may promote chemotherapy and targeted therapy drug resistance by mediating the transfer of cargo proteins, such as antiapoptotic proteins or drug efflux pumps, miRNAs, mRNAs,

lncRNAs or lipids from drug resistant cancer cells to sensitive cancer cells or to cells of the tumour microenvironment [133].

Under hypoxic conditions (a common feature of solid tumours), glucose transporters and enzymes of the glycolytic pathway are upregulated, producing and secreting metabolic acids that low pH level of the tumour microenvironment [138]. Tumour acidosis can increase the secretion and uptake of EV, enhancing cell-to-cell communication within tumours [139] and further promoting invasiveness and progression [88,140].

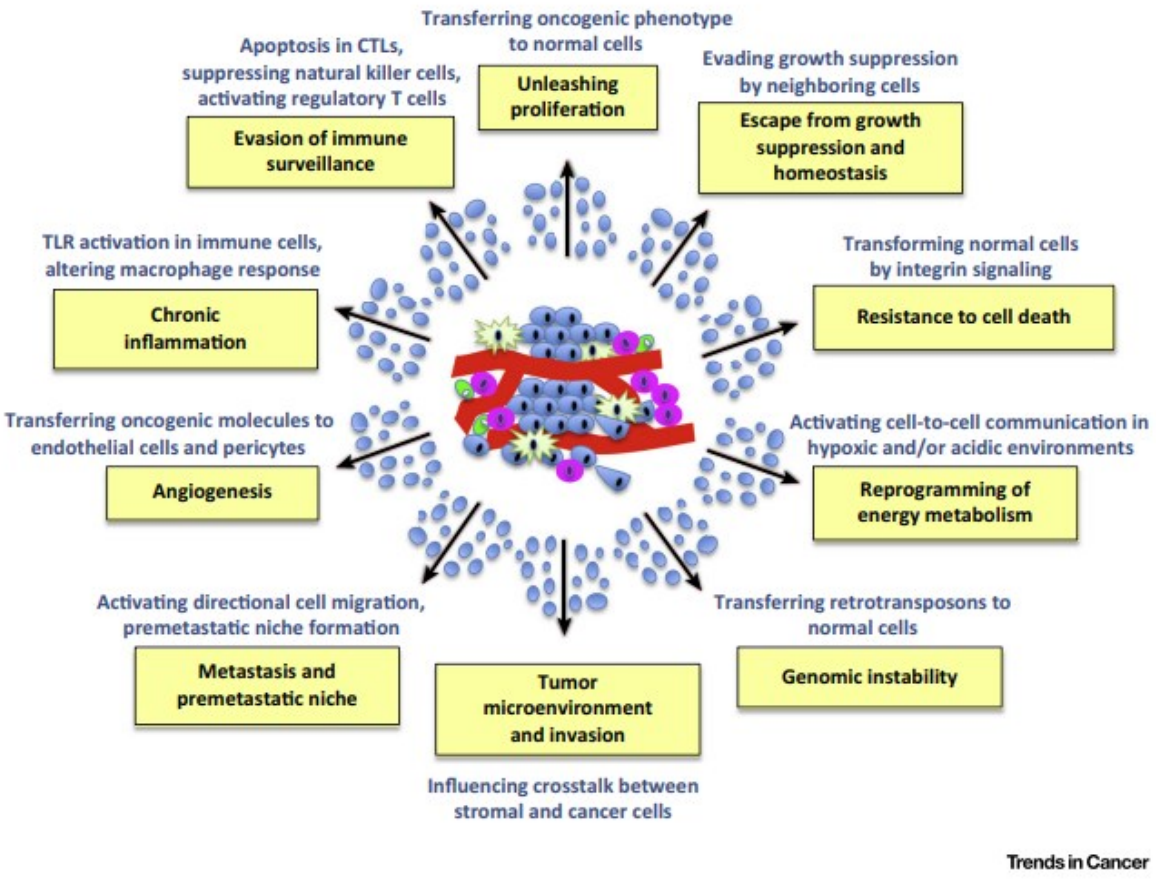

Figure 9. Extracellular vesicles and hallmarks of cancer. EV mediate the crosstalk between cancer cells and tumour microenvironment cells sustaining the acquisition of *hallmarks of cancer* capabilities. Image from [88].

2.4.3 EV for drug delivery

The new frontier of anticancer treatment is represented by antitumour targeted therapies, aimed at achieving the greatest therapeutic effect and lowest toxicity through direct, targeted and selective effects of anticancer drugs on tumour cells. Currently, the most commonly used strategies for the targeted delivery of drugs to tumour tissues for cancer treatment are based on liposomes or polymeric nanoparticles [141]. Many different types of drug delivery systems (DDS) have been investigated in the last 20 years: from liposomes, micelles, dendrimers to meso-porous silica nanoparticles, gold and super paramagnetic iron-oxide nanoparticles, carbon nanotubes, and quantum dots. Most of the technologies explored are nanocarriers of synthetic origin loaded with drugs and functionalized to recognize cancer cells and release the drug [142]; apart from liposomes most of them have not even reached the clinical trial stage.

Liposomes are round closed bilayer structures consisting of an aqueous core encapsulated by natural or synthetic phospholipids, able to encapsulate bioactive hydrophilic, amphipathic, and lipophilic molecules into the inner water phase or within the lipid bilayer [143]. Due to their efficacy in the treatment of some type of cancer, several liposomal drug products are currently available in the market [144], while others are under clinical testing (www.clinicaltrials.gov). Many liposomal products, like liposomal doxorubicin Doxil®, act with a pharmacological mechanism of passive targeting, achieving tumour targeting via the leaky tumour vasculature, according to the enhanced permeability and retention (EPR) effect [59,145]; however, having poor selectivity toward cancer cells, severe systemic side effects occur [144]. To obtain active targeting, the strategies mostly used involved modification of the liposomal surface with monoclonal antibodies, antigens, proteins, small molecules, carbohydrates, aptamers, or peptide ligands to target different receptors overexpressed on the membrane of target cells [146]; however, even these modified liposomes turned out to be hardly effective due to the presence of anatomical barrier within tumour, instability or inactivity of the targeted ligands on the liposome membrane, and failure of the ligand to trigger the binding of the target [145]. Overall, these systems suffer of insufficient targeting efficiency and translation difficulty, poor biocompatibility, poor bioavailability and stability *in vivo* as well as immunogenicity that can induce hypersensitivity reactions [144].

The ideal DDS for nanoparticles-based anticancer therapies should be characterized, after systemic administration, by long circulation, good penetration of tumour biological barriers,

enhanced and selective accumulation at tumour tissues, and efficient cellular internalization and drug release inside cancer cells [147].

In this context, extracellular vesicles (EV), in particular exosomes and microvesicles, have great potential. EV are natural membrane-derived particles surrounded by a phospholipid bilayer, released by cells in the human body to operate as mediators of the intercellular communication by efficiently delivering their parental cell-derived molecular cargo to recipient cells [148]. For these reasons, EV have gained much interest in the drug delivery field. Their structure and biological properties of natural carriers make EV suitable carriers for drug delivery because they can penetrate through anatomical barriers, keep stability, and maintain sufficient binding effects compared to the liposomal counterpart [145]. In the delivery of active compounds and *theranostics* (drugs combined to simultaneously diagnose and treat medical conditions) the advantages of EV compared to synthetic DDS are:

i) innate limited immunogenicity and cytotoxicity, due to their endogenous origin and high biocompatibility [149];
ii) high bioavailability and stability *in vivo*, benefiting from endogenous biogenesis machinery and expression of complement regulators or "don't eat me" signal [145];
iii) cell targeting properties, where innate targeting abilities of EV can be achieved by selecting specific EV donor source, while acquired targeting abilities of EV can be obtained by bioengineering methods [145];
iv) greater penetration of biological barriers, including blood brain barrier [149,150];
v) protection and efficient delivery of therapeutic cargo [151];
vi) improved therapeutic efficacy and decreased systemic drug toxicity, due to their cell targeting properties and less non-specific accumulation in tissues [152];
vii) decreased opsonization and recognition by the immune system [145,152].

As drug delivery tool, EV have been tested for siRNAs [153], miRNAs [154], proteins [155], small molecule drugs [156], nanoparticles [157], and CRISPR/Cas9 [158] in suitable animal models. It is also well-demonstrated in our group the possibility to use EV to convey encapsulated therapeutic (paclitaxel, oncolytic viruses, antibodies) and diagnostic (indocyanine green) agents directly to cancer cells [159,160], improving the diagnostic and anti-cancer activity in different mouse model of cancer (genetic, syngeneic or xenograft) [159,161,162].

Many prerequisites must be satisfied for the successful clinical application of nanoparticles in the targeted drug delivery, including: i) the efficient loading with the therapeutic molecule, ii) the stability of the EVs (size, structure, drug load) during circulation in the blood stream before reaching their therapeutic target, iii) the ability to escape phagocytosis by macrophages and cells of the RES system, iv) a sufficiently long half-life in order to reach the target tissue, v) a good biocompatibility in terms of low toxicity and immunogenicity [144]. In this respect, EV properties make them ideal nanoparticles, however drug delivery remains challenging because of non-standardized isolation and purification methods, limited drug loading efficiency, poor pharmacokinetics and targeting of natural EV, low yields of isolation, challenges in comprehensive characterization, identity, purity, and quality assurance [151,163,164]. Due to these limitations, other approaches are currently being explored, such as synthetic exosomes- or extracellular vesicle-mimetics reconstructed to mimic the composition and structure of organotropic extracellular vesicles [165].

2.4.4 EV as source of biomarkers

Extracellular vesicles are mediators of the intercellular communication, and as such they are involved in many physiological and pathological processes [122]. EV have been found to circulate through many body fluids such as blood plasma and serum, urine, saliva, breast milk, amniotic fluid, cerebrospinal fluid, pleural effusion and bronchoalveolar lavage fluid. These characteristics, together with the resemblance of EV composition with the parental cell and the dynamic composition of their cargo, made circulating EV an interesting source for the discovery of biomarkers and exploitable tools for diagnostic and therapeutic purposes [166].

In carcinogenesis, EV mediate multiple biological cancer processes, including cell growth, proliferation, migration, and drug resistance, by transferring their cargo between cells [167]. Due to their nature, EV released by tumour cells contain tumour-associated RNAs, mutated DNA fragments, oncoproteins and miRNAs reflecting the content of the secreting cell [168]. Thanks to the development of sequencing and omics technologies, EV cargos are now widely studied and selective cancer-associated miRNAs, mRNAs, lncRNAs and protein modifications present in these circulating nanoparticles have been determined [167,168]. These molecules once secreted within EV can be found in and isolated from body fluids; the practical application of this concept is represented by liquid biopsy.

Liquid biopsy is a non-invasive diagnostic and real-time monitoring method, a test typically done on blood samples of cancer patients (but also cerebrospinal fluid) to detect circulating tumour DNA (ctDNA) and circulating tumour cells (CTCs) released from neoplastic tissues [169]. Liquid biopsy is a technology used in clinic for early-stage cancer detection, to plan treatment, for predicting response to cancer therapy, and for monitoring disease progression or recurrence after anticancer treatment. Since multiple blood samples can be easily taken over time, liquid biopsy may also help in understanding the molecular changes occurring in tumours (definition from NCI [170]).

EV are emerging as a new form of liquid biopsy because cancer-associated molecules found in EV can represent biomarkers for the diagnosis and prognosis of cancer patients [167]. Since cancer treatment alters the levels of circulating EV and their compositions, these alterations before and after therapy have great potential for monitoring the therapeutic response in the single patient [171]. Moreover, the dynamic examination of circulating EV and their contents can provide real-time information on therapeutic responses, including therapy resistance, in cancer patients [169,171].

3 AIM

Cancer is a leading cause of death in the world, expected to raise worldwide due to the increasing population lifespan and susceptibility to cancer risk factors [2]. Moreover, despite the advances made in surgical and medical therapies, patients often develop resistance to therapy and relapses due to the incomplete removal of cancer cells.

Colorectal cancer (CRC) is the third most common cancer, but second for mortality rate among all cancer types [4]. This is partially due to the fact that colorectal diseases are diagnosed at advanced stages, when patients may already display distant metastases, and frequently to the develop of recurrence after curative-intended surgery [22]. Surgical intervention is the primary curative option for CRC patients, aimed at achieving complete removal of primary tumour and metastases.

Currently, intraoperative tumour resection relies on human vision, experience, training, and tactile information to delineate and resect solid tumours [33]. Neoplastic tissues are resected together with a margin of normal non-tumoral tissue to ensure removal of infiltrated cancer cells and reduce the risk of relapses. However, palpation and visual inspection are not always sufficient for delineating tumour margins, since the human eye does not have the sensitivity to deeply visualize under the tissue surface [32].

The aim of my Ph.D. project was to preclinical develop an objective tool to label and circumscribe the tumour area, to guide surgeons in the intraoperative safe removal of colorectal cancer tissues. Since so far only non-specific contrast agents labelling tumour or tumours vessels have been developed and approved for the intraoperative imaging in clinic [50,172], the development of more specific probes allowing the detection of tumours with increased sensitivity and accuracy during is warranted. Contrast agents emitting fluorescence in the near-infrared (NIR) region are preferred for intraoperative imaging [173], because of the greater sensibility *in vivo* [47,48], and high compatibility of the technique with the intraoperative setting [46].

Tumour-derived Extracellular Vesicles (EV) are naturally occurring cargo delivery vesicles with an innate potential to deliver biologics and chemotherapeutic drugs to cancer tissues [161,174,175]. With the aim of developing the tool to map the exact portion of tissue interested by the neoplastic growth during the surgical procedure, we investigated EV for the selective delivery of NIRs at tumour sites. We based our tool on optical imaging of NIR fluorescent agents, formulated within EV specifically recognizing the neoplastic area and delivering the diagnostic intratumorally.

The findings of this project have identified a highly biocompatible system able to selectively target cancer cells, whose clinical translation, facilitated by the use of clinically approved NIRs and delivery systems of biological origin, could lead to personalized image-guided protocols for more effective surgery aimed at complete disease removal for cure. The tool firstly applied to CRCs may find application to other cancer types, and not only for diagnostic purposes but also for targeted therapies.

4 MATERIALS AND METHODS

Reagents

All reagents were purchased from Sigma Aldrich unless otherwise specified.

Cell Culture

LL/2 mouse lung cancer cell line, MC-38 mouse colon cancer cell line, C2C12 mouse myoblast cell line, A549 human lung cancer cell line, MCF-7 human breast cancer cell line and RAW 264.7 murine macrophage cell line were purchased from the American Type Culture Collection (ATCC, USA). The cells were cultured at 37°C and 5% CO_2 in Dulbecco's modified eagle medium (DMEM, Gibco) supplemented with 10% fetal bovine serum (FBS, Euroclone), 1% of 100 u/mL penicillin/streptomycin (Gibco) and 1% L-glutamine (Gibco). MCF-7 cells were cultured at 37°C and 5% CO_2 in RPMI medium (RPMI 1640, Gibco) supplemented with 10% fetal bovine serum (FBS, Euroclone), 1% of 100 u/mL penicillin/streptomycin (Gibco) and 1% L-glutamine (Gibco).

EV production from cell culture

To produce EV 2.6 $\times 10^6$ LL/2, 5 $\times 10^6$ MC-38, 2.6 $\times$ 10^6 A549, 4.5 $\times$ 10^6 MCF-7 and 2.5 $\times$ 10^6 C2C12 cells were plated into T-175 flask in medium supplemented with 10% FBS. The FBS growth media was ultracentrifuged overnight for 18 h at 110,000 x g at 4°C using Optima L-80K ultracentrifuge (Beckman Coulter) with rotor type 50.2T (Beckman Coulter) to remove EV present in the serum. EV were isolated from the conditioned media using differential centrifugation steps. First the conditioned media was centrifuged at 1,500 x g for 10 min at 4°C to pellet cells and debris (Rotanta-460, Hettich Zentrifugen). Then, the supernatant was collected and ultracentrifuged at 100,000 x g for 2 h at 4°C using Optima L-80 XP ultracentrifuge (Beckman Coulter) with rotor SW32Ti (Beckman Coulter). The supernatant was removed, and the EV-containing pellets were resuspended in 100 µL phosphate-buffered saline PBS (Merck) and stocked at - 80 °C before use.

Patient selection

All the patients enrolled in the study were CRC patients with i) histological diagnosis of metastatic colorectal adenocarcinoma (stage IV); ii) one or more resectable target lesions in the

liver with a diameter >10 mm; and iii) presence, in the resected tumour lesion, of a vital component allowing a sample volume of approximately 1 cm^3 for the PDX protocol. The clinical features of the patients recruited for PDX generation are listed in Table 1.

Table 1. Clinical features of CRC patients recruited for PDX generation.

Patient number	Age	Sex	Primary tumor (previously removed)	Stage	Histology Genotype	Serum Markers
I	51	F	Left colon (sigmoid)	pT4a, N1a, M1 Synchronous liver M+	Adenocarcinoma G2 RAS/BRAF wild type	CEA: 1.5 CA 19.9: 24
II	63	M	Right colon	pT1, N1, M0 Metachronous liver M+	Adenocarcinoma G2 KRAS: mutated (G12V)	CEA: 5.69
III	69	M	Right colon	pT3, N1a, M1 Synchronous liver M+	Adenocarcinoma G2 KRAS: mutated (Codon 13)	CEA: 4.40 CA 19.9: 8.4
IV	73	F	Right colon	pT4, N0, M0 Metachronous liver M+	Adenocarcinoma G2 KRAS wild type	CEA: 1.5
V	54	F	Left colon (sigmoid)	pT2, N0, M0 Metachronous liver M+	Adenocarcinoma G2-G3 KRAS wild type	CEA: 2.05 CA 19.9: 8.0
VI	70	F	Right colon	pT3, N0, M1a Synchronous liver M+	Adenocarcinoma G2 RAS/BRAF wild type	CEA:2.84 CA 19.9: 18.4
VII	77	F	Right colon	pT3, N1, M1 Synchronous liver M+	Adenocarcinoma G3 BRAF mutated (V600E) KRAS/ NRAS wild type	CEA: 5.2
VIII	70	M	Left colon (sigmoid)	pT3, N2, M1 Synchronous liver M+	Adenocarcinoma G2-G3 RAS/BRAF wild type	CEA: 51

EV preparation from human blood

Venous blood (30 mL) was collected from patients scheduled for surgical removal of CRC liver metastases and admitted to the *Hepato-Pancreato-Biliary Unit of the National Cancer Institute, IRCCS* of Milan. As a control, blood samples were also collected from healthy volunteers. The blood was immediately processed after collection to obtain the plasma. Briefly, blood was centrifuged at 2,500 x g for 15 min at RT to remove blood cells and prevent platelet activation and release of platelet-derived EV. The supernatants were transferred into new tubes and the samples were centrifuged again at 2,500 x g for 15 min at RT. Plasma were then processed to isolate plasma-derived EV by ultracentrifugation at 100,000 x g for 2 h at 4 °C using Optima L-80 XP ultracentrifuge (Beckman Coulter) with rotor SW32Ti (Beckman Coulter). Supernatants were removed and the EV-containing pellets were resuspended in 100 µL phosphate-buffered saline (PBS, Merck) and stocked at -80 °C before use.

Size distribution analysis by nanoparticle tracking analysis (NTA)

Size distribution and concentration of EV-LL2, EV-C2C12, patient and healthy donor-derived EV formulations were analysed by NTA using Nanosight model LM14 (Nanosight) equipped with blue (404 nm, 70 mV) laser and sCMOS camera. NTA was performed for each sample by recording three 90s videos, subsequently analysed using NTA software 3.0 (Nanosight). The detection threshold was set to level 5 and camera level to 15.

Western blotting

For immunoblotting, EV were isolated from cell culture media, and patients' and healthy volunteers' blood as described above. After ultracentrifugation, supernatants were removed and the EV-containing pellets were resuspended in a proper volume of 1X RIPA buffer (150 mM NaCl; 1% NP-40; 0.5% sodium deoxycholate; 0.1% SDS; 50 mM Tris-HCl, pH 8.0) supplemented with protease inhibitor cocktail (Roche). EV protein concentrations were quantified using a Bradford or BCA assay kit (Thermo Scientific). 20µg of EV protein lysates were boiled at 95°C for 5 min, separated on 4-10% SDS-PAGE using beta-mercaptoethanol as a reducing agent and transferred into nitrocellulose membranes (Amersham). The membranes were then blocked in 5% non-fat dry milk in TBS-T (0.2% Tween-20) at RT and incubated overnight with primary antibodies against CD63 (SAB4301607 Sigma, 1:1000), TSG101 (4A10 Abcam, 1:500), CD9 (C9993 Sigma, 1:500), CD81 (B-11 Santa Cruz, 1:100) and MASP1 (LS-C372833 LSBio, 1:500). The immunoreactive bands were visualized with chemiluminescence using ECL Western Blotting Analysis System according to the manufacturer's instructions (Amersham). Densitometry quantifications of the autoradiographic signals were performed with the Kodak imaging system (Gel Logic 2200) software.

Zeta potential analysis by electrophoretic light scattering

Zeta potential was measured using ZetaSizer Nano (Malvern, UK). Samples were diluted in a volume of 800µL of MilliQ water and injected in the capillary flow (DTS1070 folded capillary cell) for the measurement. Three parallel measurements were performed on each sample.

Cryo-Electron Microscopy

Cryo-EM images were acquired with a FEI Talos Arctica 200 kV FEG electron microscope equipped with a FEI Falcon 3EC direct electron detector and Volta Phase-plate. Prior to Cryo-EV imaging, samples were vitrified on a FEI Vitrobot IV apparatus, and processed as reported [176].

Loading of EV with fluorescent agents

EV from LL/2 and MC-38 cells were loaded with the lipophilic dye DiD (1,1'-Dioctadecyl-3,3,3',3'-Tetramethylindodicarbocyanine, 4-Chlorobenzenesulfonate Salt) as previously described [161,174] by incubating for 1 hour at RT 1×10^8-5×10^9 EV with 5µL of DiD (Biotium) per mL of EV suspension in PBS. Next, the samples were centrifuged at 150,000 x g for 3 h to pellet the EV. The supernatant containing unbound DiD was removed, and the EV-pellet was washed by suspending it in PBS and pelleting it again at 150,000 x g. EV from LL/2, MC-38, A549 and C2C12 cells were loaded with indocyanine green (ICG), prepared by incubating 1×10^8-5×10^9 EV in PBS for 12 h at 4°C with 10µg/mL ICG (Sigma). Next, the samples were centrifuged at 150,000 x g for 3 h to pellet the EV. The supernatant containing unbound ICG was removed, and the EV-pellet was washed by suspending it in PBS and pelleting it again at 150,000 x g.

For the study in patient-derived xenografts, EV were loaded with ICG by incubating $1\text{-}5 \times 10^8$ EV in PBS for 12 h at 4°C with 50µg/mL ICG (Sigma). Next, the samples were centrifuged at 150,000 x g for 3 h to pellet the EV. The supernatants containing unbound ICG were removed, and the pellet was washed by suspending it in PBS and pelleting it again at 150,000 x g.

Generation of patient-derived xenograft (PDX)

Stable PDX models were generated from stage IV CRC patients undergoing surgical removal of liver metastases according to clinical decisions. Patient-derived cancer xenografts were prepared on the same day of tumour harvesting. Briefly, immediately after removal, a tumour sample of approximately 1 cm^3 was harvested and placed in the MACS® Tissue Storage Solution for preservation and transport. From the sample, fragments of about 3 mm^3 were obtained and immersed in Matrigel® for 20 min. Then, 2 xenografts of approximately 100 mm^3 prepared from each fragmented tumour lesion were subcutaneously implanted into the hips of

6- to 8-week-old immunodeficient female SCID mice [177]. After inoculation, the mice were followed daily to assess their health status and once a week to assess the growth of the inoculated mass. PDX were considered properly grown and ready for the imaging experiment when the inoculated lesions reached a volume of 300-400 mm^3. This condition was met at a median of 6 weeks (range 4-8 weeks) after the injection.

The experimental animals were maintained at the animal house of the *National Cancer Institute, IRCCS Foundation* of Milan under standard conditions and veterinary supervision of the Institutional and National Animal Welfare Committee, which previously approved the study protocol (Authorization 401/2019-PR).

Sampling and histology on the resected tumour specimens were conducted by human pathologists of the Pathology Department at the *National Cancer Institute, IRCCS Foundation* of Milan (Italy).

In vivo biodistribution study

C57Bl/6NCrl (Charles River, MGI: 2683688) and MMTV-NeuT (The Jackson Laboratory, MGI: 1930204) mice were maintained at the animal facility of the University of Milan under standard conditions according to institutional guidelines. After an acclimatization period of 14 days, murine syngeneic grafts were established by subcutaneous injections of 2×10^6 LL/2 and 1×10^6 MC38 cells into the neck of 12-week-old C57Bl/6 male mice. When tumour size reached a diameter of about 5-10 mm we performed the following treatments: DiD (5 µL per mL of EV suspension in PBS), EV-DiD-LL2 (10^8 particles/tumour), EV-DiD-MC38 (10^8 particles/tumour), ICG (10 ug/mL), EV-ICG-LL2 (10^8 particles/tumour), EV-ICG-A549 (10^8 particles/tumour), EV-ICG-C2C12 (10^8 particles/tumour), EV-ICG-patient (10^8 particles/tumour), EV-ICG-healthy (10^8 particles/tumour). Treatments were administered intravenously (i.v.) (50µL), by retro-orbital injection, to tumour-bearing mice.

SCID mice were maintained at the animal house of the *National Cancer Institute, IRCCS Foundation* of Milan under standard conditions according to institutional guidelines. EV injections in PDX mice (2-4 $\times10^9$ EV-ICG/kg) were performed when the tumour size reached a diameter of ~10 mm.

In vivo and *ex vivo* fluorescence imaging

In vivo and *ex vivo* fluorescence imaging were carried out 24 h after EV treatment using the IVIS Spectrum Imaging System (PerkinElmer, Waltham, MA, USA) with suitable filters (Cy5.5, ICG). During *in vivo* imaging sessions, mice were anaesthetized and kept under anaesthesia using Isoflurane (Isoflurane-Vet; Merial, Lyon, France) (5 min for dorsal view and 5 min for lateral view). For *ex vivo* imaging, mice were sacrificed by cervical dislocation and imaging of selected organs was carried out immediately after death over an exposition time of 1 second. Fluorescence emission from selected body areas and of excised organs was assessed using the Living Image Software 4.6 (PerkinElmer), following the manufacturer instructions for fluorescence background subtraction.

Nano-scale liquid chromatographic high resolution mass spectrometry (nLC-HRMS)

For proteomics, EV were isolated from patients' and healthy volunteers' blood as described above. After ultracentrifugation the supernatant was removed, and the pellet was washed by suspending it in PBS and pelleting it again at 100,000 x g. Then, supernatants were removed and the EV-containing pellets were resuspended in a proper volume of Urea 8M lysis buffer (Urea 8M; 50 mM NaCl; 50 mM Tris-HCl, pH 8.0) supplemented with protease inhibitor cocktail (Roche). The protein concentration of the EV samples was quantified using a BCA assay kit (Thermo Scientific). Equal pools of EV from different patients and healthy subjects were constituted for each experimental group (PDEV, healthy-EV, healed-EV, relapsed-EV).
10µg of EV protein lysate/group were diluted in 50 mM ammonium bicarbonate, reduced with dithiothreitol (DTT) at a final concentration of 5 mM for 30 min at 55°C, and then alkylated with 15 mM iodoacetamide for 20 min in the dark at RT. Trypsin digestion (1/20 w/w, Roche, USA) was carried out at 37 °C overnight. The resulting peptides were analysed by nLC using a Dionex Ultimate 3000 nano-LC system (Sunnyvale CA, USA). Mass spectrometry (MS) spectra were acquired in a m/z range of 375-1500 Da at 120,000 resolutions. Each sample was analysed in three technical triplicates.

In vitro assay of EV uptake

Raw 264.7 macrophages were plated at the density of 60,000 cells/well in a 24-well plate at day 0. At day 2, cells were treated for 4 h with: PBS, EV-ICG-MCF7, EV-ICG-C2C12, EV-ICG-patient, EV-ICG-healthy, and free ICG (0.8μM). ICG was loaded into EV as described above, while the amount of ICG encapsulated into EV was determined by reading EV fluorescence with a standard curve of fluorescence of ICG concentrations. Flow cytometry analyses of fluorescent cells were performed on at least 10,000 events by using BD FACSVerse (BD Biosciences) equipped with 633 nm lasers. Fluorescence pulses were detected using 783/56 nm collection filter. Results were analysed with BD FACSuite software (BD Biosciences).

Immunohistochemical and fluorescence analysis

For histological analysis, xenograft tumour tissues were fixed in 4% formaldehyde solution for 24 h, then dehydrated with ethanol, washed with xylene and paraffin-embedded. For haematoxylin-eosin staining the samples were cut into 4 μm thick sections, while one section of every two was cut into 10 μm thick sections for fluorescence imaging. The slides were then analysed using a confocal microscope (Nikon A1R laser scanning confocal microscope) to acquire the fluorescence signals released by ICG. Images of ICG fluorescence were then superpositioned with those from adjacent sections stained with haematoxylin-eosin, acquired with a Virtual Slide Microscope (Olympus VS120).

Ethical approval animal experimentation

All animal experimentation was carried out in accordance with the ARRIVE and European Guidelines for Animal Care, and in the full observation of the Directive 2010/63/UE. All animal experiments were approved by the Italian Ministry of Research and University (permission and authorization n° 12-12-30012012, 547/2015, 214/2020) and the University Animal Welfare Committee, and regulated by a departmental panel of experts.

Ethical approval human material

All human specimens (blood samples for EV extraction and tumour tissues for xenograft generation) were obtained in compliance with a specific protocol approved by the Institutional Ethic and Scientific Review Board of the *National Cancer Institute, IRCCS Foundation* of Milan (Italy), after having received the signed informed consent of all the patients. The biological human material collected for this study was used in accordance with the Declaration of Helsinki.

Statistical analysis

Data analyses were performed using GraphPad Prism 8 software (GraphPad Prism Inc. San Diego, CA, USA). Statistical significance was calculated by using one-way ANOVA with Sidak's or Tukey's multiple comparison test, and Student's t-test as indicated in the figures.

5 RESULTS

5.1 Production of EV formulations from cancer cells

Previous studies carried out in our lab demonstrated the capability of murine cancer-derived EV to deliver *in vitro* and *in vivo* oncolytic adenoviruses and chemotherapeutic drugs to the same tumour that originated the vesicles [161,174,175]. Therefore, we started evaluating the possibility to use these cancer-derived EV to specifically deliver fluorescent near infrared (NIR) probes commercially available (such as the carbocyanine DiD [178] and the clinically approved ICG [52]) to target different tumour types in mouse models of cancer.

NIRs and the near-infrared fluorescence imaging, working at wavelengths in the 700–900 nm range, are particularly promising in the surgical oncology field because tissue autofluorescence is minimal in this range, allowing a high signal-to-background ratio [47].

We used mouse lung (LL/2) and colon (MC38) cancer cells to produce EV formulations by an ultracentrifugation method developed in our lab and to generate tumour engraftment in immunocompetent C57Bl/6 wild type mice. EV formulations were characterized in terms of particle size distribution by NTA (Figure 10A) and of expression of specific EV biomarkers such as TGS101, CD63 and CD9 [179] by western blot analysis (Figure 10B). In addition, dynamic light scattering (DLS) and cryo-EM experiments confirmed the negative zeta-potential and shape integrity of EV (Figure 10C-D).

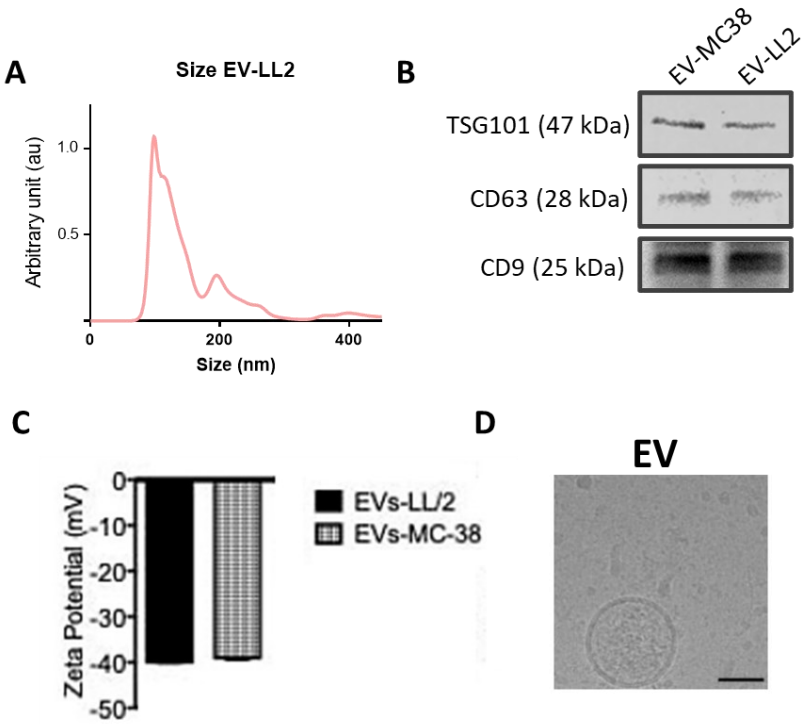

Figure 10. Characterization of murine lung and colon cancer-derived EV. (A) Size distribution of EV formulation from LL2 cells determined by nanoparticle tracking analysis (NTA). (B) Immunoblot analysis of EV marker Tumour Susceptibility Gene-101 (TSG101) and tetraspanin proteins (CD63 and CD9) in EV-preparations. (C) Surface charge of EV-LL2 and EV-MC38 obtained by DLS analysis. Bars represent means ± SD of three independent experiments. (D) Cryo-EM image of EV, scale bar 100 nm. Figure adapted from [180].

5.2 Heterologous and cross-species tumour tropism of cancer-derived EV

To study the delivery at tumour sites of NIRs encapsulated within extracellular vesicles of cancer origin, EV isolated from LL2 and MC38 cancer cells were loaded with the fluorescent dye DiD (DiIC18(5); 1,1′-dioctadecyl-3,3,3′,3′-tetramethylindodicarbocyanine, 4-chlorobenzenesulfonate salt) [178] or with ICG [52] to obtain the corresponding EV-DiD and EV-ICG formulations. The biodistribution of EV formulations was evaluated by measuring the fluorescent emission related to the particle biodistribution through *in vivo* and *ex vivo* imaging methodologies.

When 1E08 particles/tumour of EV-DiD-LL2 were intravenously administered to the mice engrafted with the same cell line originating the vesicles, the *in vivo* imaging acquisition of the fluorescence carried out 24 h after the treatment showed an accumulation of the probe at the tumour site, as confirmed also by *ex vivo* imaging analysis of the fluorescence emitted by the dissected organs that showed a positive signal mostly in the tumour and in the liver (Figure 11A). When administered alone (not formulated into EV) the dye didn't produce a preferential accumulation of the fluorescence in any tissue except for the liver and kidneys, where the signal could be mainly ascribed to autofluorescence (liver) or accumulation of the dye in the cell of the excretion organ (kidney) (Figure 11A). These data confirmed the homing ability of EV formulations to the same tumour originating the vesicles [180].

To verify whether the selective biodistribution of EV was dependent from the tumour originating the vesicles, we crossed the experimental groups by treating with EV-DiD-LL2 formulations mice bearing colon cancer tumours from MC38 cells and with EV-DiD-MC38 formulations mice bearing lung cancer tumours from LL2 cells. In both models, the *in vivo* and *ex vivo* imaging revealed a fluorescent accumulation in the tumour (in addition to the autofluorescence of the liver), indicative of a tumour tropism of cancer-derived EV regardless their origin (Figure 112B) [180].

Tumours originated by syngeneic engraftment may differ from those spontaneously originating in the tissue in terms of encapsulation or neo-vascularization [181], thus possibly affecting the permeability of the fluorescent dye to the tumour. Therefore, we tested the ability of EV to target the tumour tissue in the MMTV-NeuT transgenic mouse model, which spontaneously display carcinoma of the mammary gland [182]. In MMTV-NeuT mice, our results confirmed the tumour-specific tropism of EV also for spontaneous tumours, since EV-LL2 loaded with DiD mainly accumulated in the mammary tumour, when compared to free DiD (Figure 11C). To minimize the background detection of liver autofluorescence at DiD wavelengths, we used the fluorescent NIR indocyanine green (ICG) [183] for the characterization of EV biodistribution. The results showed a tumour-specific tropism when the fluorescent probe was loaded into the vesicles (EV-ICG-LL2 formulation), not detected when ICG was administered alone, and also giving a significantly less background autofluorescence especially in the liver compared to DiD (Figure 11C) [180].

To rule out the existence of a species-specific mechanism of tumour homing, we loaded ICG into EV derived from the human lung cancer cells A549 to obtain the corresponding EV formulation (EV-ICG-A549) and measured EV biodistribution in MMTV-NeuT mice bearing mammary cancer. The imaging carried out 24 h after the treatment demonstrated that human EV were also able to target murine tumours, thus proving the cross-species and cancer-wide targeting abilities of cancer-derived EV (Figure 11D) [180].

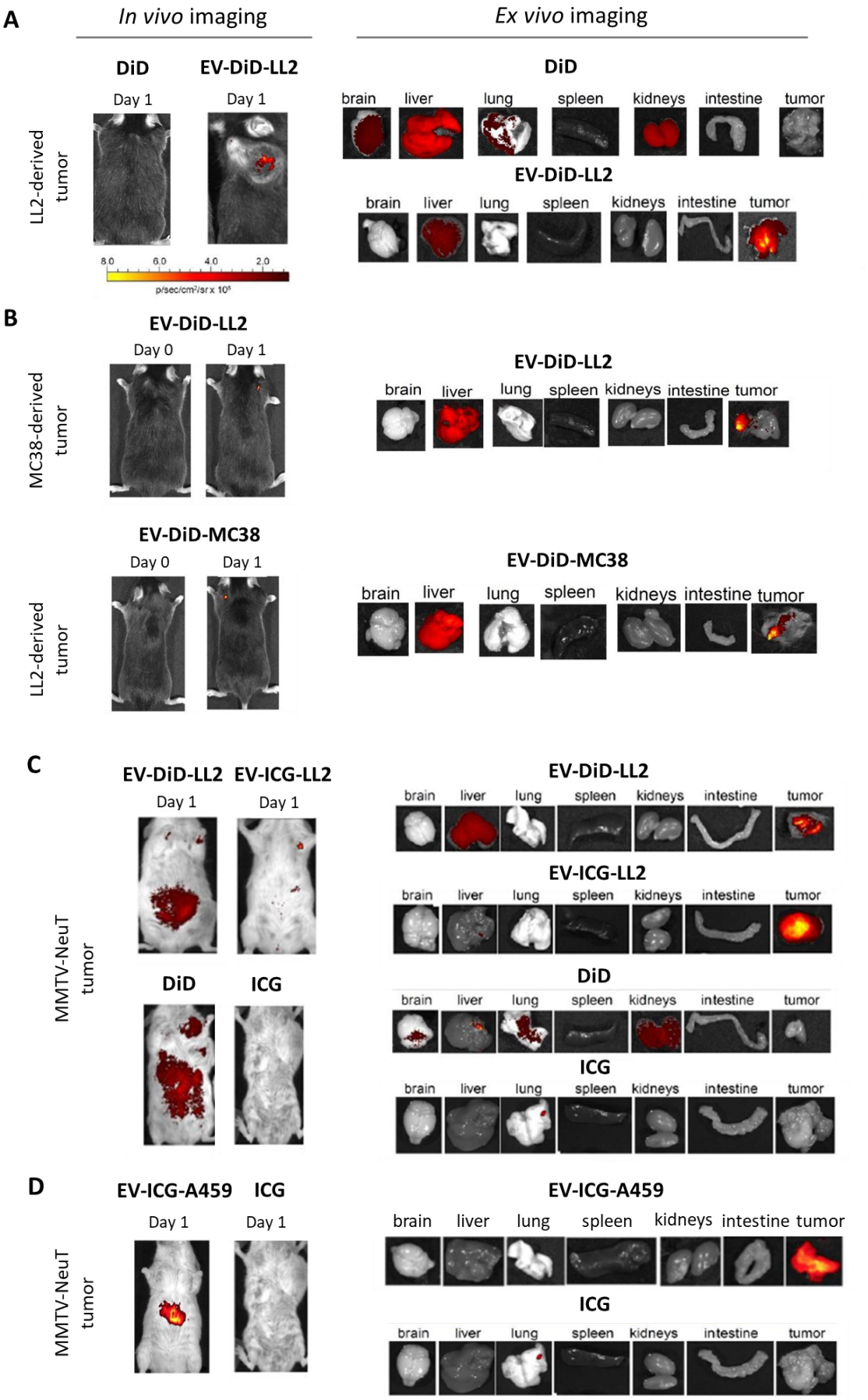
A
In vivo imaging
Ex vivo imaging
DiD
EV-DiD-LL2
Day 1
Day 1
LL2-derived tumor
8.0
6.0
4.0
2.0
p/sec/cm²/sr x 10⁵
DiD
brain
liver
lung
spleen
kidneys
intestine
tumor
EV-DiD-LL2
brain
liver
lung
spleen
kidneys
intestine
tumor
B
EV-DiD-LL2
Day 0
Day 1
MC38-derived tumor
EV-DiD-LL2
brain
liver
lung
spleen
kidneys
intestine
tumor
EV-DiD-MC38
Day 0
Day 1
LL2-derived tumor
EV-DiD-MC38
brain
liver
lung
spleen
kidneys
intestine
tumor
C
EV-DiD-LL2
EV-ICG-LL2
Day 1
Day 1
MMTV-NeuT tumor
DiD
ICG
EV-DiD-LL2
brain
liver
lung
spleen
kidneys
intestine
tumor
EV-ICG-LL2
brain
liver
lung
spleen
kidneys
intestine
tumor
DiD
brain
liver
lung
spleen
kidneys
intestine
tumor
ICG
brain
liver
lung
spleen
kidneys
intestine
tumor
D
EV-ICG-A459
ICG
Day 1
Day 1
MMTV-NeuT tumor
EV-ICG-A459
brain
liver
lung
spleen
kidneys
intestine
tumor
ICG
brain
liver
lung
spleen
kidneys
intestine
tumor

Figure 11. Homologous, heterologous and cross-species tumour tropism of EV derived from cultured cancer cells. *In vivo* and *ex vivo* imaging images of tumour bearing mice i.v. treated 24 h with cancer-derived EV loaded with fluorescent markers (1E08 particles/tumour). Representative images of the photon emission (fluorescence) in the tumour area and in 7 organs explanted from tumour-bearing mice showing in (A) the *homologous tropism* of EV-DiD-LL2 for lung LL/2-derived tumours compared to DiD alone, in (B) the *heterologous tropism* of EV-DiD-LL2 and EV-DiD-MC38 for colon MC38- and lung LL2-derived tumours, respectively, and in (C) the *heterologous tropism* of EV-DiD-LL2 and EV-ICG-LL2 for mammary tumours in NeuT mice compared to DiD and ICG alone, and in (D) the *cross-species tropism* of human derived EV-ICG-A459 for murine breast tumours in NeuT mice compared to ICG. Figure adapted from [180].

Altogether, these results demonstrated that cancer EV hold conservative homing features that allow tumour recognition independently from the tumour type and the species originating the vesicles [180].

5.3 Absence of tumour tropism in non-cancer derived EV

The generalized tumour tropism of EV could be attributed either to phagocytosis or other peculiar activities of malignant cells or to some specific and conserved mechanism of EV's uptake [107,184,185].

To exclude the first hypothesis and verify whether the tumour homing ability was a feature held by all EV isolated from cultured immortalized cell lines or not, we tested the biodistribution of non-cancerous EV derived from murine C2C12 myoblasts. When loaded with ICG and injected in C57Bl/6 mice bearing tumours derived from LL2 lung cancer cells, EV-ICG-C2C12 formulation couldn't target the tumour, showing no preferential accumulation of the fluorescence at the tumour site (Figure 12).

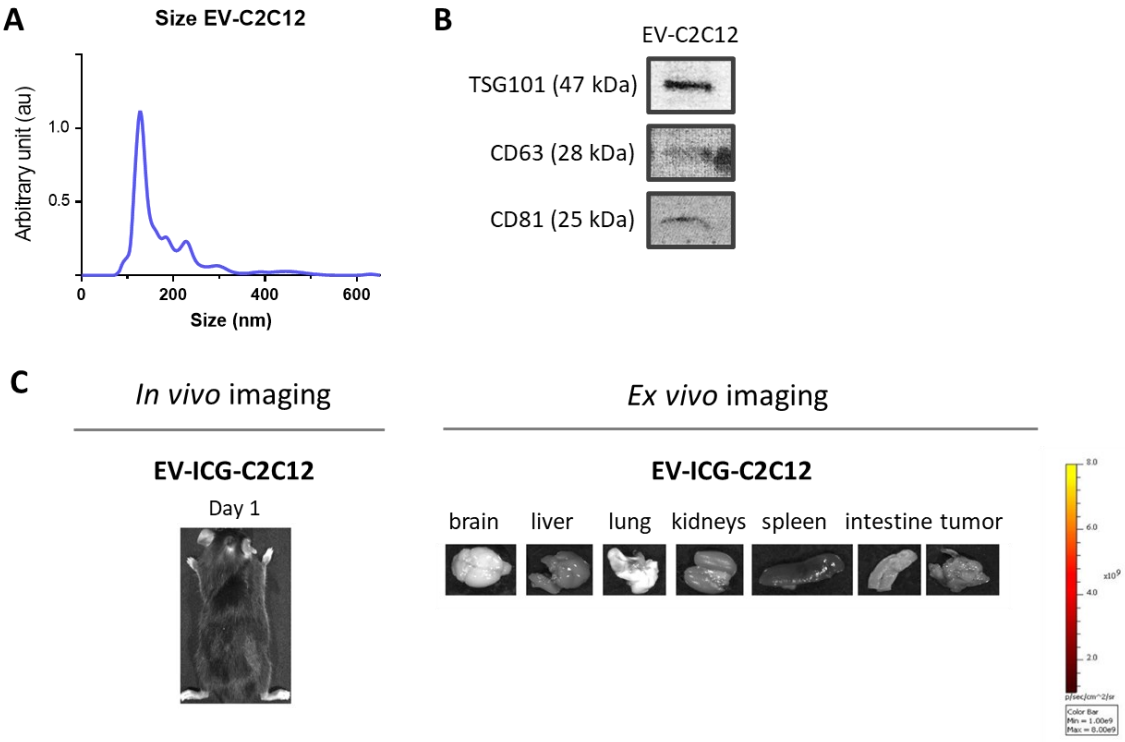

Figure 12. Absence of tumour tropism in not cancer-derived EV. (A) Size distribution of EV preparation from C2C12 cells determined by nanoparticle tracking analysis (NTA). (B) Immunoblot analysis of EV marker Tumour Susceptibility Gene-101 (TSG101) and tetraspanin proteins (CD63 and CD81) in the EV preparation. (C) *In vivo* and *ex vivo* imaging representative images of a mouse bearing a LL2-derived tumour i.v. treated 24 h with EV isolated from the murine C2C12 myoblast cell line and loaded with ICG (1E08 particles/tumour). No positive fluorescent signal was detected in the tumour area and in the 7 organs explanted.

Collectively, our results indicated that the tumour uptake of vesicles did not depend solely on cancer cells and their phagocytic activity but was also dependent on the nature of EV, whose generation from cancer cells appeared to be essential for the tumour recognition [180].

5.4 Patient-derived EV but not EV from healthy subjects recognize tumours grown in experimental mouse models

Although the targeting abilities of cancer EV suggest their possible use as drug delivery tool, the potential immunogenicity and delivery of oncogenic products of EV derived from cancer cell lines generate some concerns and limit their potential application and translation in the clinical setting. These problems could be overcome with the use of autologous EV isolated from

the patient's blood, thus, we investigated whether in the plasma of cancer patients could be found EV characterized by the same tumour tropism observed for EV isolated from cancer cell-lines.

5.4.1 Isolation and characterization of EV from plasma

To test the hypothesis that EV released by tumours in the bloodstream of cancer patients display the same tumour-specific tropism observed in EV produced by malignant cell lines [180], in collaboration with Professor Mazzaferro V. of the *National Cancer Institute, IRCCS Foundation* of Milan we extracted EV from the plasma of colorectal cancer patients: all CRC enrolled in the study were patients with liver metastasis (stage IV), a tumour type with features similar to those of MC38 cell line used in previous experiments [161,175,180], and presented defined histological and clinical criteria [186]. As negative control, we also extracted EV from the plasma of healthy volunteers.

Plasma-derived EV were produced according to the ultracentrifugation method developed in our lab (see Methods) and characterized in terms of particles concentration and size distribution by NTA, showing nanoparticles with a prevalence of exosomes (Figure 13A). EV isolation was further confirmed by immunoblot detection of typical EV markers (in compliance with the ISEV international guidelines) [187], while cryo-EM studies demonstrated EV morphology and integrity (Figure 13B-C).

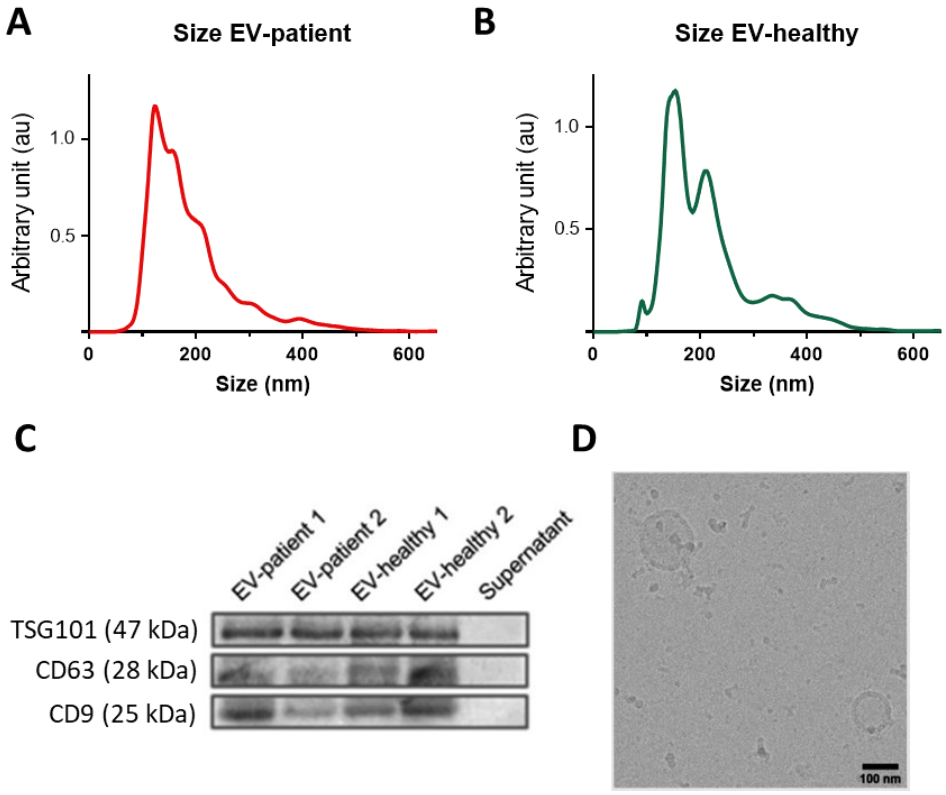

Figure 13. Shape, size-distribution and marker expression characterization of plasma EV from CRC patients and healthy volunteers. (A-B) Mean particle size distribution of plasma EVs of patients and healthy donors obtained by nanoparticle tracking analysis (NTA). (C) Expression analysis of EV marker proteins Tumour Susceptibility Gene-101 (TSG101) and tetraspanin proteins (CD63 and CD9) in plasma-derived EV from patients or healthy donors. (D) Cryo-electron microscopy image of EV from Patient1, scale bar: 100 nm. Figure adapted from [186].

5.4.2 Selective tumour tropism of patient-derived EV in engrafted and spontaneous mouse models of cancer

To test the ability of plasma-derived EV to migrate into neoplastic tissues, we first evaluated their biodistribution at 24 h (the time point we observed accumulation of EVs derived from cancer cell lines) in C57Bl/6 wild type mice engrafted with the syngeneic MC38 colon cancer cell line. EV derived from the plasma of patients and healthy subjects were loaded with ICG and a total of 1E08 EV-ICG/tumour was administered by i.v. injection into tumour-bearing mice. By following the biodistribution of ICG-loaded EV through the *in vivo* and *ex vivo* fluorescence imaging technique, we showed that EV derived from the plasma of patients displayed specific tropism for tumour tissues since a specific fluorescence signal arising from the tumour was detected both *in vivo* in the region of tumour growth and *ex vivo* in the explanted

tissue (Figure 14A). Similar results were obtained in mice bearing spontaneous breast tumours [182], where patient-derived EV selectively accumulated ICG fluorescence at tumour sites (Figure 14A-B) [186], in agreement with the heterologous tumour recognition ability of cancer-derived EV previously reported [180].

Conversely, EV circulating in the blood of healthy volunteers did not display such characteristic biodistribution profile, showing no targeting abilities towards the tumour tissue since no specific fluorescence signal arising from tumour sites was detected neither in the MC38 tumour model nor in the MMTV-NeuT transgenic (Figure 14C-D) [186].

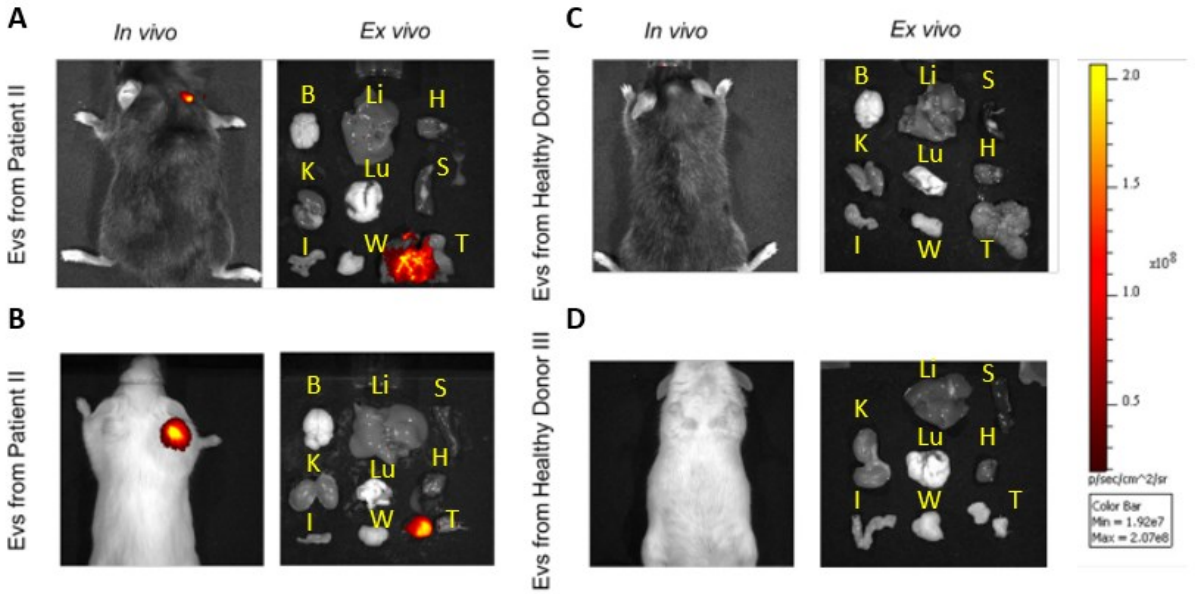

Figure 14. Selective tumour tropism of EV derived from the plasma of CRC patients. *In vivo* and *ex vivo* imaging representative images of ICG fluorescence of MC-38 tumour-bearing mice (black mice) and mammary tumour-bearing mice (NeuT, white mice) injected with EV isolated from the blood of healthy volunteers (left panels A and B) or patients' EV (right panels C and D) and labelled with ICG. Patient-derived EV showed tropism for tumours originated in mice engrafted with MC-38 cancer cells and for spontaneous mammary cancer arose in NeuT mice, while no signal was detected in both cancer models injected with healthy donor-derived EV. B: brain; Li: liver; S: spleen; K: kidneys; Lu: lung; H: heart; I: intestine; W: white adipose tissue; T: tumor. Figure from [186].

To rule out the possibility that the different biodistribution profile of patients and healthy donors-derived EV could be due to some difference in the purification of EV from the plasma of patients and healthy subjects, we carried out liquid chromatography (LC) and mass-spectrometry (MS) analyses to quantify possible serum proteins contamination (like albumin and lipoproteins) that could affect the biodistribution of the dye [188]. However, LC and MS

analyses showed comparable protein profiles in EV isolated and detected the presence of albumin and some lipoproteins whose expression did not differ between EV of patients and healthy donors (Figure 15). Moreover, also the ratio between the number of particles and the protein content was similar between the preparations [186].

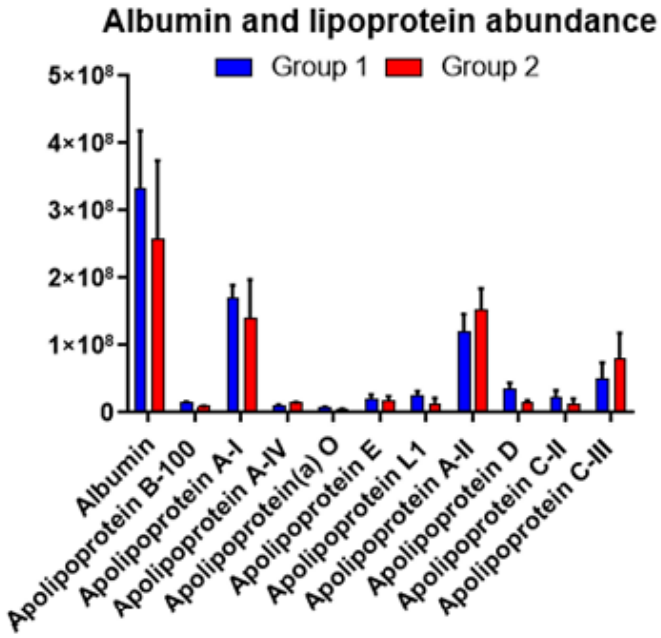

Figure 15. Serum proteins profile in plasma-derived EV of patients and healthy donors. LC and MS quantitation showing the content, i.e. abundance, of albumin and lipoproteins in EV isolated from the plasma of CRC patients (group 1, blue bars) and healthy donors (group 2, red bars). No significant statistically differences were detected between the two EV groups (p values calculated by Sidak's multiple comparison test).

Overall, these results provided evidence of the existence of autologous EV circulating in the blood of CRC patients, but not in the blood of healthy volunteers, endowed with specific cancer tropism abilities that allow tumour recognition when injected in tumour-bearing mice [186].

5.5 Mechanism of tumour homing: identification of candidate proteins possibly driving tumour tropism

To exert their functions EV have to interact, bind and be internalized by recipient cells to release their active cargo. It is known that EV of different cellular origin possess distinct and innate targeting characteristics responsible for the tropism for particular cells or tissues [189].

The protein content of EV is one of the features known to influence and direct EV targeting: some proteins like integrins, tetraspanins or fibronectin were reported to drive EV tropism towards certain tissues like lungs, liver, pancreas, brain and neuronal cells [137,190–192]. Only few studies carried out by other groups described the tropism of tumour cell-derived exosomes for their cells of origin, as also reported by us [180,193,194], but, so far, the biological mechanism and the molecular determinants underlying this tumour homing abilities are still unknown.

5.5.1 Proteomic analysis of EV derived from the plasma of CRC patients and healthy volunteers

Since EV can show different targeting abilities by expressing various surface proteins [195], the tumour tropism exhibited by patient-derived EV (PDEV) and shared by EV released from cancer cells could be conferred by a set of proteins specifically expressed on the surface of PDEV of tumoral origin, and capable of interacting with cancer cells.

To identify these molecules which could possibly explain the tumour targeting ability of PDEV, we carried out proteomic analyses on EV extracted from the plasma of both CRC patients and healthy subjects (control group) to characterize the protein signature of PDEV and find out proteins differentially expressed in the two EV populations.

Nano-scale liquid chromatographic high resolution mass spectrometry (nLC-HRMS) was performed on pools of PDEV displaying *in vivo* tumour targeting and of healthy-EV not exhibiting *in vivo* tumour targeting (Figure 16). From the instrumental and bioinformatics analyses performed on three technical replicates per EV sample, the absolute and relative protein abundances and the proteins differentially expressed among the two EV groups were obtained.

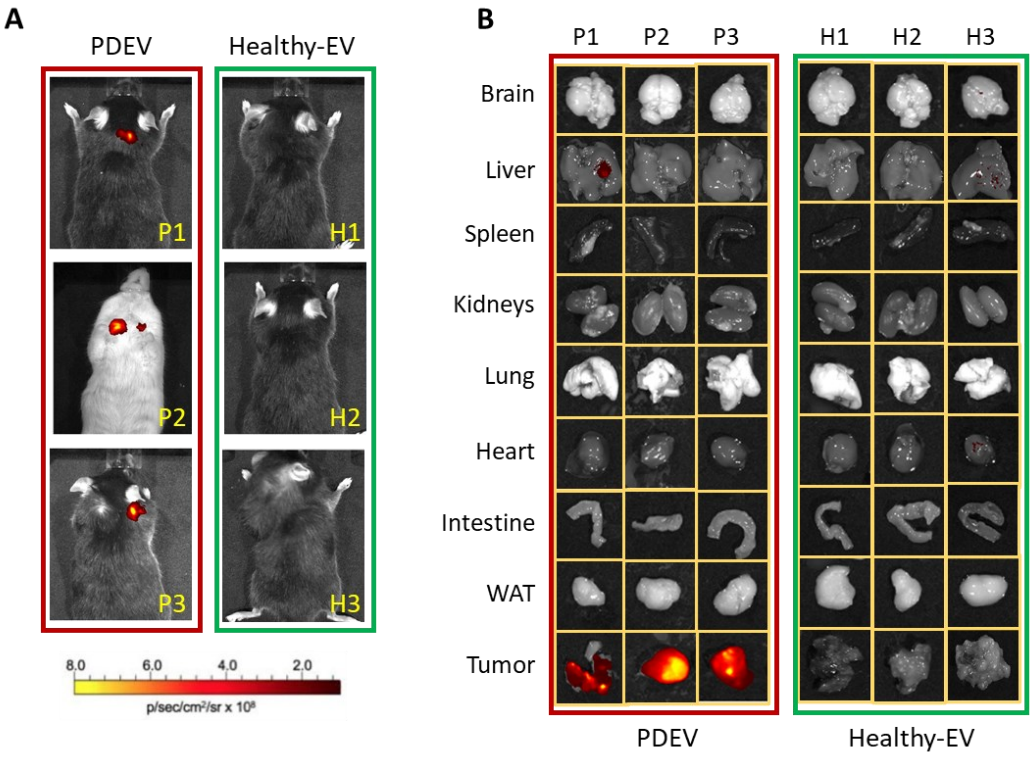

Figure 16. Tumour targeting of EV isolated from CRC patients and healthy volunteers and subjected to mass spectrometry analyses. *In vivo* and *ex vivo* imaging representative images of ICG fluorescence of tumour-bearing mice i.v. treated with EV extracted from the plasma of three representative patients (P1, P2, P3) and healthy subjects (H1, H2, H3) and labelled with ICG. All PDEV displayed the characteristic tumour tropism while no fluorescence signal was detected in mice injected with healthy-EV. WAT: white adipose tissue.

A total of 426 proteins were identified from nLC-HRMS analysis and among them 26 proteins resulted more expressed (abundance ratio ≥2) in PDEV when compared with Healthy-EV, while 16 proteins resulted less expressed (abundance ratio ≤0.5) in PDEV (Figure 17B). Among the most expressed proteins in PDEV, a number of potential candidates for a direct or cell-mediated interaction with cancer cells were present, while candidate proteins that could prevent EV's uptake or modify their half-life were found among the down-regulated proteins in PDEV, as shown by the GO mapping (Figure 17C). Interestingly, in this sense we found in the healthy-EV control group some proteins belonging to the same biological pathway related to the complement-mediated clearance mechanisms.

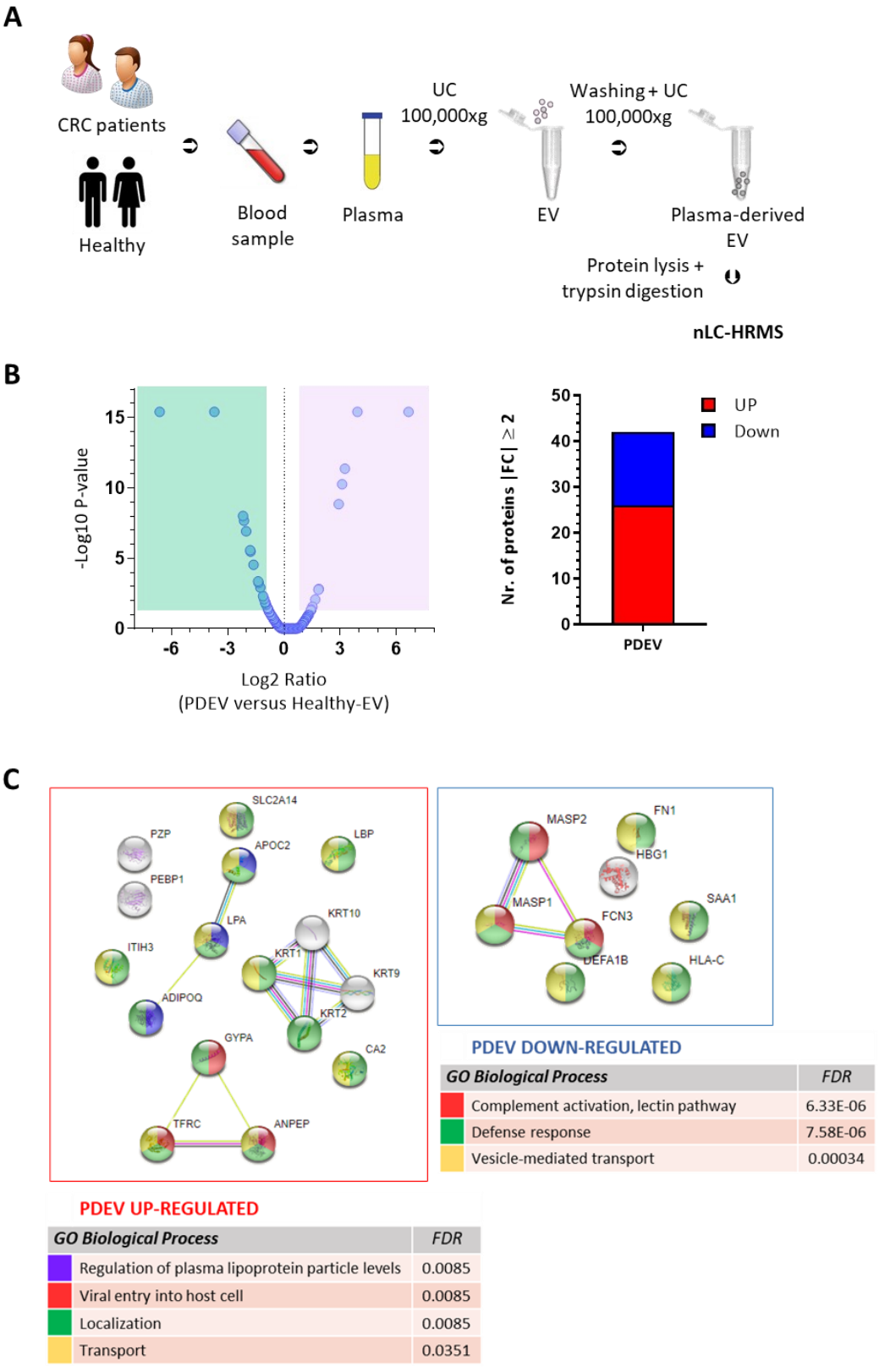

Figure 17. Mass spectrometry characterization of plasma-derived EV from CRC patients and healthy donors. (A) Workflow scheme of proteomics analysis. Briefly: EV were isolated from the plasma of colorectal cancer patients and healthy donors by ultracentrifugation at 100,000 xg; after washing and additional ultracentrifugation steps, plasma-derived samples were lysate and proteins

digested before nano-scale liquid chromatographic high resolution mass spectrometry analysis. (B) Volcano plot of proteins identified in patients and healthy's EV by nLC-HRMS. Besides, histogram representing in red the number of proteins most expressed in PDEV compared to Healthy-EV (UP, 26 proteins; fold-change ≥ 2, adjust P-Value <0.5) and in blue the number of proteins less expressed in PDEV compared to Healthy-EV (Down, 16 proteins; fold-change ≤ 0.5, adjust P-Value <0.05). (C) Protein-protein interaction network and Gene Ontology analysis of biological processes enriched for the proteins up- (red square and table) and down-regulated (blue square and table) in PDEV (False Discovery Rate <0.05). The colour of each node in the interaction view is related to functions attributed for each protein as indicated in the corresponding table. Interactions and GO were retrieved by using STRING database [196].

Based on these evidence, we hypothesized that PDEV could have an impaired clearance from circulation than healthy-EV, possibly due to a reduced interaction with resident and circulating immune cells (like macrophages), which are the main responsible for the clearance of injected nanoparticles [197,198]. The impaired clearance would allow PDEV to accumulate in the tumour tissue taking advantage of the greater permeability of tumour vessels: in this condition, the longer is EV's circulation time, greater are the chances of EV to accumulate to the tumour since nanoparticles between 50nm and 150nm can extravasate from the leaky tumour vasculature thanks to the enhanced permeability and retention (EPR) effect [199]. However, the hypothesis of a reduced clearance of EV of cancer origin is not sufficient *per se* to explain the whole mechanism of tumour targeting since following extravasation EV need to be internalized by recipient cancer cells to release their cargo (i.e. ICG) inside the cytoplasm and this requires an active uptake mechanism.

We initially tested the hypothesis of a lower uptake of cancer-derived EV *in vitro* by treating immortalized cultured macrophages (RAW 264.7) with ICG-loaded EV obtained from the breast cancer cell line MCF-7 (these EV showed tumour tropism [180]), from the plasma of CRC patients, from non-transformed C2C12 myoblasts and from healthy donors; 4 h after treatment we quantified the EV uptake by measuring the fluorescence-emitting macrophages by FACS analysis. The results showed a greater trend in the uptake of healthy-EV and EV from C2C12 cells (negative for tumour tropism) compared to PDEV and EV from MCF-7 cells, respectively, 4 h after the treatment (Figure 18).

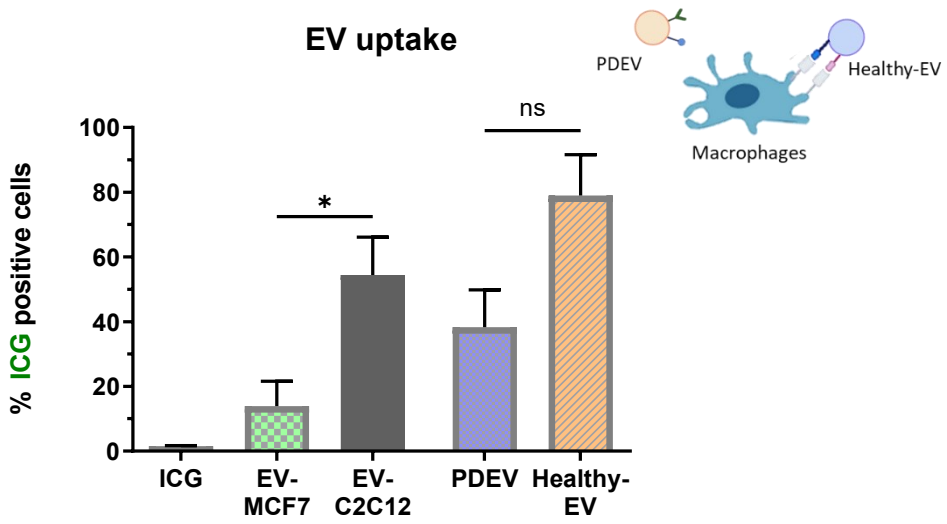

Figure 18. *In vitro* assay of EV's uptake by RAW 264.7 macrophages. Bar chart showing ICG positive cells over vehicle (PBS) treated cells as a measure of the amount of vesicle incorporation into macrophage-like cells; measures were obtained 4 h after treatment with EV from MCF7 cells, C2C12 cells, CRC patients (PDEV) and healthy volunteers loaded with ICG and a comparable amount of free ICG (0.8µM) as control. Data are represented as mean ± SEM of different subjects and experiments. The trend is statistically significant in EV-MCF7 *vs* EV-C2C12. * $p < 0.05$ calculated by Student's unpaired t-test.

These preliminary data further supported the hypothesis of acquired abilities of patients and cancer-derived EV to escape the normal clearance mechanisms, resulting in a different interaction capability of EV endowed or not endowed with tumour targeting with cells of the mononuclear phagocyte system (MPS), mostly represented by macrophages.

5.5.2 Proteomics of plasma EV from patients before and after the surgical tumour resection

EV circulating in the plasma of oncological patients and healthy subjects represent a mixed population of EV secreted into the bloodstream from the very different cells and organs of the body. Therefore, only a sub-population of EV of tumoral origin is likely to be the one displaying the specific tumour tropism in the plasma of oncological patients. This subpopulation might be enriched in the patient's plasma by the relative resistance to the clearance mechanism of cancer-derived EV (Figure 18). In order to identify specific markers characterizing the cancer-derived EV subpopulation, we compared the proteomic profile of EV circulating in the blood of CRC patients before and after the surgical removal of the neoplastic tissue. To this aim, we collected

EV from blood samples of CRC patients in the follow-up phase after surgery (on average six months after the surgical tumour resection) and followed the clinical disease course of the single patient in the surveillance follow-up phase. From this clinical monitoring activity, we identified patients experiencing tumour relapse within 3-10 months after the first oncology check-up when we performed EV collection, and patients still in complete remission 20 months after surgery. Accordingly, we performed nano-scale liquid chromatographic high resolution mass spectrometry (nLC-HRMS) on pools of PDEV extracted before the surgical tumour resection and of EV from patients in complete remission (healed-EV) and with tumour relapse (relapsed-EV) collected after surgery. From mass spectrometry analyses performed on three technical replicates per EV sample, we obtained the absolute and relative protein abundances between each EV group.

Then, we analysed the expression of the set of proteins differentially expressed between PDEV and healthy-EV in EV obtained from patients after surgery to identify relevant molecules whose expression significantly changed after the removal of the neoplastic tissue (Figure 19A).
By comparing the protein signature of PDEV, healthy-EV and EV from patients in complete remission (healed-EV) we found a common expression pattern for 11 proteins in PDEV when compared to EV from both healthy and healed subjects: these proteins are either highly present in PDEV with a low expression in both healthy and healed subjects or poorly expressed in PDEV with a high expression in healthy and healed subjects (Figure 19B). Moreover, 6 out of 11 of these proteins did not significantly modify their expression level in EV of patients with tumour relapse after surgery (relapsed-EV) (Figure 19C), suggesting that these proteins might "label" the presence of latent residual disease. Interestingly, among these proteins we found MASP1 and MASP2, two proteins with enzymatic activity involved in the lectin pathway of the complement system, responsible for the activation of the complement cascade in the innate and adaptive immune responses [200], that reconnect with the impaired clearance hypothesis formulated for PDEV.

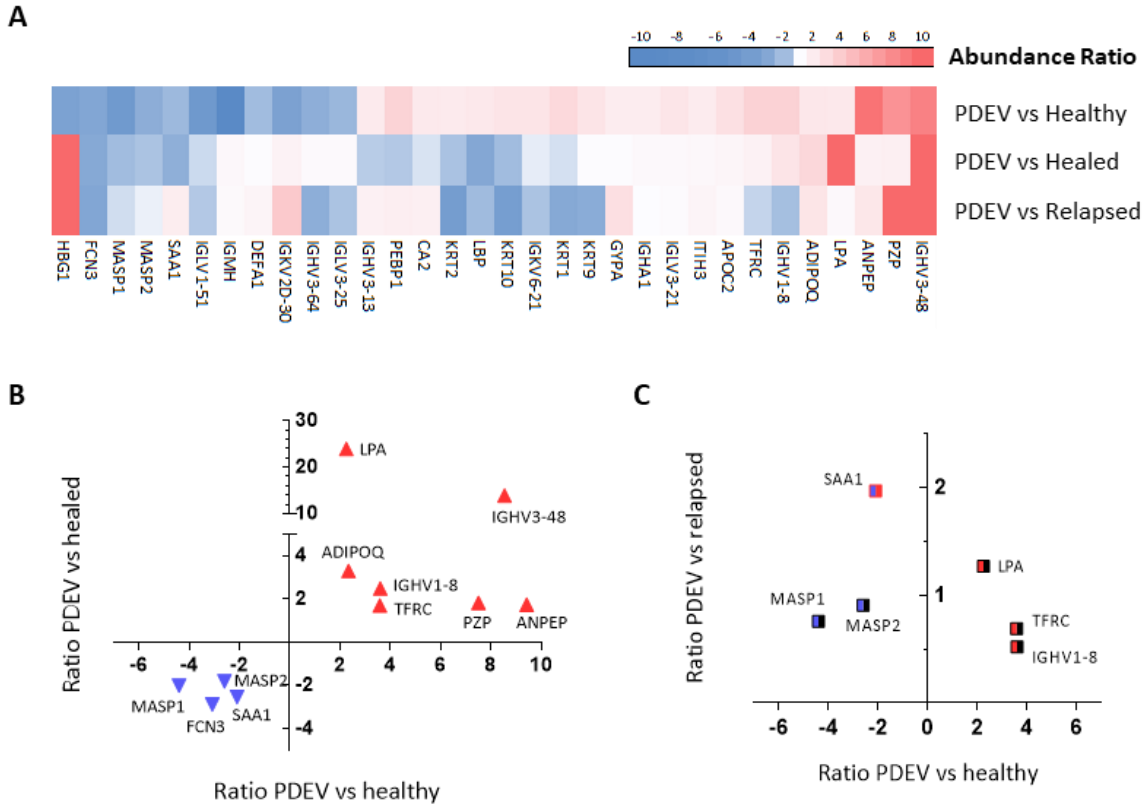

Figure 19. Proteomics of PDEV before and after the surgical tumour resection. (A) Heatmap of abundance ratios of the proteins differentially present in PDEV before and after tumour resection showing the differential expression in PDEV when compared to Healthy-EV, Healed-EV and Relapsed-EV in proteomics analyses. Ratios are pictured in a colour scale from red (high-relative expression in PDEV) to blue (low-relative expression in PDEV). (B) Graph showing the correspondence in the relative expression (abundance ratio) for the set of proteins with similar trend in PDEV when compared to Healthy-EV (x axis) and Healed-EV (y axis). Red triangles indicate proteins highly expressed in PDEV (FC≥2) with a low expression in both healthy and healed subjects, blue triangles indicate proteins with a low expression in PDEV (FC≤0.5), while displaying a high expression in both healthy and healed subjects. (C) Graph showing the correspondence in the abundance ratio for the proteins in (B) with a different trend in PDEV when compared to Healthy-EV (x axis) and Relapsed-EV (y axis). Half-red squares indicate proteins highly expressed in PDEV compared to Healthy-EV (FC≥2) but with similar expression in patients before and after surgery with tumour relapse; half-blue squares indicate proteins low-expressed in PDEV compared to Healthy-EV (FC≤0.5) but with similar expression in patients before surgery and after tumour relapse.

These data identified a protein "signature" characterizing the PDEVs: these proteins might be involved in the mechanism underlying the tumour tropism and could be tested for their possible clinical application as disease markers.

Based on the collected evidence, we here propose a model to explain the tumour targeting abilities of patient-derived EV. We have hypothesized three fundamental phases in the mechanism of tumour tropism: (a) half-life in the blood, (b) targeting, and (c) cargo delivery (Figure 20).

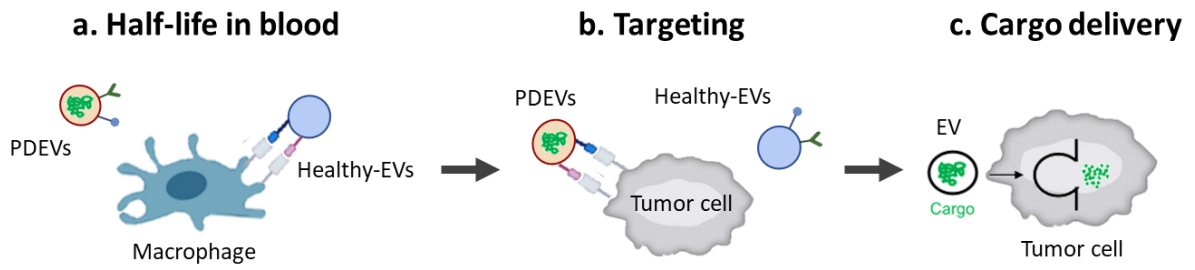

Figure 20. Stages of the mechanism of EV tumour tropism. Proposed model for the targeting of tumours tissues by cancer and patient-derived EV (PDEV). Three main phases are expected to be involved: a) escape from the macrophage-mediated removal from the blood circulation that increase the half-life of EV of cancer origin; b) selective targeting of tumour cells through specific ligand-receptor interactions between patient-EV and cancer cells, and c) internalization and delivery of EV cargo inside cancer cells.

In the first stage, and most likely the limiting one, cancer and patient-derived EV with increased intrinsic half-life in the bloodstream are likely to accumulate in tumour tissues, taking advantage of the greater permeability of tumour vessels. The increased half-life in blood of patient-EV would be the result of acquired abilities to escape the normal clearance mechanisms, mostly mediated by macrophage cells. These abilities could be ascribed to the reduced expression in patient-EV of proteins of the complement system, like MASP1 (Mannan-binding lectin serine protease 1), MASP2 (Mannan-binding lectin serine protease 2) and FCN3 (Ficolin-3), resulting in a lower opsonization and phagocytosis or lysis of EV. On the opposite, these proteins enriched in EV derived from healthy subjects could lead to the clearance of most of the normal injected EV. Patient-EV accumulating in the tumour tissue must specifically target and interact with cancer cells to be internalized and release their cargo inside the cytoplasm. In order to accomplish that, in the targeting stage, surface receptors of patient-EV are likely to interact with specific ligands expressed by cancer cells: proteins like TFRC (transferrin receptor 1), known to facilitate clathrin-mediated endocytosis [201], or ANPEP (Aminopeptidase N), a receptor for tumour-homing peptides [202], enriched in EV from patients could mediate the direct

interaction and targeting of tumour cells, leading to the final release of EV cargo inside cancer cells in the ultimate delivery step (Figure 20).

5.6 Clinical applications of patient-derived EV (PDEV)

5.6.1 PDEV as drug delivery systems of theranostics in autologous transplantation

In the previous section, we demonstrated that EV extracted from the plasma of CRC patients recognize and selectively accumulate at tumours when i.v. administered in engrafted and spontaneous mouse models of cancer (section 5.4.2). However, human colorectal cancer is known to be very heterogenous [203].

To confirm that the observed tropism was not due to specific features of the murine model of cancer not representative of human CRC, the ability of patient-derived EV (PDEV) to recognize their tumour of origin was assessed in a mouse model closely reflecting the human malignant disease: patient derived xenografts (PDX) [204,205].

PDX were generated by implanting liver metastasis of CRC patients in immunodeficient SCID mice [177], while EV were isolated from the plasma of patients before the surgical tumour resection, as described in Figure 21, and stocked at -80ºC for the targeting test in the corresponding PDX model.

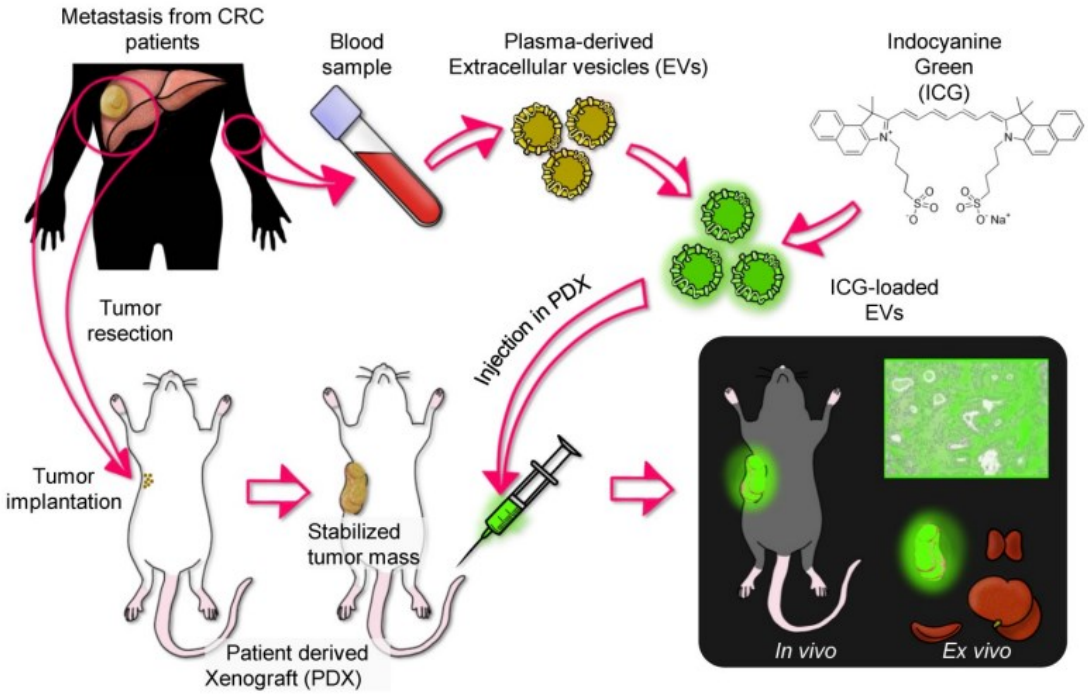

Figure 21. Experimental design of the test of EV purified from CRC patients in PDX models. Liver metastases were excised from CRC patients and implanted in SCID mice to generate PDX, while EV were isolated from the blood of the same patients collected before surgery. After tumour growth, PDEV were loaded with ICG and administered by i.v. injections in mice bearing tumours from the same patient of the vesicles; 24 h after the treatment *in vivo* and *ex vivo* imaging were performed [186].

To test their homing ability, PDEV were loaded with ICG and administered by i.v. injection into corresponding PDX mice after the tumour from the same patient was growth at about 300-400 mm^3 dimension. The i*n vivo* imaging performed 24 h after treatments showed accumulation of ICG fluorescence in the tumour area in all mice tested (Figure 22A), as also confirmed by *ex vivo* imaging detailing the specific fluorescent emission arising from the tumour tissues (Figure 22B). All tumours were selectively labelled by ICG-loaded PDEV, while no specific fluorescence signal from the tumour was detected when tumour bearing mice were i.v. injected with ICG not formulated with PDEVs (Figure 23) [186].

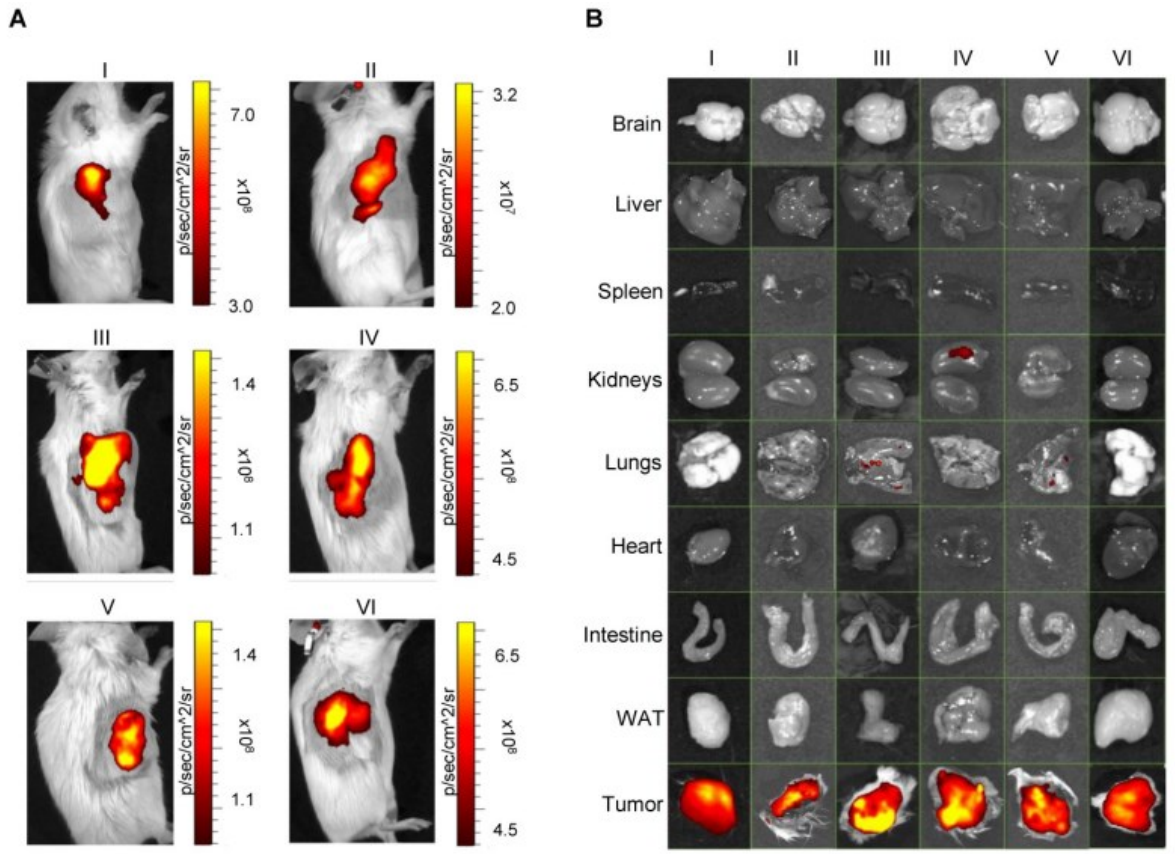

Figure 22. Patient derived-EV recognize corresponding tumours grown in PDX mice. Pseudo-colour images of ICG fluorescence in PDX mice. (A) *In vivo* imaging of n=6 PDX mice (I to VI) injected with ICG-loaded EV derived from the plasma of the same patients originating the tumour and PDX model, and (B) *ex vivo* imaging of related dissected organs showing tumours selectively labelled with PDEV-ICG in all PDX mice. WAT: white adipose tissue. [186]

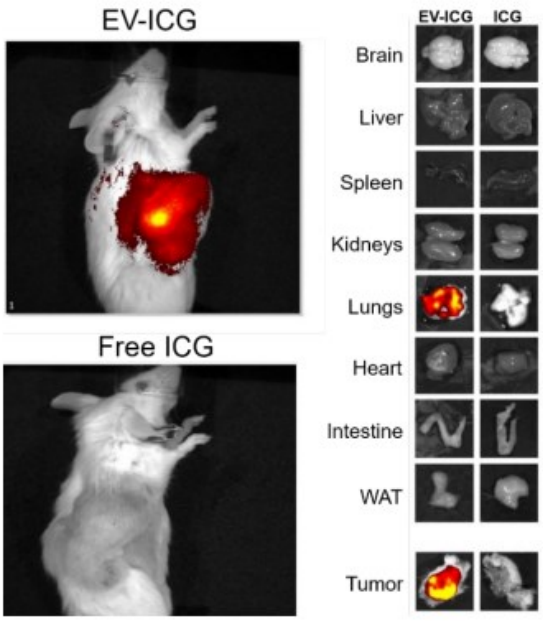

Figure 23. Free ICG does not accumulate at tumours. Pseudo-colour images of ICG fluorescence in PDX mice injected with patient-derived EV (EV-ICG) or the same amount of ICG not formulated with PDEVs (free ICG). Left and right panels showing *in vivo* and *ex vivo* imaging, respectively. [186]

We further confirmed what we observed at the macroscopic level by fluorescence imaging with the microscopy analysis of haematoxylin-eosin staining and ICG-related fluorescence of sections of CRC xenograft tumour tissue: these analyses provided evidence that ICG accumulated in the neoplastic tissue but not in the normal surrounding tissue (Figure 24) [186].

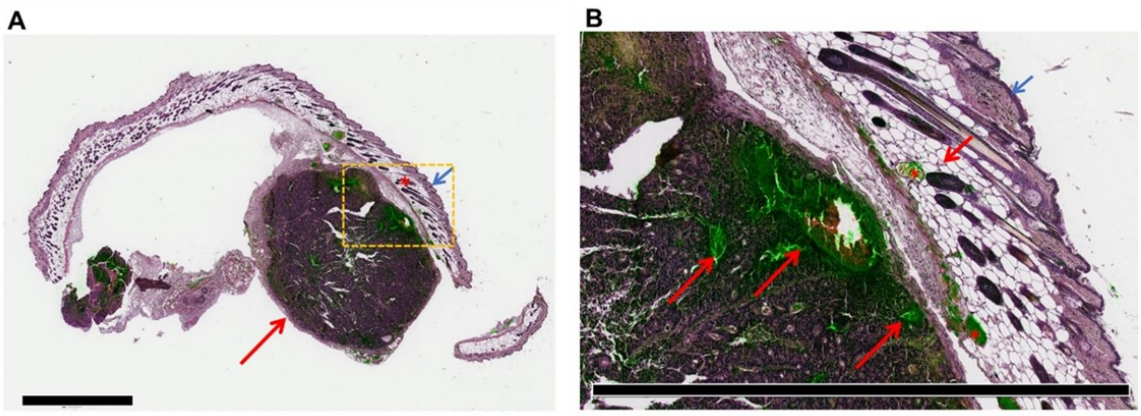

Figure 24. ICG fluorescence delivered by EV selectively accumulates in the neoplastic tissue. Microscopic view of haematoxylin-eosin staining (violet) and ICG fluorescence (green) of a representative xenograft tumour tissue. (A) Section of tissue showing the tumour nodule (long arrow) located underneath the subcutaneous layer (short arrow: cutis; asterisk: subcutis). Scale bar: 2 mm. (B) Details of the tumour tissue (yellow box in panel A) showing ICG accumulation in cancer cells (long red arrow) and tumour necrosis (asterisk: ipodermal vascular spaces; short blue arrow: cutis; short red arrow: subcutis). Scale bar: 2 mm. [186]

With these experiments we demonstrated that patient-derived EVs recognize corresponding tumours grown in PDX mouse models, and deliver ICG inside tumour cells.

Overall, the results confirmed that patients-derived EV are indeed endowed with selective tropism for cancer tissues and gave a proof-of-principle demonstration of the possible translational use of patients' EV for targeting patient tumours and delivering fluorescent agents directly inside cancer cells through the infusion of autologous EV. The innate abilities of patients' EV to recognize tumours can therefore be exploited for the design of protocols where EV are loaded with diagnostics for the detection of neoplastic tissues, therapeutics (e.g.

chemotherapeutic drugs) for targeted cancer therapies or theranostics for combined diagnostic and therapy.

We are currently working on the first-in-human demonstration of the feasibility of the protocol where EV are extracted from the plasma of CRC patients, loaded with ICG and then reinfused in the same patient for the intraoperative detection of CRCs during the surgical tumour resection procedure (Figure 25).

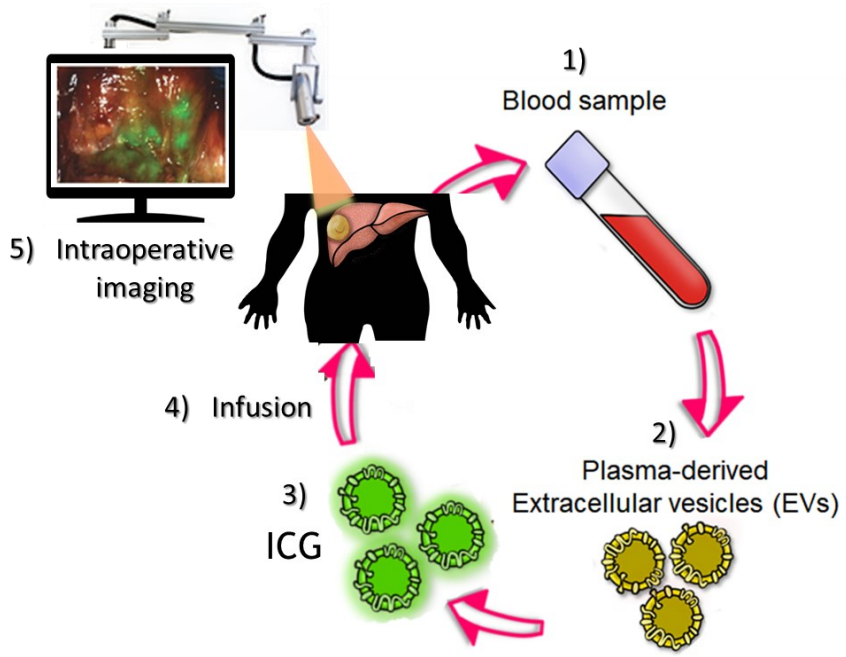

Figure 25. Transplantation protocol of autologous EV for cancer-specific targeting. In the transplantation protocol, autologous EV directly isolated from patient's blood are manipulated *ex vivo* to insert diagnostics (i.e. ICG) and subsequently re-infused in the same patient to intraoperative visualize cancer tissues. With EV of autologous origin, the immunogenicity and oncogenicity concerns related to exogenous EV could be overcome since patients' EV are fully biocompatible, have physiological pharmacokinetic properties and give the chance for a standardized production.

5.6.2 PDEV as source of biomarkers in CRC disease

Proteomic analyses identified the mannan-binding lectin serine protease 1 (MASP1) among the candidate molecules potentially relevant for the tumour tropism and as potential biomarker for liquid biopsy [206,207]. Interestingly, MASP1 is involved in the innate response: a serine protease that normally function in the alternative pathway of the complement system. The lectin pathway is usually triggered upon binding of mannan-binding lectin (MBL), collect-11 and ficolins to sugar moieties on microbial surface which leads to association and activation of proteases MASP1 and MASP2. The role of MASP1 is to start the proteolytic cascade activating MASP2, which cleaves C4 and C2 forming the C3 convertase (C4b2a), or directly C2 or C3 molecule the key component of complement reaction. Activation of the complement cascade subsequently leads to opsonization by C3b molecules, phagocytosis by specialized phagocytic cells, and lysis of target microorganisms through the formation of the membrane-attack complex (MAC) [208].

Although high serum levels of the MASP2 protein were associated with recurrence and poor survival of colorectal cancer and ovarian cancer [209,210] and, together with high MASP1 serum levels, with progression and worse prognosis in cervical cancer [211], little is known about the connection between MASP1 and extracellular vesicles.

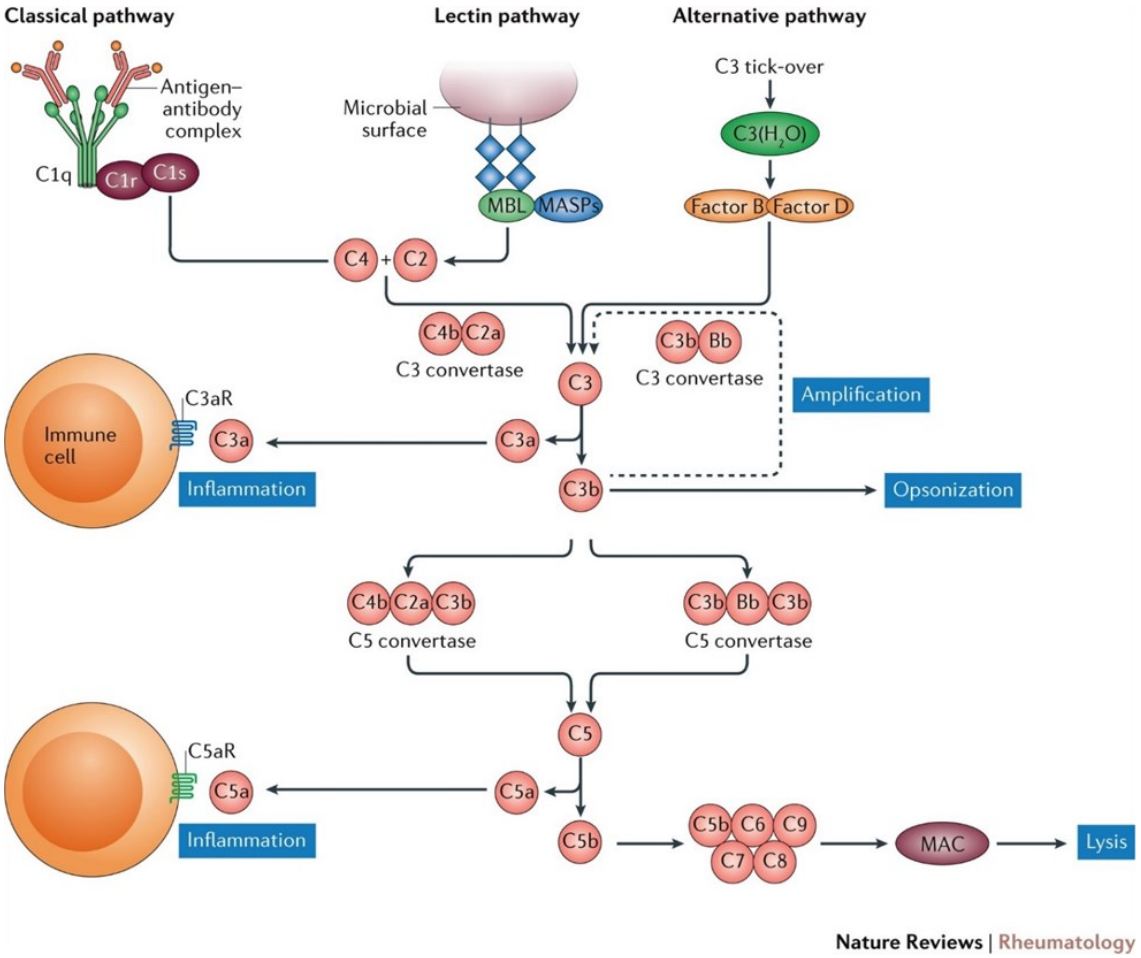

Figure 26. The three pathways of complement system activation. The classical pathway is activated following binding of the C1q molecule to antigen-antibody immune complexes. The lectin pathway is triggered by binding of recognition molecules (mannose-binding lectin (MBL), collectins and ficolins) to carbohydrate structures on the pathogen surface, which activates the MBL-associated serine proteases MASP-1 and MASP-2. The alternative pathway is continuously activated at a low level as a result of spontaneous C3 hydrolysis. After activation, a cascade of proteolytic reactions leads to the formation of anaphylatoxin C3a and the opsonin C3b. Next, pro-inflammatory anaphylatoxins C5a and C5b are generated to form the membrane attack complex (MAC). Figure from [212].

Our proteomics data on EV isolated from the plasma of CRC patients before surgery (PDEV), healthy donors and patients in complete remission or experiencing relapse after tumour resection showed 4.5-fold reduced levels of MASP1 protein in PDEV when compared to EV from healthy subjects. In EV from patients in complete remission (Healed-EV), MASP1 abundance was not at the same level of that of healthy subjects although was still 2-fold higher than that of PDEV. However, when we looked at MASP1 in EV from patients developing tumour recurrence, its levels did not significantly change when compared to EV from patients with tumours (0.8-fold change) (Figure 27A-B). These preliminary data suggest that the expression levels of MASP1 in plasma EV might predict the presence of CRC disease, while

cannot be used as a prognostic marker of therapeutic efficacy, although a definitive statement on this aspect could only be obtained with longitudinal studies in which the level of MASP1 expression in the EV are monitored in each patient in time.

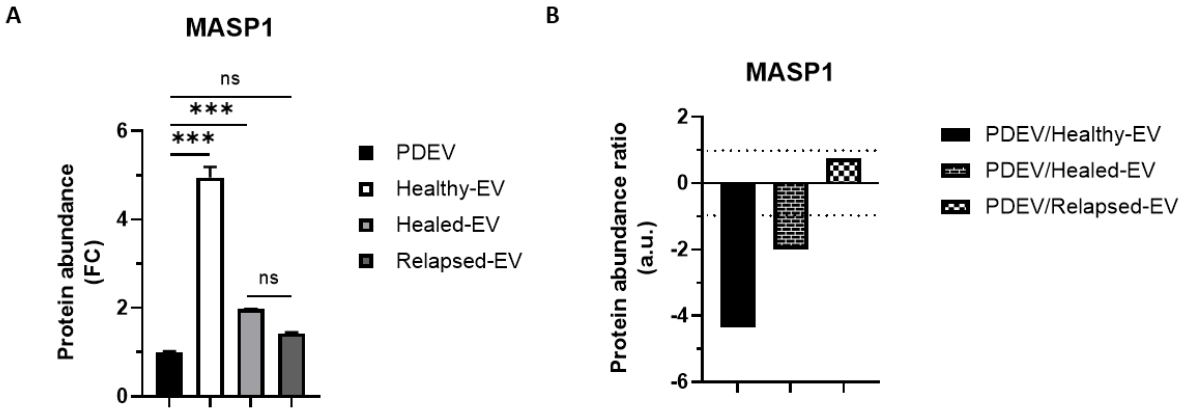

Figure 27. Mass spectrometry MASP1 levels in EV from CRC patients before and after the surgical tumour resection. nLC-HRMS data of MASP1 protein levels in plasma EV extracted from CRC patients, healthy volunteers, CRC patients in complete remission and with tumour relapse after surgery. (A) Histogram showing relative MASP1 protein abundances in PDEV, Healthy-EV, Healed-EV and Relapsed-EV groups as fold-change over the PDEV group. Differences in abundance among EV groups are statistically different as indicated. *** $p < 0.001$ calculated by one-way ANOVA and Tukey's multiple comparison test; ns: not significant (B) Bar chart displaying abundance ratios of MASP1 protein in PDEV vs Healthy-EV, PDEV vs Healed-EV and PDEV vs Relapsed-EV. Negative values indicate a 4.5-fold and 2-fold higher levels of MASP1 in Healthy-EV and Healed-EV compared to PDEV, respectively. Positive value indicates a 0.8-fold change expression of MASP1 in PDEV compared to Relapsed-EV.

To verify whether the differential expression of the MASP1 protein in EV derived from the plasma of colorectal cancer patients and healthy donors was real and therefore to also validate proteomics data, we carried out western blot analyses to detect and measure the expression of MASP1 in PDEV and Healthy-EV. Explorative immunoblot experiments performed initially on two representative patients and on two representative controls revealed expression of MASP1 protein in EV from healthy donors, while no signal was detected in EV from patients (Figure 28A-B).

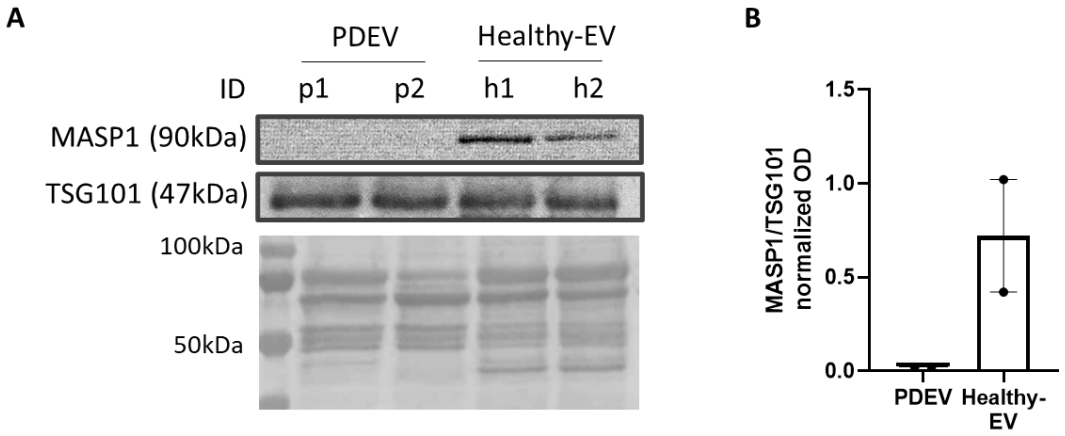

Figure 28. MASP1 expression is reduced in EV from CRC patients compared to EV from healthy subjects. Explorative western blot analysis of MASP1 expression in EV isolated from the plasma of two CRC patients and two healthy volunteers. (A). Immunodetection of the target protein MASP1 and of EV marker protein Tumour Susceptibility Gene-101 (TSG101) in plasma-derived EV from patients (p1, p2) or healthy donors (h1, h2). 20ug of EV protein lysate were analysed, confirmed by ponceau staining. (B) Bar chart representing the densitometry quantification of the autoradiographic signals (MASP1 vs TSG101) in PDEV and Healthy-EV.

After these preliminary experiments, the analysis was extended on a greater number of CRC patients and healthy subjects in order to confirm the results. The immunoblot analysis indicated that MASP1 expression is clearly higher in plasma-derived EV from healthy subjects than EV from patients with colon cancer, albeit with a little inter-individual variability, confirming the observations and data coming from mass spectrometry (Figure 29A-B).

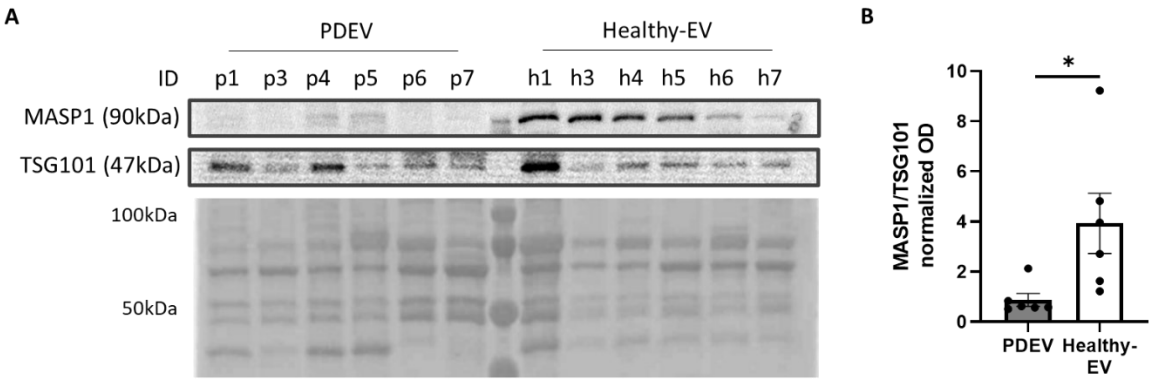

Figure 29. MASP1 levels are significantly lower in EV derived from the plasma of CRC patients. Extended western blot analysis of MASP1 expression in EV from six CRC patients and six healthy volunteers. (A). Expression analysis of MASP1 and of EV marker protein Tumour Susceptibility Gene-101 (TSG101) in plasma-derived EV from patients (p1, p3, p4, p5, p6, p7) or healthy donors (h1, h3,

h4, h5, h6, h7). (B) Bar chart representing the densitometry quantification of the autoradiographic signals (MASP1 vs TSG101) in all PDEV and Healthy-EV tested. * $p < 0.05$ calculated by Student's unpaired t-test.

Altogether, these data strongly support the role of extracellular vesicles-associated MASP1 as candidate disease biomarker for colorectal cancer in liquid biopsy. Further investigations will also deepen its possible role in the early diagnosis of recurrence of disease in patients underwent surgical tumour resection.

6 DISCUSSION

Despite advances made in surgical and medical therapies, cancer is still a major cause of death in the world; colorectal cancer (CRC), in particular, still has a high mortality rate due to the aggressivity, invasiveness and tendency of the disease to spread and develop metastases [4]. Surgery is the first treatment option for CRCs, aimed at achieving complete removal of primary tumour and metastases. The surgical procedure of tumour resection is based on surgical intervention planning through imaging scans and test usually performed before surgery, while during surgery the intraoperative resection of cancerous tissues is entrusted to the surgeon's vision and ability. Surgeons resect neoplastic tissues along with a surrounding margin of normal healthy tissue according to established surgical protocol and guidelines [10,17], in order to achieve complete removal of cancer cells and reduce the risk of relapses. However, a high percentage of patients experience relapses often within the first 2-years after curative treatment [22]. Thus, tactual exploration and visual inspection may not always sufficient for delineating tumour margins and perform a complete excision without leaving behind occult cancer cells, resulting in residual disease. Since the human eye does not have the sensitivity to deeply visualize under the tissue surface, intraoperative tools able to delineate and visualize the disease tissue need to be implemented, to enhance its identification during the surgical procedure beyond the simple visual inspection and palpation.

Molecular imaging focuses on the non-invasive quantitation and visualization of molecular processes as they occur *in vivo*, allowing the investigation of physiological processes within the context of a living organism [48]. Imaging applied to oncological surgery has the potential to provide surgeons with innovative tools for the detection of the neoplastic tissue and the definition of resection margins. Among all the technologies, the intraoperative fluorescence imaging with near-infrared (NIR) probes is one of the most promising; contrast agents working in the NIR region (at wavelengths between 700-1000 nm) have greater sensibility *in vivo*, due to the lower autofluorescence, deeper tissue penetration and reduced interference of molecules constituting human tissues in the NIR spectrum [47,48]. However, so far only two non-specific contrast agents labelling tumour or tumours vessels have been developed and approved for the use in the intraoperative imaging in clinic: indocyanine green (ICG) and methylene blue [50,172]. Thus, the development of more specific probes able to reveal with great precision the whole area influenced by the tumour growth, including the margins of invasion, is warranted.

My PhD project focused on the investigation of novel drug delivery systems of natural origin named *Extracellular Vesicles* for the development of a tool, based on optical imaging of NIR

fluorescent agents, to specifically label and circumscribe the tumour area and guide surgeons in the removal of the neoplastic tissue, CRCs *in primis*.

Extracellular vesicles (EV) are lipid membrane-enclosed particles ranging from nano to micrometric sizes, naturally secreted by many cells into the extracellular environment (including biofluids) as mediators for cell-cell communication [213]; EV carry and transfer many and different kind of bioactive molecules, including protein, lipids, nucleic acids (DNA, mRNAs, miRNAs), and sugars, from donors to recipient cells in order to influence biological functions [81]. Their structure and biological properties of natural carriers, which provide several therapeutic advantages in the delivery of active compounds compared to liposomes and synthetic nanocarriers [148], have gained them much interest in the drug delivery field by the scientific community over the years.

Starting from the evidence collected by our group demonstrating the capabilities of tumour-derived EV to deliver encapsulated biologics and chemotherapeutic drugs (e.g. oncolytic viruses and paclitaxel) to cancer tissues [161,174,175], we developed a method to isolate and load extracellular vesicles with NIRs commercially available, such as DiD [178] and the clinically approved diagnostic ICG [52], to follow their biodistribution *in vivo* through the fluorescence imaging technique. With this system, we demonstrated that EV isolated from cultured immortalized cancer cell-lines selectively target tumour tissues in genetic and syngeneic mouse models of cancer (Figure 11) [180]. We proved that the tumour tropism exhibited by cancer-derived EV, heterologous and cross-species, is conserved among EV of tumoral origin, independently from the tumour type and the species originating the vesicles (Figure 11A-D) [180]. Interestingly, non-cancerous EV derived from immortalized myoblasts did not show any tumour tropism, pointing to EV generation form cancer cells as essential for the tumour recognition (Figure 12C).

The targeting abilities of cancer EV indicated their possible use as drug delivery tool, however their potential application and translation in clinic would have been limited by the potential immunogenicity and oncogenicity of EV derived from cancer cell lines. To overcome these problems, we investigated EV isolated from the blood of colorectal cancer patients and discovered autologous EV derived from the plasma of patients displaying specific tropism for tumour tissues (Figure 14A-B) [186], in agreement with the heterologous tumour recognition ability of cancer EV (Figure 11) [180]. We proved that such population of tumour-targeting vesicles did not circulate in the blood of healthy subjects (Figure 14C-D) [186], suggesting that

the sub-population of EV of tumoral origin is likely the one displaying the specific tumour tropism in the plasma of oncological patients.

To characterize this sub-population of EV and identify the molecular determinants underlying the tumour homing abilities of patient-derived EV (PDEV), we used a proteomic approach to identify proteins differentially expressed in PDEV compared to EV derived from healthy volunteers and possibly responsible for the selective tumour tropism. From mass spectrometry we identified potential candidates that could mediate the direct interaction and targeting of cancer cells by PDEV; surprisingly, we also found in PDEV a reduced expression of proteins implicated in the clearance mechanisms of EV into the blood circulation, hence possibly indicating a longer half-life of PDEV in the bloodstream (Figure 17C). We tested the hypothesis of the impaired clearance of PDEV and cancer EV *in vitro* and observed that EV endowed with tumour targeting were less captured by scavenger macrophages than EV not endowed with tumour targeting, further supporting the hypothesis of acquired abilities of patients and cancer-derived EV to escape the normal clearance mechanisms (Figure 18). Also data obtained from the comparison of the protein cargo of EV circulating in the blood of CRC patients before and after the surgical removal of the neoplastic tissue reconnect with and sustain the relative resistance to the clearance mechanism of PDEV and cancer EV (Figure 19). The hypothesis of a reduced clearance of EV of cancer origin is not sufficient to explain the whole mechanism of tumour targeting, which also requires an active step of targeting and uptake.
With the evidence collected during this project we defined a model for the tumour targeting of patient-derived EV, consisting of these three fundamental steps: i) escape from the macrophage-mediated clearance mechanisms that increase half-life and circulation time in the blood, thus allowing EV of cancer origin to accumulate in the tumour tissue; ii) selective targeting of tumour cells mediated by specific ligand-receptor interactions between PDEV and cancer cells, and finally iii) internalization and delivery of EV cargo inside cancer cells (Figure 20).

The study conducted in my PhD thesis on EV extracted from the plasma of patients before tumour resection and of patients in the follow-up phase after surgery aimed at characterizing the cancer-derived EV subpopulation enriched in the plasma of non-operated patients to identify specific markers. The data acquired on EV from patients and healthy subjects, and from patients experiencing tumour relapse or in complete remission after surgery (Figure 19) not only identified specific proteins as possible candidates for the mechanism of cancer tropism, but also outlined a cancer-specific protein signature that could represent a diagnostic marker

easily detectable from blood samples and potentially useful not only for cancer prediction and prevention in screening programs but also in follow-up surveillance for the detection of recurrent disease. The elucidation of the mechanism underlying the specific tumour tropism of patient-derived EV represents a key issue: the identification of the "minimal requirements" for the tumour targeting would pave the way to the synthetic reconstruction of biocompatible delivery systems specifically targeting cancer cells for the intraoperatory imaging and for the tumour-specific delivery of anticancer therapies. The mechanism has not yet been demonstrated but we are working on the screening of some of the molecules identified to test their ability to drive the tumour homing of patient-derived EV.

As drug delivery tool, autologous EV have the advantage, over EV derived from cancer cell-lines, of being fully biocompatible, not immunogenic nor oncogenic, have physiological pharmacokinetic properties and allow standardized production. We demonstrated that autologous EV circulating in the blood of CRC patients are endowed with specific cancer tropism abilities that allow tumour recognition when injected in tumour-bearing mice (Figure 14A-B) [186]. To enable translation into the clinical setting, EV should be able to target human tumours and deliver their content (i.e. ICG) inside cancer cells. We proved that patient-derived EVs are indeed able to target corresponding tumours (derived from the same patient who generated the EV) grown in Patient-Derived Xenograft (PDX) models (Figure 22); furthermore, we showed that encapsulation into EV protect ICG from rapid clearance and excretion (Figure 23), providing at the same time deliver and accumulation of ICG in the neoplastic tissue but not in the normal surrounding tissue (Figure 24) [186]. These findings provided a first proof-of-principle demonstration of the possible translational use of patients' EV for targeting patient tumours and delivering fluorescent agents directly inside cancer cells through the infusion of autologous EV. The innate abilities of patients' EV to recognize tumours can therefore be exploited for the design of protocols where EV are loaded with diagnostics for the detection of neoplastic tissues (Figure 25), therapeutics for targeted cancer therapies or theranostics for combined diagnostic and therapy.

However, some issues will need to be further addressed before proceeding with the clinical application of autologous transplantation protocols, including: i) an extended toxicological study to evaluate potential short and long-term effects of the treatment, ii) the determination of the effective dose of EVs and ICG in humans and the impact of the protocol scale-up on treatment efficacy, iii) the application of Good Manufacturing Practices (GMP) to the

production of the formulations to reach the clinical grade of the procedure and satisfy regulatory requirements. Currently, many isolation methods of EV are available, but since these methods all involve multistep procedures, the final production results in low yield and/or low purity of EV [144]. The amount of EV that can be extracted from patients will have to be considered, in compliance with the ethics of patients' management. Finally, the entire procedure will require standardization of isolation and purification of EV, characterization, identity, purity, and quality assurance of the formulations according to GMP production.
The feasibility of the protocol for the first-in-human demonstration of the autologous EV transplantation for the intraoperative detection of CRCs during the surgical tumour resection procedure is currently under investigation, in collaboration with the surgeons of the *National Cancer Institute, IRCCS Foundation* of Milan.

Circulating EV are emerging as a new form of liquid biopsy because cancer-associated molecules found in EV can represent biomarkers for the diagnosis and prognosis of cancer patients [167]. During my PhD we discovered a new promising biomarker of colorectal disease, associate with EV found in plasma: the mannan-binding lectin serine protease 1 (MASP1). We identified MASP1 among the candidate molecules potentially relevant for the tumour tropism; as biomarker, our data strongly support the role of extracellular vesicles-associated MASP1 for the prediction of CRC disease: MASP1 expression in plasma-derived EV from patients is significantly reduced compared to plasma-derived EV from healthy donors (Figure 27-28-29). Further investigations will also deepen its possible role in the early diagnosis of recurrence of disease in patients underwent surgical tumour resection; at present, our data showed that in EV from patients in complete remission MASP1 expression was higher (at the time of EV collection) than that of patients before surgery but not at the same level of that of healthy subjects (Figure 27): a possible reason is that at the time of EV collection patients were still recovering from surgery. Additional longitudinal studies will also clarify the possible role of MASP1 as a prognostic marker of therapeutic efficacy.

To conclude, the selective intratumor cell delivery of therapeutics and diagnostics is one of the main challenges of cancer therapy and still represents a major unmet need. In my thesis, we have demonstrated the existence of pathotropic extracellular vesicles, circulating in the blood of oncological patients, with innate abilities to recognize tumours. We have developed methods to isolate these natural nanoparticles and to load into them biologics, diagnostics and

chemotherapeutics drugs for the selective delivery to tumour tissues. The use of autologous EV fully biocompatible and of diagnostic and therapeutic agents clinically approved might be the starting point for the development of personalized diagnostic strategies and anticancer therapies based on autologous EV, to improve cancer management and ultimately patient outcomes.

Future studies will focus on the development of the protocol and quality controls for the transplantation of autologous EV loaded with ICG for the intraoperative resection of CRCs, and on the evaluation of more formulations to be encapsulated in PDEVs for novel diagnostic, therapeutic and theranostic applications. Moreover, the research will concentrate on the characterization of the mechanism underlying the tumour tropism of EV of tumoral origin; particularly interesting will be deciphering the biological significance in tumorigenesis of a communication mechanism entailing a travel back-forward of EV released by the patient's tumour in the bloodstream. We may also foresee that an in-depth characterization of the molecular determinants responsible of the tumour tropism of patient-derived EVs will lead to the discovery of cancer-specific biomarkers with prognostic and diagnostic potential.

7 ACKNOWLEDGMENTS

I am grateful to all the people who made possible to carry out this project; everyone's contribution was essential for the success of the project and for my personal growth.

I would like to thank my Professor Paolo Ciana, and all the people I have worked with for the past 5 years. It was a great journey!!

Adriana Maggi, Elisabetta Vegeto, Alessandro Villa, Mariangela Garofalo, Electra Brunialti, Nicoletta Rizzi, Monica Rebecchi, Clara Meda, Giulia Dell'Omo, Simona Vincenti, Sara Della Torre, Giovanna Pepe, Federica Mornata, Mara Barone, Lucia Zardi, Cristina Frazzica, Francesca Stucchi, Elisa Adobati, Jessica Dellavedova, Cecile Cueni, Sara Settembrini, Elisabetta Crippa and Fereshteh Shojaeighahrizjani.

I would also like to thank Professor Vincenzo Mazzaferro, Paolo Belotti and Nicolò Simonotti of the *Istituto Nazionale dei Tumori - Fondazione IRCCS* for all the clinical work and support.

Part of this work was carried out in collaboration with the Department of Oncology and Hemato-Oncology of the *Università degli Studi di Milano*.

Part of this work was also carried out in OMICs, an advanced mass spectrometry platform established by the *Università degli Studi di Milano*.

This work has been supported by MIUR under Grant "Departments of excellence Italian Law n.232, 11th December 2016", AIRC - Foundation for cancer research under IG 2020 - ID. 24914 project and has been awarded by the Seed4Innovation scouting program of *Fondazione UNIMI* of the *Università degli Studi di Milano*.

8 REFERENCES

1. Definition of cancer - NCI Dictionary of Cancer Terms - National Cancer Institute. https://www.cancer.gov/publications/dictionaries/cancer-terms/def/cancer.
2. Sung, H. *et al.* Global Cancer Statistics 2020: GLOBOCAN Estimates of Incidence and Mortality Worldwide for 36 Cancers in 185 Countries. *CA. Cancer J. Clin.* **71**, 209–249 (2021).
3. Bosetti, C. *et al.* National burden of cancer in Italy, 1990–2017: a systematic analysis for the global burden of disease study 2017. *Sci. Reports 2020 101* **10**, 1–10 (2020).
4. Zorzi, M. *et al.* Trends of colorectal cancer incidence and mortality rates from 2003 to 2014 in Italy. *Tumori* **105**, 417–426 (2019).
5. Murphy, G. *et al.* Sex Disparities in Colorectal Cancer Incidence by Anatomic Subsite, Race and Age. *Int. J. Cancer* **128**, 1668 (2011).
6. Ewing, I., Hurley, J. J., Josephides, E. & Millar, A. The molecular genetics of colorectal cancer. *Frontline Gastroenterol.* **5**, 26–30 (2014).
7. Phipps, A. I., Chan, A. T. & Ogino, S. Anatomic Subsite of Primary Colorectal Cancer and Subsequent Risk and Distribution of Second Cancers. *Cancer* **119**, 3140 (2013).
8. Kuipers, E. J. *et al.* COLORECTAL CANCER. *Nat. Rev. Dis. Prim.* **1**, 15065 (2015).
9. Hamilton, S. R. Carcinoma of the colon and rectum. *World Heal. Organ. Classif. tumors. Pathol. Genet. tumors Dig. Syst.* 105–119 (2000).
10. AIOM 2018 COLORECTAL TUMOURS Guidelines | AIOM. https://www.aiom.it/en/aiom-2018-colorectal-tumours-guidelines/.
11. AJCC Cancer Staging Handbook. *AJCC Cancer Staging Handb.* (2010) doi:10.1007/978-0-387-88443-1.
12. Adloff, M., Arnaud, J. P., Thebault, Y., Ollier, J. C. & Schloegel, M. Hepatic Metastasis from Colorectal Cancer. *Euroasian J. Hepato-Gastroenterology* **7**, 166 (2017).
13. Vukobrat-Bijedic, Z. *et al.* Cancer Antigens (CEA and CA 19-9) as Markers of Advanced Stage of Colorectal Carcinoma. *Med. Arch.* **67**, 397 (2013).
14. Breugom, A. J. *et al.* Quality assurance in the treatment of colorectal cancer: the EURECCA initiative. *Ann. Oncol. Off. J. Eur. Soc. Med. Oncol.* **25**, 1485–1492 (2014).
15. Bonjer, H. J. *et al.* A randomized trial of laparoscopic versus open surgery for rectal cancer. *N. Engl. J. Med.* **372**, 1324–1332 (2015).
16. M, B. *et al.* Survival after laparoscopic surgery versus open surgery for colon cancer: long-term outcome of a randomised clinical trial. *Lancet. Oncol.* **10**, 44–52 (2009).
17. Nelson, H. *et al.* Guidelines 2000 for colon and rectal cancer surgery. *J. Natl. Cancer Inst.* **93**, 583–596 (2001).
18. Xie, Y. H., Chen, Y. X. & Fang, J. Y. Comprehensive review of targeted therapy for colorectal cancer. *Signal Transduct. Target. Ther. 2020 51* **5**, 1–30 (2020).
19. Jonker, D. J. *et al.* Cetuximab for the Treatment of Colorectal Cancer. *http://dx.doi.org/10.1056/NEJMoa071834* **2**, 2040–2048 (2009).

20. McCormack, P. L. & Keam, S. J. Bevacizumab: a review of its use in metastatic colorectal cancer. *Drugs* **68**, 487–506 (2008).

21. Elferink, M. A. G., de Jong, K. P., Klaase, J. M., Siemerink, E. J. & de Wilt, J. H. W. Metachronous metastases from colorectal cancer: a population-based study in North-East Netherlands. *Int. J. Colorectal Dis.* **30**, 205–212 (2015).

22. Van Der Stok, E. P., Spaander, M. C. W., Grünhagen, D. J., Verhoef, C. & Kuipers, E. J. Surveillance after curative treatment for colorectal cancer. *Nat. Rev. Clin. Oncol.* **14**, 297–315 (2017).

23. Hermanek, P. & Wittekind, C. Residual tumor (R) classification and prognosis. *Semin. Surg. Oncol.* **10**, 12–20 (1994).

24. Tomlinson, J. S. *et al.* Actual 10-year survival after resection of colorectal liver metastases defines cure. *J. Clin. Oncol.* **25**, 4575–4580 (2007).

25. Ayez, N. *et al.* Outcome of microscopic incomplete resection (R1) of colorectal liver metastases in the era of neoadjuvant chemotherapy. *Ann. Surg. Oncol.* **19**, 1618–1627 (2012).

26. Siegel, R. L., Miller, K. D. & Jemal, A. Cancer statistics, 2019. *CA. Cancer J. Clin.* **69**, 7–34 (2019).

27. Wilhelmsen, M. *et al.* Determinants of recurrence after intended curative resection for colorectal cancer. *http://dx.doi.org/10.3109/00365521.2014.926981* **49**, 1399–1408 (2014).

28. Park, M. S. *et al.* Histopathologic factors affecting tumor recurrence after hepatic resection in colorectal liver metastases. *Ann. Surg. Treat. Res.* **87**, 14–21 (2014).

29. Lintoiu-Ursut, B., Tulin, A. & Constantinoiu, S. Recurrence after hepatic resection in colorectal cancer liver metastasis-Review article-. *J. Med. Life* **8**, 12 (2015).

30. Minami, Y. & Kudo, M. Radiofrequency Ablation of Liver Metastases from Colorectal Cancer: A Literature Review. *Gut Liver* **7**, 1 (2013).

31. De Jong, M. C. *et al.* Rates and patterns of recurrence following curative intent surgery for colorectal liver metastasis: an international multi-institutional analysis of 1669 patients. *Ann. Surg.* **250**, 440–447 (2009).

32. Koch, M. & Ntziachristos, V. Advancing Surgical Vision with Fluorescence Imaging. *https://doi.org/10.1146/annurev-med-051914-022043* **67**, 153–164 (2016).

33. Lauwerends, L. J. *et al.* Real-time fluorescence imaging in intraoperative decision making for cancer surgery. *Lancet. Oncol.* **22**, e186–e195 (2021).

34. Rizzo, M. *et al.* The effects of additional tumor cavity sampling at the time of breast-conserving surgery on final margin status, volume of resection, and pathologist workload. *Ann. Surg. Oncol.* **17**, 228–234 (2010).

35. Alam, I. S. *et al.* Emerging Intraoperative Imaging Modalities to Improve Surgical Precision. *Mol. Imaging Biol.* **20**, 705–715 (2018).

36. Vahrmeijer, A. L., Hutteman, M., Van Der Vorst, J. R., Van De Velde, C. J. H. & Frangioni, J. V. Image-guided cancer surgery using near-infrared fluorescence. *Nat. Rev. Clin. Oncol.* **10**, 507 (2013).

37. Moran, M. S. *et al.* Society of Surgical Oncology-American Society for Radiation Oncology consensus guideline on margins for breast-conserving surgery with whole-breast irradiation in stages I and II invasive breast cancer. *Int. J. Radiat. Oncol. Biol. Phys.* **88**, 553–564 (2014).

38. Tewari, A. *et al.* Positive surgical margin and perioperative complication rates of primary surgical treatments for prostate cancer: a systematic review and meta-analysis comparing retropubic, laparoscopic, and robotic prostatectomy. *Eur. Urol.* **62**, 1–15 (2012).

39. Anderson, C., Uman, G. & Pigazzi, A. Oncologic outcomes of laparoscopic surgery for rectal cancer: a systematic review and meta-analysis of the literature. *Eur. J. Surg. Oncol.* **34**, 1135–1142 (2008).

40. Koller, M. *et al.* Implementation and benchmarking of a novel analytical framework to clinically evaluate tumor-specific fluorescent tracers. *Nat. Commun. 2018 91* **9**, 1–11 (2018).

41. Amso, N. N. & Shayeb, A. G. Intraoperative imaging. *Best Pract. Res. Clin. Obstet. Gynaecol.* **27**, 323–338 (2013).

42. Jokerst, J. V., Pohling, C. & Gambhir, S. S. Molecular imaging with surface-enhanced Raman spectroscopy nanoparticle reporters. *MRS Bull.* **38**, 625–630 (2013).

43. Xu, M. & Wang, L. V. Photoacoustic imaging in biomedicine. *Rev. Sci. Instrum.* **77**, 041101 (2006).

44. Kruger, R. A. *et al.* Thermoacoustic CT: imaging principles. *https://doi.org/10.1117/12.386316* **3916**, 150–159 (2000).

45. Dhawan, A. P. Nuclear Medicine Imaging Modalities. *Med. Image Anal.* 139–155 (2011) doi:10.1002/9780470918548.CH6.

46. James, M. L. & Gambhir, S. S. A molecular imaging primer: Modalities, imaging agents, and applications. *Physiol. Rev.* **92**, 897–965 (2012).

47. Frangioni, J. V. In vivo near-infrared fluorescence imaging. *Curr. Opin. Chem. Biol.* **7**, 626–634 (2003).

48. Hilderbrand, S. A. & Weissleder, R. Near-infrared fluorescence: application to in vivo molecular imaging. *Curr. Opin. Chem. Biol.* **14**, 71–79 (2010).

49. DSouza, A. V., Lin, H., Henderson, E. R., Samkoe, K. S. & Pogue, B. W. Review of fluorescence guided surgery systems: identification of key performance capabilities beyond indocyanine green imaging. *https://doi.org/10.1117/1.JBO.21.8.080901* **21**, 080901 (2016).

50. van Manen, L. *et al.* A practical guide for the use of indocyanine green and methylene blue in fluorescence-guided abdominal surgery. *J. Surg. Oncol.* **118**, 283 (2018).

51. Tummers, W. S. *et al.* Recommendations for reporting on emerging optical imaging agents to promote clinical approval. *Theranostics* **8**, 5336 (2018).

52. Schaafsma, B. E. *et al.* The clinical use of indocyanine green as a near-infrared fluorescent contrast agent for image-guided oncologic surgery. *Journal of Surgical Oncology* vol. 104 323–332 (2011).

53. Hillary, S. L., Guillermet, S., Brown, N. J. & Balasubramanian, S. P. Use of methylene blue and near-infrared fluorescence in thyroid and parathyroid surgery. *Langenbeck's Arch. Surg.* **403**, 111 (2018).

54. Cwalinski, T. *et al.* Methylene Blue—Current Knowledge, Fluorescent Properties, and Its Future Use. *J. Clin. Med.* **9**, 1–12 (2020).

55. Ishizuka, M. *et al.* Novel development of 5-aminolevurinic acid (ALA) in cancer diagnoses and therapy. *Int. Immunopharmacol.* **11**, 358–365 (2011).

56. Boonstra, M. C. *et al.* Stromal Targets for Fluorescent-Guided Oncologic Surgery. *Front. Oncol.* **5**, (2015).

57. Rosenthal, E. L. *et al.* Safety and Tumor Specificity of Cetuximab-IRDye800 for Surgical Navigation in Head and Neck Cancer. *Clin. Cancer Res.* **21**, 3658–3666 (2015).

58. Harlaar, N. J. *et al.* Molecular fluorescence-guided surgery of peritoneal carcinomatosis of colorectal origin: a single-centre feasibility study. *lancet. Gastroenterol. Hepatol.* **1**, 283–290 (2016).

59. Maeda, H., Wu, J., Sawa, T., Matsumura, Y. & Hori, K. Tumor vascular permeability and the EPR effect in macromolecular therapeutics: A review. *J. Control. Release* **65**, 271–284 (2000).

60. Silindir-Gunay, M., Sarcan, E. T. & Ozer, A. Y. Near-infrared imaging of diseases: A nanocarrier approach. *Drug Dev. Res.* **80**, 521–534 (2019).

61. Reinhart, M. B., Huntington, C. R., Blair, L. J., Heniford, B. T. & Augenstein, V. A. Indocyanine Green :Historical Context, Current Applications, and Future Considerations. *Surg. Innov.* **23**, 166–175 (2016).

62. Alander, J. T. *et al.* A Review of Indocyanine Green FluorescentImaging in Surgery. *Int. J. Biomed. Imaging* **2012**, (2012).

63. Polom, K. *et al.* Current trends and emerging future of indocyanine green usage in surgery and oncology. *Cancer* **117**, 4812–4822 (2011).

64. Kusano, M., Kokudo, N., Toi, M. & Kaibori, M. ICG fluorescence imaging and navigation surgery. *ICG Fluoresc. Imaging Navig. Surg.* 1–474 (2016) doi:10.1007/978-4-431-55528-5.

65. Laperche, Y., Oudea, M. C. & Lostanlen, D. Toxic effects of indocyanine green on rat liver mitochondria. *Toxicol. Appl. Pharmacol.* **41**, 377–387 (1977).

66. fda & cder. HIGHLIGHTS OF PRESCRIBING INFORMATION.

67. Landsman, M. L. J., Kwant, G., Mook, G. A. & Zijlstra, W. G. Light-absorbing properties, stability, and spectral stabilization of indocyanine green. *J. Appl. Physiol.* **40**, 575–583 (1976).

68. CHERRICK, G. R., STEIN, S. W., LEEVY, C. M. & DAVIDSON, C. S. INDOCYANINE GREEN: OBSERVATIONS ON ITS PHYSICAL PROPERTIES, PLASMA DECAY, AND HEPATIC EXTRACTION. *J. Clin. Invest.* **39**, 592 (1960).

69. De Gasperi, A., Mazza, E. & Prosperi, M. Indocyanine green kinetics to assess liver function: Ready for a clinical dynamic assessment in major liver surgery? *World J. Hepatol.* **8**, 355 (2016).

70. Maarek, J. M. I. *et al.* Measurement of cardiac output with indocyanine green transcutaneous fluorescence dilution technique. *Anesthesiology* **100**, 1476–1483 (2004).

71. Yannuzzi, L. A. Indocyanine Green Angiography: A Perspective on Use in the Clinical Setting. *Am. J. Ophthalmol.* **151**, 745-751.e1 (2011).

72. Ishizawa, T. *et al.* Scientific Basis and Clinical Application of ICG Fluorescence Imaging: Hepatobiliary Cancer. *Open Surg. Oncol. J.* **2**, 31–36 (2010).

73. Baiocchi, G. L., Diana, M. & Boni, L. Indocyanine green-based fluorescence imaging in visceral and hepatobiliary and pancreatic surgery: State of the art and future directions. *World J. Gastroenterol.* **24**, 2921 (2018).

74. Ishizawa, T. *et al.* Fluorescent cholangiography illuminating the biliary tree during laparoscopic cholecystectomy. *Br. J. Surg.* **97**, 1369–1377 (2010).

75. Tanaka, E., Choi, H. S., Fujii, H., Bawendi, M. G. & Frangioni, J. V. Image-Guided Oncologic Surgery Using Invisible Light: Completed Pre-Clinical Development for Sentinel Lymph Node Mapping. *Ann. Surg. Oncol.* **13**, 1671 (2006).

76. Li, X. *et al.* Preliminary safety and efficacy results of laser immunotherapy for the treatment of metastatic breast cancer patients. *Photochem. Photobiol. Sci.* **10**, 817 (2011).

77. Gowsalya, K., Yasothamani, V. & Vivek, R. Emerging indocyanine green-integrated nanocarriers for multimodal cancer therapy: a review. *Nanoscale Adv.* **3**, 3332–3352 (2021).

78. Shirata, C. *et al.* Near-infrared photothermal/photodynamic therapy with indocyanine green induces apoptosis of hepatocellular carcinoma cells through oxidative stress. *Sci. Reports 2017 71* **7**, 1–8 (2017).

79. Voskuil, F. J. *et al.* Exploiting metabolic acidosis in solid cancers using a tumor-agnostic pH-activatable nanoprobe for fluorescence-guided surgery. *Nat. Commun. 2020 111* **11**, 1–10 (2020).

80. Théry, C. *et al.* Minimal information for studies of extracellular vesicles 2018 (MISEV2018): a position statement of the International Society for Extracellular Vesicles and update of the MISEV2014 guidelines. *J. Extracell. Vesicles* **7**, (2018).

81. Yáñez-Mó, M. *et al.* Biological properties of extracellular vesicles and their physiological functions. *Journal of Extracellular Vesicles* vol. 4 1–60 (2015).

82. Chargaff, E. & West, R. THE BIOLOGICAL SIGNIFICANCE OF THE THROMBOPLASTIC PROTEIN OF BLOOD*. (1946) doi:10.1016/S0021-9258(17)34997-9.

83. Wolf, P. The Nature and Significance of Platelet Products in Human Plasma. *Br. J. Haematol.* **13**, 269–288 (1967).

84. Bonucci, E. Fine structure and histochemistry of “calcifying globules” in epiphyseal cartilage. *Zeitschrift für Zellforsch. und Mikroskopische Anat. 1970 1032* **103**, 192–217 (1970).

85. Johnstone, R. M., Adam, M., Hammond, J. R., Orr, L. & Turbide, C. Vesicle formation during reticulocyte maturation. Association of plasma membrane activities with released vesicles (exosomes). *J. Biol. Chem.* **262**, 9412–9420 (1987).

86. Nieuwland, R. *et al.* Essentials of extracellular vesicles: posters on basic and clinical aspects of extracellular vesicles. *J. Extracell. Vesicles* **7**, (2018).

87. Van Niel, G., D'Angelo, G. & Raposo, G. Shedding light on the cell biology of extracellular vesicles. *Nat. Rev. Mol. Cell Biol. 2018 194* **19**, 213–228 (2018).

88. Kanada, M., Bachmann, M. H. & Contag, C. H. Signaling by Extracellular Vesicles Advances Cancer Hallmarks. *Trends in Cancer* **2**, 84–94 (2016).

89. Colombo, M., Raposo, G. & Théry, C. Biogenesis, Secretion, and Intercellular Interactions of Exosomes and Other Extracellular Vesicles. *http://dx.doi.org.pros1.lib.unimi.it/10.1146/annurev-cellbio-101512-122326* **30**, 255–289 (2014).

90. Dreyer, F. & Baur, A. Biogenesis and Functions of Exosomes and Extracellular Vesicles. *Methods Mol. Biol.* **1448**, 201–216 (2016).

91. Rusten, T. E., Vaccari, T. & Stenmark, H. Shaping development with ESCRTs. *Nat. Cell Biol. 2012 141* **14**, 38–45 (2011).

92. Doyle, L. M. & Wang, M. Z. Overview of Extracellular Vesicles, Their Origin, Composition, Purpose, and Methods for Exosome Isolation and Analysis. *Cells 2019, Vol. 8, Page 727* **8**, 727 (2019).

93. Mathieu, M., Martin-Jaular, L., Lavieu, G. & Théry, C. Specificities of secretion and uptake of exosomes and other extracellular vesicles for cell-to-cell communication. *Nat. Cell Biol. 2019 211* **21**, 9–17 (2019).

94. Robbins, P. D. & Morelli, A. E. Regulation of immune responses by extracellular vesicles. *Nat. Rev. Immunol. 2014 143* **14**, 195–208 (2014).

95. Tricarico, C., Clancy, J. & D'Souza-Schorey, C. Biology and biogenesis of shed microvesicles. *Small GTPases* **8**, 220 (2017).

96. Abels, E. R. & Breakefield, X. O. Introduction to Extracellular Vesicles: Biogenesis, RNA Cargo Selection, Content, Release, and Uptake. *Cell. Mol. Neurobiol. 2016 363* **36**, 301–312 (2016).

97. Kakarla, R., Hur, J., Kim, Y. J., Kim, J. & Chwae, Y. J. Apoptotic cell-derived exosomes: messages from dying cells. *Exp. Mol. Med. 2020 521* **52**, 1–6 (2020).

98. Wlodkowic, D., Telford, W., Skommer, J. & Darzynkiewicz, Z. Apoptosis and Beyond: Cytometry in Studies of Programmed Cell Death. *Methods Cell Biol.* **103**, 55 (2011).

99. Caruso, S. & Poon, I. K. H. Apoptotic Cell-Derived Extracellular Vesicles: More Than Just Debris. *Front. Immunol.* **9**, (2018).

100. Gutiérrez-Vázquez, C., Villarroya-Beltri, C., Mittelbrunn, M. & Sánchez-Madrid, F. Transfer of extracellular vesicles during immune cell-cell interactions. *Immunol. Rev.* **251**, 125 (2013).

101. Mashouri, L. *et al.* Exosomes: composition, biogenesis, and mechanisms in cancer metastasis and drug resistance. *Mol. Cancer 2019 181* **18**, 1–14 (2019).

102. Vlassov, A. V., Magdaleno, S., Setterquist, R. & Conrad, R. Exosomes: Current knowledge of their composition, biological functions, and diagnostic and therapeutic potentials. *Biochim. Biophys. Acta - Gen. Subj.* **1820**, 940–948 (2012).

103. Ha, D., Yang, N. & Nadithe, V. Exosomes as therapeutic drug carriers and delivery vehicles across biological membranes: current perspectives and future challenges. *Acta Pharm. Sin. B* **6**, 287–296 (2016).

104. Iraci, N., Leonardi, T., Gessler, F., Vega, B. & Pluchino, S. Focus on Extracellular Vesicles: Physiological Role and Signalling Properties of Extracellular Membrane Vesicles. *Int. J. Mol. Sci. 2016, Vol. 17, Page 171* **17**, 171 (2016).

105. Margolis, L. & Sadovsky, Y. The biology of extracellular vesicles: The known unknowns. *PLOS Biol.* **17**, e3000363 (2019).

106. Ratajczak, M. Z. & Ratajczak, J. Extracellular microvesicles/exosomes: discovery, disbelief, acceptance, and the future? *Leuk. 2020 3412* **34**, 3126–3135 (2020).

107. Mulcahy, L. A., Pink, R. C. & Carter, D. R. F. Routes and mechanisms of extracellular vesicle uptake. *J. Extracell. Vesicles* **3**, (2014).

108. Segura, E., Guérin, C., Hogg, N., Amigorena, S. & Théry, C. CD8+ Dendritic Cells Use LFA-1 to Capture MHC-Peptide Complexes from Exosomes In Vivo. *J. Immunol.* **179**, 1489–1496 (2007).

109. Kirchhausen, T. Clathrin. *Annu. Rev. Biochem.* **69**, 699–727 (2000).

110. Nabi, I. R. & Le, P. U. Caveolae/raft-dependent endocytosis. *J. Cell Biol.* **161**, 673–677 (2003).

111. Doherty, G. J. & McMahon, H. T. Mechanisms of endocytosis. *Annu. Rev. Biochem.* **78**, 857–902 (2009).

112. Teissier, É. & Pécheur, E. I. Lipids as modulators of membrane fusion mediated by viral fusion proteins. *Eur. Biophys. J.* **36**, 887–899 (2007).

113. Chernomordik, L. V. & Kozlov, M. M. Mechanics of membrane fusion. *Nat. Struct. Mol. Biol.* **15**, 675–683 (2008).

114. Heijnen, H. F. G., Schiel, A. E., Fijnheer, R., Geuze, H. J. & Sixma, J. J. Activated Platelets Release Two Types of Membrane Vesicles: Microvesicles by Surface Shedding and Exosomes Derived From Exocytosis of Multivesicular Bodies and □-Granules. *Blood* **94**, 3791–3799 (1999).

115. Nair, R. *et al.* Extracellular vesicles derived from preosteoblasts influence embryonic stem cell differentiation. *Stem Cells Dev.* **23**, 1625–1635 (2014).

116. Teng, X. *et al.* Mesenchymal Stem Cell-Derived Exosomes Improve the Microenvironment of Infarcted Myocardium Contributing to Angiogenesis and Anti-Inflammation. *Cell. Physiol. Biochem.* **37**, 2415–2424 (2015).

117. Baixauli, F., López-Otín, C. & Mittelbrunn, M. Exosomes and autophagy: coordinated mechanisms for the maintenance of cellular fitness. *Front. Immunol.* **5**, (2014).

118. Greening, D. W., Nguyen, H. P. T., Elgass, K., Simpson, R. J. & Salamonsen, L. A. Human Endometrial Exosomes Contain Hormone-Specific Cargo Modulating Trophoblast Adhesive Capacity: Insights into Endometrial-Embryo Interactions. *Biol. Reprod.* **94**, (2016).

119. Mitchell, M. D. *et al.* Placental exosomes in normal and complicated pregnancy. *Am. J. Obstet. Gynecol.* **213**, S173–S181 (2015).

120. Budnik, V., Ruiz-Cañada, C. & Wendler, F. Extracellular vesicles round off communication in the nervous system. *Nat. Rev. Neurosci.* **17**, 160–172 (2016).

121. Xu, R. *et al.* Extracellular vesicles in cancer — implications for future improvements in cancer care. *Nat. Rev. Clin. Oncol. 2018 1510* **15**, 617–638 (2018).

122. Yuana, Y., Sturk, A. & Nieuwland, R. Extracellular vesicles in physiological and pathological conditions. *Blood Rev.* **27**, 31–39 (2013).

123. Hanahan, D. & Weinberg, R. A. Hallmarks of cancer: the next generation. *Cell* **144**, 646–674 (2011).

124. Al-Nedawi, K. *et al.* Intercellular transfer of the oncogenic receptor EGFRvIII by microvesicles derived from tumour cells. *Nat. Cell Biol.* **10**, 619–624 (2008).

125. Antonyak, M. A. *et al.* Cancer cell-derived microvesicles induce transformation by transferring tissue transglutaminase and fibronectin to recipient cells. *Proc. Natl. Acad. Sci. U. S. A.* **108**, 4852–4857 (2011).

126. Grange, C. *et al.* Microvesicles released from human renal cancer stem cells stimulate angiogenesis and formation of lung premetastatic niche. *Cancer Res.* **71**, 5346–5356 (2011).

127. Hsu, Y. L. *et al.* Hypoxic lung cancer-secreted exosomal miR-23a increased angiogenesis and vascular permeability by targeting prolyl hydroxylase and tight junction protein ZO-1. *Oncogene 2017 3634* **36**, 4929–4942 (2017).

128. Webber, J. P. *et al.* Differentiation of tumour-promoting stromal myofibroblasts by cancer exosomes. *Oncogene* **34**, 319–333 (2015).

129. Orimo, A. *et al.* Stromal fibroblasts present in invasive human breast carcinomas promote tumor growth and angiogenesis through elevated SDF-1/CXCL12 secretion. *Cell* **121**, 335–348 (2005).

130. Liang, P. *et al.* Myofibroblasts Correlate with Lymphatic Microvessel Density and Lymph Node Metastasis in Early-stage Invasive Colorectal Carcinoma. *Anticancer Res.* **25**, 2705–2712 (2005).

131. Erdogan, B. & Webb, D. J. Cancer-associated fibroblasts modulate growth factor signaling and extracellular matrix remodeling to regulate tumor metastasis. *Biochem. Soc. Trans.* **45**, 229 (2017).

132. Luga, V. *et al.* Exosomes mediate stromal mobilization of autocrine Wnt-PCP signaling in breast cancer cell migration. *Cell* **151**, 1542–1556 (2012).

133. Xavier, C. P. R. *et al.* The Role of Extracellular Vesicles in the Hallmarks of Cancer and Drug Resistance. *Cells 2020, Vol. 9, Page 1141* **9**, 1141 (2020).

134. Costa, P. M. & De Lima, M. C. P. MicroRNAs as Molecular Targets for Cancer Therapy: On the Modulation of MicroRNA Expression. *Pharmaceuticals* **6**, 1195 (2013).

135. Taylor, D. D. & Gerçel-Taylor, C. Tumour-derived exosomes and their role in cancer-associated T-cell signalling defects. *Br. J. Cancer* **92**, 305 (2005).

136. Shimoda, M. & Khokha, R. Metalloproteinases in extracellular vesicles. *Biochim. Biophys. Acta - Mol. Cell Res.* **1864**, 1989–2000 (2017).

137. Hoshino, A. *et al.* Tumour exosome integrins determine organotropic metastasis. *Nature* **527**, 329–335 (2015).

138. Cardone, R. A., Casavola, V. & Reshkin, S. J. The role of disturbed pH dynamics and the Na+/H+ exchanger in metastasis. *Nat. Rev. Cancer* **5**, 786–795 (2005).

139. Parolini, I. *et al.* Microenvironmental pH is a key factor for exosome traffic in tumor cells. *J. Biol. Chem.* **284**, 34211–34222 (2009).

140. Wang, T. *et al.* Hypoxia-inducible factors and RAB22A mediate formation of microvesicles that stimulate breast cancer invasion and metastasis. *Proc. Natl. Acad. Sci. U. S. A.* **111**, (2014).

141. Xia, W. *et al.* Targeted Delivery of Drugs and Genes Using Polymer Nanocarriers for Cancer Therapy. *Int. J. Mol. Sci.* **22**, (2021).

142. Hossen, S. *et al.* Smart nanocarrier-based drug delivery systems for cancer therapy and toxicity studies: A review. *J. Adv. Res.* **15**, 1–18 (2019).

143. Nisini, R., Poerio, N., Mariotti, S., De Santis, F. & Fraziano, M. The multirole of liposomes in therapy and prevention of infectious diseases. *Front. Immunol.* **9**, 155 (2018).

144. Antimisiaris, S. G., Mourtas, S. & Marazioti, A. Exosomes and Exosome-Inspired Vesicles for Targeted Drug Delivery. *Pharm. 2018, Vol. 10, Page 218* **10**, 218 (2018).

145. Meng, W. *et al.* Prospects and challenges of extracellular vesicle-based drug delivery system: considering cell source. *https://doi.org/10.1080/10717544.2020.1748758* **27**, 585–598 (2020).

146. Nogueira, E., Gomes, A. C., Preto, A. & Cavaco-Paulo, A. Design of liposomal formulations for cell targeting. *Colloids Surfaces B Biointerfaces* **136**, 514–526 (2015).

147. Yong, T. *et al.* Extracellular vesicles for tumor targeting delivery based on five features principle. *J. Control. Release* **322**, 555–565 (2020).

148. Van Der Meel, R. *et al.* Extracellular vesicles as drug delivery systems: Lessons from the liposome field. *Journal of Controlled Release* vol. 195 72–85 (2014).

149. Armstrong, J. P. K. & Stevens, M. M. Strategic design of extracellular vesicle drug delivery systems. *Adv. Drug Deliv. Rev.* **130**, 12 (2018).

150. Tominaga, N. *et al.* Brain metastatic cancer cells release microRNA-181c-containing extracellular vesicles capable of destructing blood–brain barrier. *Nat. Commun.* **6**, (2015).

151. Klyachko, N. L., Arzt, C. J., Li, S. M., Gololobova, O. A. & Batrakova, E. V. Extracellular Vesicle-Based Therapeutics: Preclinical and Clinical Investigations. *Pharm. 2020, Vol. 12, Page 1171* **12**, 1171 (2020).

152. Fuhrmann, G., Neuer, A. L. & Herrmann, I. K. Extracellular vesicles – A promising avenue for the detection and treatment of infectious diseases? *Eur. J. Pharm. Biopharm.* **118**, 56–61 (2017).

153. El-Andaloussi, S. *et al.* Exosome-mediated delivery of siRNA in vitro and in vivo. *Nat. Protoc. 2012 712* **7**, 2112–2126 (2012).

154. Li, L. *et al.* γδTDEs: An Efficient Delivery System for miR-138 with Anti-tumoral and Immunostimulatory Roles on Oral Squamous Cell Carcinoma. *Mol. Ther. Nucleic Acids* **14**, 101 (2019).

155. Haney, M. J. *et al.* Exosomes as Drug Delivery Vehicles for Parkinson's Disease Therapy. *J. Control. Release* **207**, 18 (2015).

156. Zhuang, X. *et al.* Treatment of Brain Inflammatory Diseases by Delivering Exosome Encapsulated Anti-inflammatory Drugs From the Nasal Region to the Brain. *Mol. Ther.* **19**, 1769 (2011).

157. Jung, K. O., Jo, H., Yu, J. H., Gambhir, S. S. & Pratx, G. Development and MPI tracking of novel hypoxia-targeted theranostic exosomes. *Biomaterials* **177**, 139 (2018).

158. Lin, Y. *et al.* Exosome–Liposome Hybrid Nanoparticles Deliver CRISPR/Cas9 System in MSCs. *Adv. Sci.* **5**, 1700611 (2018).

159. Garofalo, M. *et al.* Systemic administration and targeted delivery of immunogenic oncolytic adenovirus encapsulated in extracellular vesicles for cancer therapies. *Viruses* **10**, (2018).

160. Garofalo, M. *et al.* Antitumor effect of oncolytic virus and paclitaxel encapsulated in extracellular vesicles for lung cancer treatment. *J. Control. Release* **283**, 223–234 (2018).

161. Garofalo, M. *et al.* Extracellular vesicles enhance the targeted delivery of immunogenic oncolytic adenovirus and paclitaxel in immunocompetent mice. *J. Control. Release* **294**, 165–175 (2019).

162. Yong, T. *et al.* Tumor exosome-based nanoparticles are efficient drug carriers for chemotherapy. *Nat. Commun.* **10**, 1–16 (2019).

163. Herrmann, I. K., Wood, M. J. A. & Fuhrmann, G. Extracellular vesicles as a next-generation drug delivery platform. *Nat. Nanotechnol. 2021 167* **16**, 748–759 (2021).

164. Dang, X. T. T., Kavishka, J. M., Zhang, D. X., Pirisinu, M. & Le, M. T. N. Extracellular Vesicles as an Efficient and Versatile System for Drug Delivery. *Cells 2020, Vol. 9, Page 2191* **9**, 2191 (2020).

165. Li, Y. J. *et al.* Artificial exosomes for translational nanomedicine. *J. Nanobiotechnology 2021 191* **19**, 1–20 (2021).

166. Ciferri, M. C., Quarto, R. & Tasso, R. Extracellular Vesicles as Biomarkers and Therapeutic Tools: From Pre-Clinical to Clinical Applications. *Biol. 2021, Vol. 10, Page 359* **10**, 359 (2021).

167. Lane, R. E., Korbie, D., Hill, M. M. & Trau, M. Extracellular vesicles as circulating cancer biomarkers: opportunities and challenges. *Clin. Transl. Med. 2018 71* **7**, 1–11 (2018).

168. Skog, J. *et al.* Glioblastoma microvesicles transport RNA and proteins that promote tumour growth and provide diagnostic biomarkers. *Nat. Cell Biol. 2008 1012* **10**, 1470–1476 (2008).

169. Zhou, E. *et al.* Circulating extracellular vesicles are effective biomarkers for predicting response to cancer therapy. *EBioMedicine* **67**, 103365 (2021).

170. Definition of liquid biopsy - NCI Dictionary of Cancer Terms - National Cancer Institute. https://www.cancer.gov/publications/dictionaries/cancer-terms/def/liquid-biopsy.

171. König, L. *et al.* Elevated levels of extracellular vesicles are associated with therapy failure and disease progression in breast cancer patients undergoing neoadjuvant chemotherapy. *Oncoimmunology* **7**, (2018).

172. Alander, J. T. *et al.* A Review of indocyanine green fluorescent imaging in surgery. *International Journal of Biomedical Imaging* vol. 2012 (2012).

173. Yi, X. M., Wang, F. L., Qin, W. J., Yang, X. J. & Yuan, J. L. Near-infrared fluorescent probes in cancer imaging and therapy: an emerging field. *Int. J. Nanomedicine* **9**, 1347–1365 (2014).

174. Garofalo, M. *et al.* Systemic Administration and Targeted Delivery of Immunogenic Oncolytic Adenovirus Encapsulated in Extracellular Vesicles for Cancer Therapies. *Viruses* **10**, (2018).

175. Garofalo, M. *et al.* Antitumor effect of oncolytic virus and paclitaxel encapsulated in extracellular vesicles for lung cancer treatment. *J. Control. Release* **283**, (2018).

176. Thompson, R. F., Walker, M., Siebert, C. A., Muench, S. P. & Ranson, N. A. An introduction to sample preparation and imaging by cryo-electron microscopy for structural biology. *Methods* **100**, 3–15 (2016).

177. Bosma, M. J. & Carroll, A. M. The SCID Mouse Mutant: Definition, Characterization, and Potential Uses. *http://dx.doi.org/10.1146/annurev.iy.09.040191.001543* **9**, 323–350 (2003).

178. Progatzky, F., Dallman, M. J. & Celso, C. Lo. From seeing to believing: labelling strategies for in vivo cell-tracking experiments. *Interface Focus* **3**, (2013).

179. Yoshioka, Y. *et al.* Comparative marker analysis of extracellular vesicles in different human cancer types. *J. Extracell. Vesicles* **2**, (2013).

180. Garofalo, M. *et al.* Heterologous and cross-species tropism of cancer-derived extracellular vesicles. *Theranostics* **9**, 5681–5693 (2019).

181. Guy, C. T. *et al.* Expression of the neu protooncogene in the mammary epithelium of transgenic mice induces metastatic disease. *Proc. Natl. Acad. Sci. U. S. A.* **89**, 10578 (1992).

182. Muller, W. J., Sinn, E., Pattengale, P. K., Wallace, R. & Leder, P. Single-step induction of mammary adenocarcinoma in transgenic mice bearing the activated c-neu oncogene. *Cell* **54**, 105–115 (1988).

183. FOX, I. J. & WOOD, E. H. Indocyanine green: physical and physiologic properties. *Mayo Clin. Proc.* **35**, 732–744 (1960).

184. Feng, D. *et al.* Cellular Internalization of Exosomes Occurs Through Phagocytosis. *Traffic* **11**, 675–687 (2010).

185. McKelvey, K. J., Powell, K. L., Ashton, A. W., Morris, J. M. & McCracken, S. A. Exosomes: Mechanisms of Uptake. *Journal of Circulating Biomarkers* vol. 4 (2015).

186. Villa, A. *et al.* Transplantation of autologous extracellular vesicles for cancer-specific targeting. *Theranostics* **11**, 2034 (2021).

187. Théry, C. *et al.* Minimal information for studies of extracellular vesicles 2018 (MISEV2018): a position statement of the International Society for Extracellular Vesicles and update of the MISEV2014 guidelines. *J. Extracell. Vesicles* **7**, (2018).

188. Yoneya, S. *et al.* Binding properties of indocyanine green in human blood. *Invest. Ophthalmol. Vis. Sci.* **39**, 1286–1290 (1998).

189. Kooijmans, S. A. A., Schiffelers, R. M., Zarovni, N. & Vago, R. Modulation of tissue tropism and biological activity of exosomes and other extracellular vesicles: New nanotools for cancer treatment. *Pharmacol. Res.* **111**, 487–500 (2016).

190. Laulagnier, K. *et al.* Amyloid precursor protein products concentrate in a subset of exosomes specifically endocytosed by neurons. *Cell. Mol. Life Sci.* **75**, 757–773 (2018).

191. Osawa, S., Kurachi, M., Yamamoto, H., Yoshimoto, Y. & Ishizaki, Y. Fibronectin on extracellular vesicles from microvascular endothelial cells is involved in the vesicle uptake into oligodendrocyte precursor cells. *Biochem. Biophys. Res. Commun.* **488**, 232–238 (2017).

192. Rana, S., Yue, S., Stadel, D. & Zöller, M. Toward tailored exosomes: The exosomal tetraspanin web contributes to target cell selection. *Int. J. Biochem. Cell Biol.* **44**, 1574–1584 (2012).

193. Qiao, L. *et al.* Tumor cell-derived exosomes home to their cells of origin and can be used as Trojan horses to deliver cancer drugs. *Theranostics* **10**, 3474–3487 (2020).

194. Emam, S. E. *et al.* Cancer cell-type tropism is one of crucial determinants for the efficient systemic delivery of cancer cell-derived exosomes to tumor tissues. *Eur. J. Pharm. Biopharm.* **145**, 27–34 (2019).

195. Murphy, D. E. *et al.* Extracellular vesicle-based therapeutics: natural versus engineered targeting and trafficking. *Experimental and Molecular Medicine* vol. 51 (2019).

196. Szklarczyk, D. *et al.* STRING v11: protein–protein association networks with increased coverage, supporting functional discovery in genome-wide experimental datasets. *Nucleic Acids Res.* **47**, D607 (2019).

197. Parada, N., Romero-Trujillo, A., Georges, N. & Alcayaga-Miranda, F. Camouflage strategies for therapeutic exosomes evasion from phagocytosis. *J. Adv. Res.* **31**, 61–74 (2021).

198. Imai, T. *et al.* Macrophage-dependent clearance of systemically administered B16BL6-derived exosomes from the blood circulation in mice. *J. Extracell. Vesicles* **4**, 1–8 (2015).

199. Blanco, E., Shen, H. & Ferrari, M. Principles of nanoparticle design for overcoming biological barriers to drug delivery. *Nat. Biotechnol.* **33**, 941 (2015).

200. Matsushita, M., Thiel, S., Jensenius, J. C., Terai, I. & Fujita, T. Proteolytic Activities of Two Types of Mannose-Binding Lectin-Associated Serine Protease. *J. Immunol.* **165**, 2637–2642 (2000).

201. Mayle, K. M., Le, A. M. & Kamei, D. T. The Intracellular Trafficking Pathway of Transferrin. *Biochim. Biophys. Acta* **1820**, 264 (2012).

202. Pasqualini, R. *et al.* Aminopeptidase N Is a Receptor for Tumor-homing Peptides and a Target for Inhibiting Angiogenesis. *Cancer Res.* **60**, 722 (2000).

203. Sagaert, X., Vanstapel, A. & Verbeek, S. Tumor Heterogeneity in Colorectal Cancer: What Do We Know So Far? *Pathobiology* **85**, 72–84 (2018).

204. Hidalgo, M. *et al.* Patient-Derived Xenograft Models: An Emerging Platform for Translational Cancer Research. *Cancer Discov.* **4**, 998–1013 (2014).

205. Bhimani, J., Ball, K. & Stebbing, J. Patient-derived xenograft models—the future of personalised cancer treatment. *Br. J. Cancer 2020 1225* **122**, 601–602 (2020).

206. Lane, R. E., Korbie, D., Hill, M. M. & Trau, M. Extracellular vesicles as circulating cancer biomarkers: opportunities and challenges. *Clin. Transl. Med.* **7**, 1–11 (2018).

207. Tamura, T., Yoshioka, Y., Sakamoto, S., Ichikawa, T. & Ochiya, T. Extracellular vesicles as a promising biomarker resource in liquid biopsy for cancer. *Extracell. Vesicles Circ. Nucleic Acids* **2**, 148–174 (2021).

208. Beltrame, M. H., Catarino, S. J., Goeldner, I., Boldt, A. B. W. & Reason, I. J. de M. The lectin pathway of complement and rheumatic heart disease. *Front. Pediatr.* **2**, 148 (2015).

209. Ytting, H. *et al.* Mannan-Binding Lectin (MBL) and MBL-Associated Serine Protease 2 (MASP-2) Genotypes in Colorectal Cancer. *Scand. J. Immunol.* **73**, 122–127 (2011).

210. Swierzko, A. S. *et al.* Mannose-Binding Lectin (MBL) and MBL-associated serine protease-2 (MASP-2) in women with malignant and benign ovarian tumours. *Cancer Immunol. Immunother.* **63**, 1129 (2014).

211. Maestri, C. A. *et al.* MASP-1 and MASP-2 Serum Levels Are Associated With Worse Prognostic in Cervical Cancer Progression. *Front. Immunol.* **9**, 2742 (2018).

212. Trouw, L. A., Pickering, M. C. & Blom, A. M. The complement system as a potential therapeutic target in rheumatic disease. *Nat. Rev. Rheumatol. 2017 139* **13**, 538–547 (2017).

213. Raposo, G. & Stahl, P. D. Extracellular vesicles: a new communication paradigm? *Nature Reviews Molecular Cell Biology* vol. 20 509–510 (2019).

Ph.D. ACTIVITIES

Other projects

During the Ph.D. I participated to other projects not included in this thesis.

- Study of estrogen receptor α and the early molecular events underlying the neoplastic transformation of the mammary gland;
- Identification of early prognostic and diagnostic markers and new targets for the development of chemopreventive strategies in breast cancer.

Teaching experiences

April 2021
Position: remote lecturer "Principi di chemioterapia antitumorale e principali classi di farmaci".
Supervisor: Professor Paolo Ciana.
Institute: Faculty of Medicine and Surgery, University of Milan, Italy.

March 2021
Position: remote lecturer "Diabete mellito".
Supervisor: Professor Paolo Ciana.
Institute: Faculty of Medicine and Surgery, University of Milan, Italy.

May 2020
Position: remote lecturer "Diabete mellito".
Supervisor: Professor Paolo Ciana.
Institute: Faculty of Medicine and Surgery, University of Milan, Italy.

March 2020
Position: remote lecturer "Principi generali di chemioterapia antitumorale e principali classi di farmaci".
Supervisor: Professor Paolo Ciana.
Institute: Faculty of Medicine and Surgery, University of Milan, Italy.

March 2020
Position: remote lecturer "Farmaci del sistema gastrointestinale".
Supervisor: Professor Paolo Ciana.
Institute: Faculty of Medicine and Surgery, University of Milan, Italy.

June 2019
Position: lecturer "Farmaci antinfiammatori steroidei e non steroidei", "Farmaci per il trattamento della gotta", "Farmaci per il trattamento dell'artrite reumatoide".
Supervisor: Professor Paolo Ciana.
Institute: Faculty of Medicine and Surgery, University of Milan, Italy.

28-31 January 2019
Position: teaching activity for the laboratory of "Biotecnologie farmacologiche avanzate".
Supervisor: Professor Adriana Maggi.
Institute: Faculty of Pharmacy, University of Milan, Italy.

Tutoring of master's degree thesis

2021 - ongoing: Sara Settembrini, Master Course in Pharmaceutical Chemistry and Technology.

2020 - ongoing: Cecile Cueni, Master Course in Medical Biotechnology and Molecular Medicine.

2019 - 2020: Elisa Adobati, Master Course in Pharmaceutical Chemistry and Technology. "Studio iniziale sul meccanismo molecolare implicato nel riconoscimento tumore-specifico di vescicole extracellulari di origine neoplastica".

2019 - 2020: Cristina Frazzica, Master Course in Pharmaceutical Biotechnology.
"Analisi trascrittomica dei segnali modulati dal recettore degli estrogeni alfa nelle fasi iniziali della tumorigenesi mammaria".

2018 - 2019: Lucia Zardi, Master Course in Pharmacy.
"Evidenze di un nuovo meccanismo di azione del recettore degli estrogeni e dell'attività anti-proliferativa del tamoxifene durante le prime fasi di sviluppo della neoplasia mammaria".

2018: Andrea Maugeri, Master Course in Pharmacy.
"Strumenti diagnostici, prognostici e terapeutici per la chemioprevenzione del carcinoma mammario".

Congresses

D. Crescenti, A. Villa, M. Garofalo, V. Mazzaferro, P. Ciana. *Extracellular vesicles-based targeted delivery of diagnostic agents to neoplastic tissues*. Annual PhD Student School 2021. 11-14 October 2021, Gargnano (BS). Oral presentation.

D. Crescenti, A. Villa, M. Garofalo, V. Mazzaferro, P. Ciana. *Targeted delivery of diagnostic agents to neoplastic tissues: preclinical development of nanoparticles-based systems for the intraoperatory labelling of tumor sites*. PhD Seminars. 20 May 2021. Remote presentation.

Villa A, Garofalo M, **Crescenti D**, Rizzi N, Brunialti E, Vingiani A, Belotti P, Sposito C, Franzè S, Cilurzo F, Pruneri G, Recordati C, Giudice C, Giordano A, Tortoreto M, Stefanello D, Manenti G, Zaffaroni N, Mazzaferro V, Ciana P. *Transplantation of autologous extracellular vesicles for cancer-specific targeting*. 40º CONGRESSO NAZIONALE della SOCIETÀ ITALIANA di FARMACOLOGIA, 9-13 Marzo 2021, Digital Edition. Poster.

Crescenti D, Villa A, Garofalo M, Brunialti E, Mazzaferro V, Ciana P. *Veicolazione di agenti diagnostici mirata ai tessuti neoplastici: sviluppo preclinico di sistemi basati su nanoparticelle per la marcatura intraoperatoria dei siti tumorali*. Congresso DiSS 2020, November 13 2020, Virtual Meeting. Selected for poster and oral presentation.

D. Crescenti, A. Villa, M. Garofalo, V. Mazzaferro, P. Ciana. *Cancer-targeted delivery of diagnostic agents: development of nanoparticles-based systems for the intraoperatory labelling of tumor sites*. Annual School IV Edition. 25-28 June 2020, Chiesa in Valmalenco (SO). Oral presentation.

D. Crescenti, M. Garofalo, A. Villa, E. Brunialti, P. Belotti, V. Mazzaferro, P. Ciana. *Development of NIR probes and delivery systems selectively labelling tumor sites*. Next Step X, La giovane ricerca avanza. September 18, Milan 2019. Oral presentation.

D. Crescenti, M. Garofalo, A. Villa, V. Mazzaferro, P. Ciana. *Development of NIR probes and delivery systems selectively labelling tumor sites*. Spring School III Edition. 11-14 April 2019, Chiesa in Valmalenco (SO). Oral presentation.

Third mission

RicercaMIx Blog (http://www.ricercamix.org/author/daniela-crescenti/)

18 June 2021 - "Vescicole extracellulari: un cavallo di Troia nella lotta contro i tumori".

27 January 2020 - "Sirtuine: dalla dieta alla terapia anti-cancro".

Publications

Crescenti D, et al. *Changing of proteomic landscape of circulating extracellular vesicles in colorectal cancer patients*. (In preparation).

Crescenti D, et al. *Tamoxifen resistant pathway during early breast cancer progression*. (In preparation).

Villa A, Garofalo M, **Crescenti D**, Rizzi N, Brunialti E, Vingiani A, Belotti P, Sposito C, Franzè S, Cilurzo F, Pruneri G, Recordati C, Giudice C, Giordano A, Tortoreto M, Stefanello D, Manenti G, Zaffaroni N, Mazzaferro V, Ciana P. *Transplantation of autologous extracellular vesicles for cancer-specific targeting*. Theranostics. 2021 Jan 1;11(5):2034-2047.

Garofalo M, Villa A, Brunialti E, **Crescenti D**, Dell'Omo G, Kuryk L, Mazzaferro V, Ciana P. *Cancer-derived EVs show tropism for tissues at early stage of neoplastic transformation*. Nanotheranostics. doi:10.7150/ntno.47226.

Garofalo M, Villa A**, Crescenti D**, Marzagalli M, Kuryk L, Limonta P, Mazzaferro V, Ciana P. *Heterologous and cross-species tropism of cancer-derived extracellular vesicles*. Theranostics 2019; 9(19):5681-5693. doi:10.7150/thno.34824.

Dell'Omo G, **Crescenti D,** Vantaggiato C, Parravicini C, Borroni AP, Rizzi N, Garofalo M, Pinto A, Recordati C, Scanziani E, Bassi FD, Pruneri G, Conti P, Eberini I, Maggi A, Ciana P - *Inhibition of SIRT1 deacetylase and p53 activation uncouples the anti-inflammatory and chemopreventive actions of NSAIDs*. Br J Cancer. 2019 Mar.

Garofalo M, Saari H, Somersalo P, **Crescenti D,** Kuryk L, Aksela L, Capasso C, Madetoja M, Koskinen K, Oksanen T, Mäkitie A, Jalasvuori M, Cerullo V, Ciana P, Yliperttula M – *Antitumor effect of oncolytic virus and paclitaxel encapsulated in extracellular vesicles for lung cancer treatment*. J Control Release. 2018 Jun 1.